

# Heteroatom-Induced Molecular Asymmetry Tunes Quantum Interference in Charge Transport through Single-Molecule Junctions

*Yang Yang<sup>1#</sup>, Markus Gantenbein<sup>2#</sup>, Afaf Alqorashi<sup>3#</sup>, Junying Wei<sup>1</sup>, Sara Sangtarash<sup>3</sup>, Duan Hu<sup>1</sup>, Hatef Sadeghi<sup>3</sup>, Rui Zhang<sup>1</sup>, Jiuchan Pi<sup>1</sup>, Lichuan Chen<sup>1</sup>, Xiaoyan Huang<sup>1</sup>, Ruihao Li<sup>1</sup>, Junyang Liu<sup>1</sup>, Jia Shi<sup>1</sup>, Wenjing Hong<sup>\*1</sup>, Colin J. Lambert<sup>\*3</sup>, Martin R. Bryce<sup>\*2</sup>*

1. State Key Laboratory of Physical Chemistry of Solid Surfaces, Pen-Tung Sah Institute of Micro-Nano Science and Technology, College of Chemistry and Chemical Engineering, iChEM, Xiamen University, 361005, Xiamen, China

2. Department of Chemistry, Durham University, DH1 3LE, Durham, UK

3. Department of Physics, Lancaster University, LA1 4YB, Lancaster, UK

This manuscript is dedicated to the memory of Professor Thomas Wandlowski.

## AUTHOR INFORMATION

### Corresponding Author

\* Wenjing Hong, Email: [whong@xmu.edu.cn](mailto:whong@xmu.edu.cn)

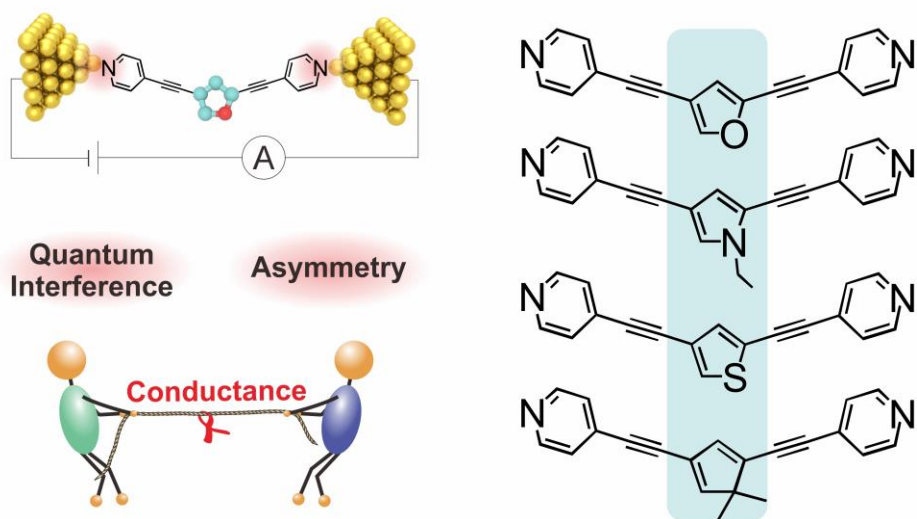
\* Martin R. Bryce, Email: [m.r.bryce@durham.ac.uk](mailto:m.r.bryce@durham.ac.uk)

\* Colin J. Lambert, Email: [c.lambert@lancaster.ac.uk](mailto:c.lambert@lancaster.ac.uk)

## ABSTRACT

We studied the interplay between quantum interference (QI) and molecular asymmetry in charge transport through a single molecule. Eight compounds with five-membered core rings were synthesized and their single-molecule conductances were characterized using the mechanically controllable break junction (MCBJ) technique. It is found that the symmetric molecules are more conductive than their asymmetric isomers and there is no statistically-significant dependence on the aromaticity of the core. In contrast, we find experimental evidence of destructive QI in five-membered rings, which can be tuned by implanting different heteroatoms into the core ring. Our findings are rationalized by the presence of anti-resonance features in the transmission curves calculated using non-equilibrium Green's functions. This novel mechanism for modulating QI effects in charge transport via tuning of molecular asymmetry will lead to promising applications in the design of single-molecule devices.

## TOC Graphic



## 1. INTRODUCTION

Quantum interference (QI) effects have recently attracted great interest in studies of the charge transport at the single-molecule scale.<sup>1-6</sup> As determined by the phases of the partial de Broglie waves traversing different paths,<sup>7-9</sup> QI provides a unique way to tune the single-molecule conductance by orders of magnitude without incorporating substituent groups, extending molecular length or changing the surrounding environment of the molecule. To date most reports of QI in cyclic molecules have been restricted to compounds with central six-membered rings.<sup>10-14</sup> Although it has not been observed experimentally, QI in central five-membered rings is suggested to be a promising way to vary the molecular topology and increase structural diversity of single-molecule devices.<sup>15</sup>

The incorporation of heteroatoms into a central difunctionalized five-membered  $\pi$ -system leads to the structural asymmetry of the molecular junctions. Parks et al demonstrated that through modification of the symmetry of a single-molecule junction by axially stretching the molecule, the spin states, magnetic anisotropy, and thus the electron flow through the junction can be tuned.<sup>16</sup> Our recent studies also suggest that an asymmetric pyridine (2,4-disubstituted) modifies the pattern of QI within the core of the molecular backbone and promotes charge transport through single-molecule junctions.<sup>17</sup> Therefore, five-membered heterocyclic cores provide a logical diversification of the known structural platforms and enable an investigation of the interplay of QI effects and structural asymmetry of the core unit in charge transport through single-molecule junctions.

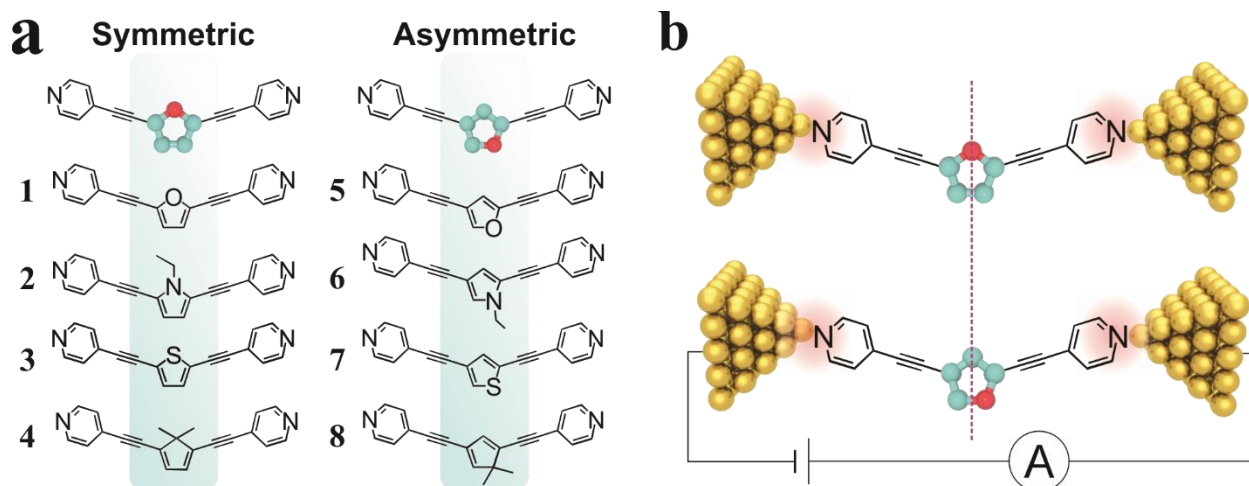
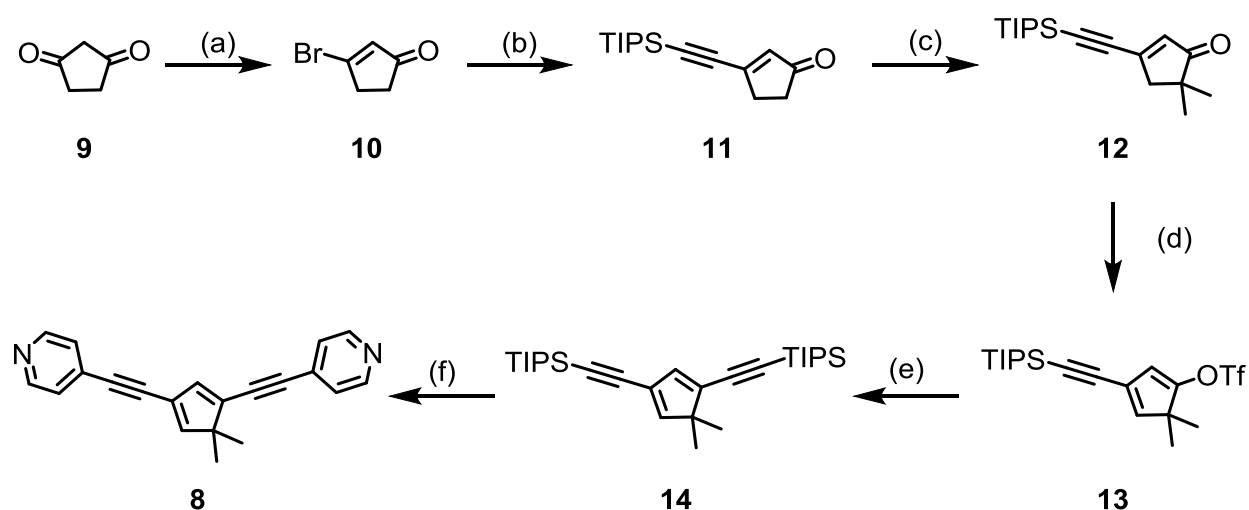


**Figure 1.** (a) Molecules with five-membered core units studied in this work. (b) Schematic of a molecular junction. The vertical dashed line shows the symmetry (top structure) and asymmetry (bottom structure) with respect to the core unit.

Herein we study the single-molecule conductances of a series of eight compounds of the type X-Y-X. As shown in Figure 1a and Figures S3-1 and S3-2 in the SI, the furan (**1**, **5**), pyrrole (**2**, **6**), thiophene (**3**, **7**) and cyclopentadiene cores (**4**, **8**) are rigid and planar. There are three notable features in their molecular design: (i) all of the molecules have terminal pyridyl anchoring units (X) at both ends; (ii) each molecule has one of four different five-membered core units (Y), and (iii) the core is either symmetrically substituted (i.e. 2,5-difunctionalized; **1-4**) or asymmetrically substituted (i.e. 2,4-difunctionalized; **5-8**). These compounds provide a unique opportunity to investigate two issues. First, whether the QI effect is general for other conjugated systems, besides those previously studied with aromatic six-membered central rings.<sup>10-14</sup> Second, what is the interplay between QI and structural asymmetry in charge transport through five-membered core units?

## 2. EXPERIMENTAL SECTION

The synthesis and detailed characterization of compounds **1-8** are given in the SI. The general synthetic strategy to the symmetrical target structures **1-4** was as follows. The core-unit 2,5-disubstituted with bromine (thiophene, pyrrole, and furan) or triflate (cyclopentadiene) was reacted with two equivalents of TIPS-protected acetylene under Sonogashira conditions. After a two-pot reaction sequence of desilylation with tetrabutylammonium fluoride and subsequent Sonogashira coupling with 4-iodopyridine, compounds **1-4** were obtained in good yields. The synthesis of the asymmetric isomers **5-8** was more challenging. This was especially the case for derivative **8** (Scheme 1) as the formation of C-C bonds at the 2,4-positions of cyclopentadiene under mild conditions, to our knowledge is not known in the literature. It is worth noting that the alkyne units at C(2) and C(4) were attached sequentially: this strategy should, therefore, be versatile for the attachment of different functionality at these positions.



**Scheme 1.** Synthesis of **8**. Reagents and Conditions: (a)  $\text{PPh}_3$ ,  $\text{Br}_2$ , TEA,  $\text{CH}_2\text{Cl}_2$ ,  $0\text{ }^\circ\text{C}$  to rt, 2 h, 71%; (b)  $\text{PdCl}_2(\text{PPh}_3)_2$ , CuI, TIPS-A, DIPA, 10 min, 94%; (c) LiHMDS, MeI, THF,  $-78\text{ }^\circ\text{C}$  to rt,

12 h, 64%; (d) KHMDS, Comins' reagent, THF, -78 °C to rt, 12 h, 87%; (e) TIPSA, PdCl<sub>2</sub>(PPh<sub>3</sub>)<sub>2</sub>, CuI, TEA, THF, rt, 4 h, 91%; (f) TBAF (1 M in THF), THF, rt, 30 min, then 4-iodopyridine, PdCl<sub>2</sub>(PPh<sub>3</sub>)<sub>2</sub>, CuI, THF, DIPA, 40 °C, 12 h, 61% (over two steps).

The mechanically controllable break junction (MCBJ) technique was used to measure the single-molecule conductances of compounds **1-8**. A schematic drawing of the molecular junction is shown in Figure 1b, while details of the electrical characterization are reported in our previous paper.<sup>18</sup> Briefly, we use an Au wire tip of 99.99% purity for the in-situ fabrication of nanometer-sized separation. The target compounds were pre-pared as 0.2 mM solutions in TMB (mesitylene) as solvent. The experiments were carried out in ambient conditions at room temperature by employing a homebuilt *I-V* converter with a sampling rate of 10 kHz. For each conductance histogram, at least 1,000 individual curves were collected without any data selection.

### 3. RESULTS AND DISCUSSION

Figures 2a and 2c display individual conductance traces of **1-4** and **5-8** recorded during the opening process of the MCBJ operation. The corresponding conductance histograms are given in Figures 2b and Figure 2d, respectively. Figures 2a-f are plotted in a semi-logarithmic scale in order to cover the whole measuring range, and the conductance values are reported in units of the conductance quantum ( $G_0=2e^2/h$ ). As shown in Figure 2a, after an abrupt jump from the sudden rupture of the last gold-gold atomic contact, clear conductance plateaus were observed which could be attributed to the single molecular junctions.

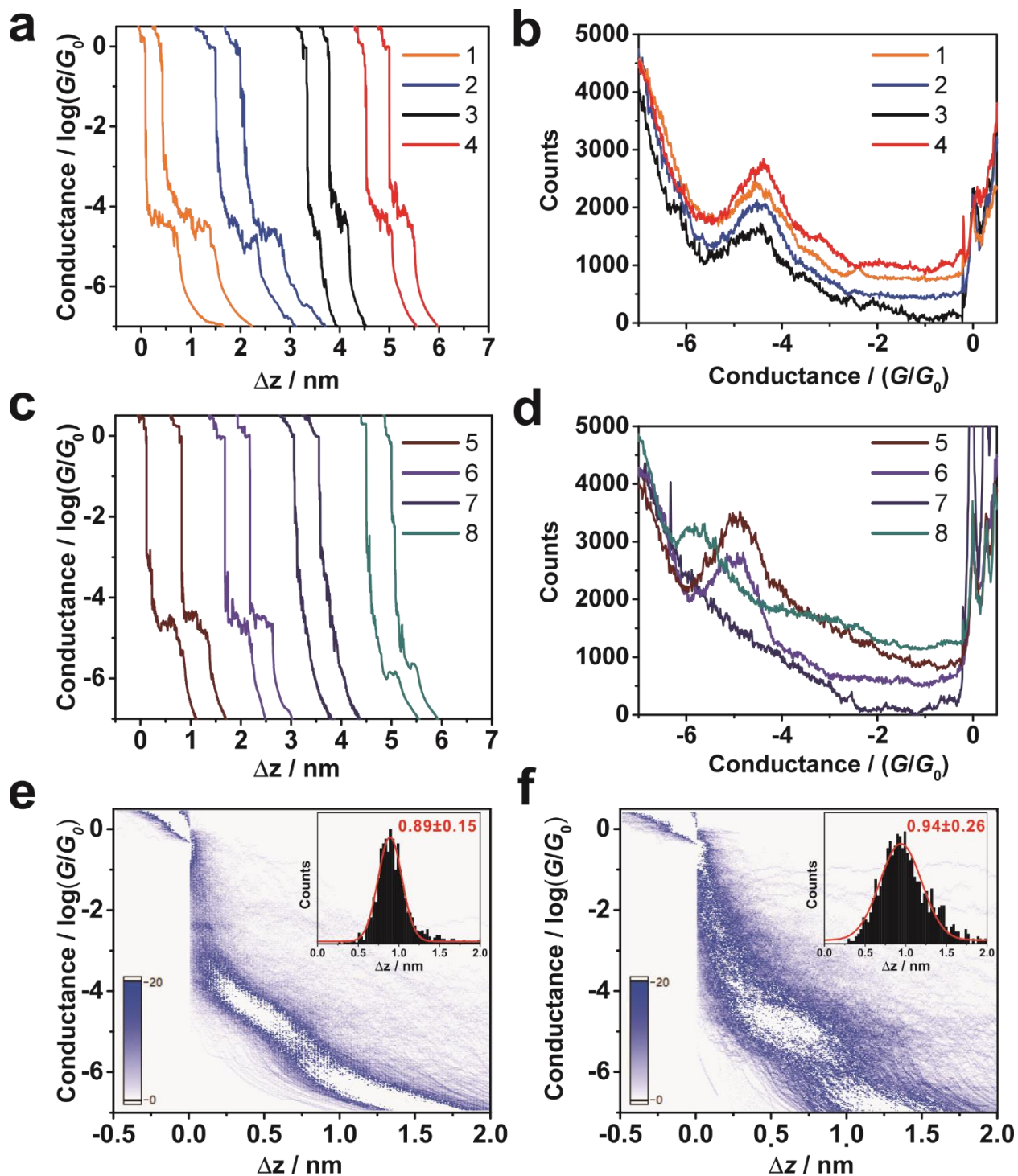


**Figure 2.** Typical conductance traces for compounds 1-4 (a) and 5-8 (c), respectively. One-dimensional conductance histograms for compounds 1-4 (b) and 5-8 (d), respectively. Two-

dimensional conductance-distance clouds of compounds **1** (e) and **5** (f), respectively. The curves in (b) and (d) are shifted for clarity, while the original histograms are given in the SI.

**Table 1.** Single-molecule conductances and lengths measured in MCBJ measurements.

Compounds	Measured Conductance / $\log(G/G_0)^a$	Measured Length / nm
<b>1</b>	$-4.54 \pm 0.37$	$1.39 \pm 0.15$
<b>2</b>	$-4.57 \pm 0.54$	$1.38 \pm 0.18$
<b>3</b>	$-4.63 \pm 0.36$	$1.36 \pm 0.16$
<b>4</b>	$-4.49 \pm 0.60$	$1.38 \pm 0.13$
<b>5</b>	$-4.94 \pm 0.40$	$1.44 \pm 0.26$
<b>6</b>	$-5.03 \pm 0.35$	$1.47 \pm 0.23$
<b>7</b>	$< -6^b$	/
<b>8</b>	$-5.85 \pm 0.34$	$1.40 \pm 0.16$

<sup>a</sup> Error bars are based on the Gaussian fitting of conductance all-data-point one-dimensional histograms. The conductance of the symmetric isomers **1-4** divided by the conductance of the corresponding asymmetrical isomers **5-8**, respectively, gives the following values: **1/5** = 2.5; **2/6** = 2.9; **3/7** = >23.4; **4/8** = 22.9. <sup>b</sup> This is an assumed value, not a measured value. As discussed in the text, we conclude that the conductance of molecule **7** is below the instrumental sensitivity of our *I-V* converter, i.e.,  $< 10^{-6} G_0$ .

The emergence of conductance plateaus in Figure 2a results in the discernible peaks in Figure 2b, which are centered at the very similar values of  $10^{-4.54 \pm 0.37} G_0$ ,  $10^{-4.57 \pm 0.54} G_0$ ,  $10^{-4.63 \pm 0.36} G_0$ , and  $10^{-4.49 \pm 0.60} G_0$  for compounds **1-4**, respectively. The plateaus and peaks are attributed to the most favorable microscopic configuration of the molecular junctions, which were further verified by the location of the intensive cloud in the corresponding two-dimensional conductance-distance histograms, as shown in Figures 2e and 2f for compounds **1** and **5**. The comparable data for the other compounds and pure solvent are given in the SI. Based on the above-mentioned data analysis, Table 1 summarizes the single-molecule conductances and the lengths of

compounds **1-8** obtained from MCBJ measurements, where the length was calibrated by adding 0.5 nm considering the snap-back effect.<sup>18</sup> In Table 1, error bars are based on the Gaussian fitting of the one-dimensional conductance histograms and the plateau displacement distributions. For compound **7** there is no distinct plateau in the individual trace, or peak in the conductance histogram, implying that the single-molecule conductance is out of the measuring range of our *I-V* converter, i.e., it is lower than  $10^{-6} G_0$ . We emphasize that we repeatedly attempted to measure the conductance of molecule **7** with the same result on each occasion. In these experiments, all the aspects of the instrumentation were checked, such as the notched-wire chip, the mechanical components, as well as the *I-V* converter. Compound **7** is stable to storage under ambient laboratory conditions, so decomposition of the molecules cannot explain this unexpected result. We cannot prove that molecule **7** is binding in the junction, but there is no logical reason why it should not bind, given that all the other seven molecules clearly do bind and reproducibly give measurable conductance data.

The data show that for the symmetric compounds **1-4** there is no statistical variation of conductance with the bridging atom (S, N, O or C). It is instructive to compare these results with the work of Chen et al on a series of compounds having similar structures to **1**, **3**, and **4**.<sup>19</sup> The only difference is that each compound studied by Chen et al was wired to gold electrodes by aminophenyl anchors, while the compounds studied here are wired by pyridyl anchors. The molecular lengths in both studies are similar. Amino anchors lead to HOMO-dominated conductances,<sup>20</sup> while pyridyl anchors lead to LUMO-dominated conductances,<sup>21</sup> respectively. For the amino anchors the clear trend in conductance was cyclopentadiene > furan > thiophene. This led Chen et al to conclude that “aromaticity decreases single-molecule junction conductance”.<sup>19</sup> However, we conclude that for the symmetrical compounds **1-4** the pyridyl

anchor dominates the conductance, and there is no statistically-significant dependence on the aromaticity of the core. Transport between the electrodes can occur through a continuous linearly-conjugated “butadiene-type” pathway involving the four  $sp^2$ -hybridized carbon atoms in **1-4**. We also note that the single-molecule conductances of our pyridyl compounds are consistently lower than for the amino anchored analogs due to the different anchoring groups.<sup>22</sup>

Compounds **5-8** have isomeric structures and comparable lengths with **1-4**. However, the single-molecule conductance values of **5-8** are consistently lower than that of the series **1-4** as listed in Table 1, giving the direct evidence of destructive QI. This is logical based on a simple resonance structure analysis of the cores disubstituted at the 2,4 positions,<sup>23</sup> suggesting the QI rule in the conventional six-membered rings is also valid for five-membered rings. In contrast to **1-4**, there is only weak effective coupling through the system in **5-8** as these molecules do not offer a linearly conjugated pathway between the two leads. Connecting the substituents at the 2,4-positions of the core (compounds **5-8**) corresponds to cross-conjugation,<sup>4,24</sup> thus resulting in destructive QI. This finding is reminiscent of data for six-membered phenyl core units, where destructive QI has been observed in the case of non-conjugated *meta* couplings,<sup>10-14</sup> and of our recent work with polycyclic core units, which established that the resonance energy of the core influences single-molecule conductance.<sup>25</sup> In the present case, there is no effective conjugated pathway in molecules **5-8**, therefore, the heteroatom in **5-7**, or the  $sp^3$  carbon atom in **8**, plays a more important role in determining the conductance than in series **1-4**.

For compounds **5-8**, the electronegativity decreases in the sequence O (3.44) > N (3.04) > S (2.58)  $\approx$  C (2.55) from the periodic table of electronegativity by the Pauling scale, thus for the studied compounds, the degree of asymmetry decreases in the sequence **5** > **6** > **7**  $\approx$  **8**. The degrees of asymmetry are tuned by the electronegativity of the heteroatom in **5-7**, or the  $sp^3$

carbon atom in **8**. As listed in Table 1, the lowest conductance values are obtained for **7** and **8**, where the heteroatoms have the lowest electronegativities, suggesting a strong correlation between the molecular asymmetry, electronegativity and single-molecule conductance.

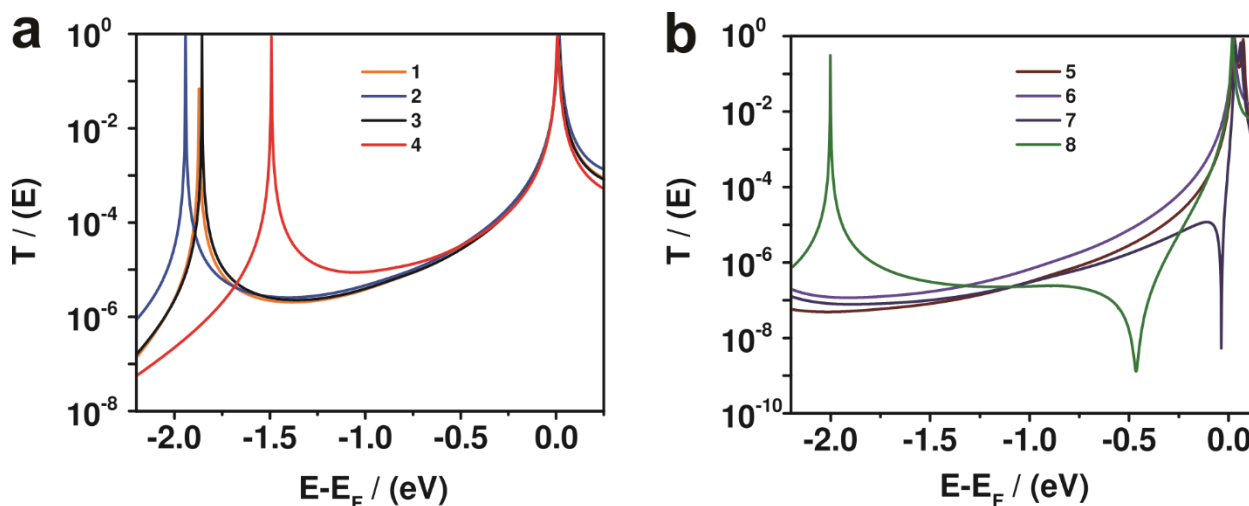


**Figure 3.** DFT results of the transmission coefficients for (a) compounds **1-4** and (b) **5-8**.

To investigate the interplay between structural asymmetry and QI in molecules wired between two electrodes, we calculated the transmission coefficient  $T(E)$  of electrons with energy  $E$  passing from one electrode to another through molecules shown in Figure S3-2, using the Gollum transport code.<sup>26</sup> Figure 3 shows the calculated  $T(E)$  of compounds **1-8** using the material specific mean field Hamiltonian obtained from the SIESTA implementation of density functional theory (DFT).<sup>27</sup> For molecules with pyridyl terminal groups, it is known that DFT incorrectly places the Fermi energy close to the LUMO resonance (at  $E - E_F = 0$  in Figure 3). This causes DFT to overestimate the conductance and therefore to achieve agreement with experiment, the Fermi energy should be shifted away from the LUMO towards the middle of the HOMO-LUMO gap (near  $E - E_F = -1$  eV in Figure 3).<sup>21</sup> Such a shift is consistent with

thermopower measurements of pyridyl-terminated molecules, whose positive Seebeck coefficients indicate that the Fermi energy lies in the tail of the LUMO, (in the range  $-1 \text{ eV} < E - E_F < 0$  in Figure 3).<sup>28</sup> For the symmetric compounds, Figure 3 shows that the  $T(E)$  values of **1-4** in the LUMO dominated regime  $-1 \text{ eV} < E < 0$  are quite similar, in good agreement with the experimental findings, that for the series **1-4** the conductances are almost the same. Nevertheless, in other cases the conductances of *para* compounds with pyridyl may be sensitive to the heteroatoms. For instance, recently we measured the conductances of a series of *para* compounds with polycyclic core units, i.e., dibenzothiophene, carbazole, dibenzofuran and fluorene cores, where the conductance varies as the heteroatom changes because the transmission around the LUMO peak is sensitive to the heteroatoms.<sup>25</sup>

As shown in Figure 3b, in the same energy regime  $-1 \text{ eV} < E < 0$ , the calculated  $T(E)$  of **5-8** is significantly lower than that of **1-4**. Furthermore, for compounds **7** and **8**, sharp drops in the transmission curve, i.e., the anti-resonance features, are observed in the tail of the LUMO peaks. The presence of these anti-resonances correlates with the lower measured conductances for these compounds. In contrast, for **5** and **6**, as shown in Figure 3b, there are no anti-resonances within the HOMO-LUMO gap, which correlates with the higher conductances that are measured experimentally. The absence of anti-resonance features within the HOMO-LUMO gap suggests that the high electronic asymmetry of the core unit, which originates from the greater electronegativities of the heteroatoms, moves the anti-resonance features out of the HOMO-LUMO gap of the molecular junction, and thus QI has a minor effect on the charge transport through single-molecule junctions. These theoretical results and our experimental findings suggest that molecular asymmetry affords a novel approach to tuning destructive QI and charge transport through single-molecule junctions.

## 4. CONCLUSIONS

To conclude, we investigated the synergistic effect of molecular symmetry and QI on the charge transport through single-molecule junctions with five-membered core rings. The study of 5-membered ring cores is a new and promising way to increase structural diversity of single-molecule devices. It was found that for the symmetric 2,5-disubstituted series **1-4**, the pyridyl anchors dominate the conductance and there is no statistically significant variation with core unit. In contrast, the conductances of the asymmetric 2,4-disubstituted series **5-8** are significantly lower than those of the symmetric **1-4** series, reflecting the presence of destructive QI. More importantly, the control of molecular asymmetry via the heteroatoms provides the tuning of destructive QI in the charge transport through single-molecule junctions. DFT calculations reveal that for asymmetric molecules, the electronegativity of the heteroatoms can be used to move anti-resonance features into or out of the HOMO-LUMO gap, which controls the destructive QI effect. Our work establishes a route for the design of building blocks through incorporating heteroatoms into molecular structure, and further demonstrates a novel yet simple strategy for tuning QI in single-molecule electronics via asymmetry. This has promising applications in the design of future molecular-electronic components

## ASSOCIATED CONTENT

**Supporting Information.** The Supporting Information is available free of charge on the ACS Publications website at DOI:

Synthesis and characterization of compounds **1-8**; methods and results for the single-molecule conductance measurements of solvent and compounds **1-8**; computational methods for calculating the transmission coefficients.

## **AUTHOR INFORMATION**

### **Corresponding Author**

\* Wenjing Hong, Email: whong@xmu.edu.cn

\* Colin J. Lambert, Email: c.lambert@lancaster.ac.uk

\* Martin R. Bryce, Email: m.r.bryce@durham.ac.uk

### **Author Contributions**

#Yang Yang, Markus Gantenbein and Afaf Alqorashi contributed equally to this work.

### **Notes**

The authors declare no competing financial interests.

## **ACKNOWLEDGMENTS**

We thank the National Natural Science Foundation of China (21503179, 21673195, 21722305, 21703188), the National Key R&D Program of China (2017YFA0204902), the Fundamental Research Funds for the Central Universities (Xiamen University: 20720170035) and Young Thousand Talent Project for funding work in Xiamen; EC FP7 ITN ‘MOLESCO’ project number 606728 for funding work in Durham and Lancaster; UK EPSRC grant EP/K0394/23/1 for funding instrumentation used in Durham and grants EP/N017188/1, EP/M014452/1 in Lancaster.

## REFERENCES

- (1) Baer, R.; Neuhauser, D. Phase Coherent Electronics: A Molecular Switch Based on Quantum Interference. *J. Am. Chem. Soc.* **2002**, *124*, 4200-4201.
- (2) Cardamone, D. M.; Stafford, C. A.; Mazumdar, S. Controlling Quantum Transport through a Single Molecule. *Nano Lett.* **2006**, *6*, 2422-2426.
- (3) Guedon, C. M.; Valkenier, H.; Markussen, T.; Thygesen, K. S.; Hummelen, J. C.; van der Molen, S. J. Observation of Quantum Interference in Molecular Charge Transport. *Nat. Nanotechnol.* **2012**, *7*, 305-309.
- (4) Valkenier, H.; Guedon, C. M.; Markussen, T.; Thygesen, K. S.; van der Molen, S. J.; Hummelen, J. C. Cross-Conjugation and Quantum Interference: A General Correlation? *Phys. Chem. Chem. Phys.* **2014**, *16*, 653-662.
- (5) Lambert, C. J. Basic Concepts of Quantum Interference and Electron Transport in Single-Molecule Electronics. *Chem. Soc. Rev.* **2015**, *44*, 875-888.
- (6) Su, T. A.; Neupane, M.; Steigerwald, M. L.; Venkataraman, L.; Nuckolls, C. Chemical Principles of Single-Molecule Electronics. *Nat. Rev. Mater.* **2016**, *1*, No. 16002.
- (7) Geng, Y.; Sangtarash, S.; Huang, C.; Sadeghi, H.; Fu, Y.; Hong, W.; Wandlowski, T.; Decurtins, S.; Lambert, C. J.; Liu, S.-X. Magic Ratios for Connectivity-Driven Electrical Conductance of Graphene-Like Molecules. *J. Am. Chem. Soc.* **2015**, *137*, 4469-4476.
- (8) Sangtarash, S.; Huang, C. C.; Sadeghi, H.; Sorohhov, G.; Hauser, J.; Wandlowski, T.; Hong, W. J.; Decurtins, S.; Liu, S. X.; Lambert, C. J. Searching the Hearts of Graphene-Like Molecules for Simplicity, Sensitivity, and Logic. *J. Am. Chem. Soc.* **2015**, *137*, 11425-11431.
- (9) Sangtarash, S.; Sadeghi, H.; Lambert, C. J. Exploring Quantum Interference in Heteroatom-Substituted Graphene-Like Molecules. *Nanoscale* **2016**, *8*, 13199-13205.
- (10) Solomon, G. C.; Herrmann, C.; Hansen, T.; Mujica, V.; Ratner, M. A. Exploring Local Currents in Molecular Junctions. *Nat. Chem.* **2010**, *2*, 223-228.
- (11) Arroyo, C. R.; Frisenda, R.; Moth-Poulsen, K.; Seldenthuis, J. S.; Bjornholm, T.; van der Zant, H. S. J. Quantum Interference Effects at Room Temperature in Opv-Based Single-Molecule Junctions. *Nanoscale Res. Lett.* **2013**, *8*, No. 234.
- (12) Arroyo, C. R.; Tarkuc, S.; Frisenda, R.; Seldenthuis, J. S.; Woerde, C. H. M.; Eelkema, R.; Grozema, F. C.; van der Zant, H. S. J. Signatures of Quantum Interference Effects on Charge Transport through a Single Benzene Ring. *Angew. Chem. Int. Ed.* **2013**, *52*, 3152-3155.

- (13) Manrique, D. Z.; Huang, C.; Baghernejad, M.; Zhao, X.; Al-Owaedi, O. A.; Sadeghi, H.; Kaliginedi, V.; Hong, W.; Gulcur, M.; Wandlowski, T.; Bryce, M. R.; Lambert, C. J. A Quantum Circuit Rule for Interference Effects in Single-Molecule Electrical Junctions. *Nat. Commun.* **2015**, *6*, No. 6389.
- (14) Garner, M. H.; Solomon, G. C.; Strange, M. Tuning Conductance in Aromatic Molecules: Constructive and Counteractive Substituent Effects. *J. Phys. Chem. C* **2016**, *120*, 9097-9103.
- (15) Borges, A.; Solomon, G. C. Effects of Aromaticity and Connectivity on the Conductance of Five-Membered Rings. *J. Phys. Chem. C* **2017**, *121*, 8272-8279.
- (16) Parks, J. J.; Champagne, A. R.; Costi, T. A.; Shum, W. W.; Pasupathy, A. N.; Neuscamman, E.; Flores-Torres, S.; Cornaglia, P. S.; Aligia, A. A.; Balseiro, C. A.; Chan, G. K. L.; Abruña, H. D.; Ralph, D. C. Mechanical Control of Spin States in Spin-1 Molecules and the Underscreened Kondo Effect. *Science* **2010**, *328*, 1370-1373.
- (17) Liu, X. S.; Sangtarash, S.; Reber, D.; Zhang, D.; Sadeghi, H.; Shi, J.; Xiao, Z. Y.; Hong, W. J.; Lambert, C. J.; Liu, S. X. Gating of Quantum Interference in Molecular Junctions by Heteroatom Substitution. *Angew. Chem. Int. Ed.* **2017**, *56*, 173-176.
- (18) Hong, W.; Valkenier, H.; Meszaros, G.; Manrique, D. Z.; Mishchenko, A.; Putz, A.; Garcia, P. M.; Lambert, C. J.; Hummelen, J. C.; Wandlowski, T. An Mcbj Case Study: The Influence of Pi-Conjugation on the Single-Molecule Conductance at a Solid/Liquid Interface. *Beilstein J. Nanotechnol.* **2011**, *2*, 699-713.
- (19) Chen, W.; Li, H.; Widawsky, J. R.; Appayee, C.; Venkataraman, L.; Breslow, R. Aromaticity Decreases Single-Molecule Junction Conductance. *J. Am. Chem. Soc.* **2014**, *136*, 918-920.
- (20) Dell'Angela, M.; Kladnik, G.; Cossaro, A.; Verdini, A.; Kamenetska, M.; Tamblyn, I.; Quek, S. Y.; Neaton, J. B.; Cvetko, D.; Morgante, A.; Venkataraman, L. Relating Energy Level Alignment and Amine-Linked Single Molecule Junction Conductance. *Nano Lett.* **2010**, *10*, 2470-2474.
- (21) Bagrets, A.; Arnold, A.; Evers, F. Conduction Properties of Bipyridinium-Functionalized Molecular Wires. *J. Am. Chem. Soc.* **2008**, *130*, 9013-9018.
- (22) Hong, W.; Manrique, D. Z.; Moreno-Garcia, P.; Gulcur, M.; Mishchenko, A.; Lambert, C. J.; Bryce, M. R.; Wandlowski, T. Single Molecular Conductance of Tolanes: Experimental

and Theoretical Study on the Junction Evolution Dependent on the Anchoring Group. *J. Am. Chem. Soc.* **2012**, *134*, 2292-2304.

(23) Markussen, T.; Stadler, R.; Thygesen, K. S. The Relation between Structure and Quantum Interference in Single Molecule Junctions. *Nano Lett.* **2010**, *10*, 4260-4265.

(24) Pedersen, K. G. L.; Borges, A.; Hedegard, P.; Solomon, G. C.; Strange, M. Illusory Connection between Cross-Conjugation and Quantum Interference. *J. Phys. Chem. C* **2015**, *119*, 26919-26924.

(25) Gantenbein, M.; Wang, L.; Al-Jobory, A. A.; Ismael, A. K.; Lambert, C. J.; Hong, W. J.; Bryce, M. R. Quantum Interference and Heteroaromaticity of Para- and Meta-Linked Bridged Biphenyl Units in Single Molecular Conductance Measurements. *Sci. Rep.* **2017**, *7*, No. 1794.

(26) Ferrer, J.; Lambert, C. J.; García-Suárez, V. M.; Manrique, D. Z.; Visontai, D.; Oroszlany, L.; Rodríguez-Ferradás, R.; Grace, I.; Bailey, S. W. D.; Gillemot, K.; Hatf, S.; Algharagholy, L. A. Gollum: A Next-Generation Simulation Tool for Electron, Thermal and Spin Transport. *New J. Phys.* **2014**, *16*, No. 093029.

(27) José, M. S.; Emilio, A.; Julian, D. G.; Alberto, G.; Javier, J.; Pablo, O.; Daniel, S.-P. The Siesta Method for Ab Initio Order- N Materials Simulation. *J. Phys-Condens. Mat.* **2002**, *14*, 2745-2779.

(28) Rincon-Garcia, L.; Evangeli, C.; Rubio-Bollinger, G.; Agrait, N. Thermopower Measurements in Molecular Junctions. *Chem. Soc. Rev.* **2016**, *45*, 4285-4306.

# Supporting Information

## Heteroatom-Induced Molecular Asymmetry Tunes Quantum Interference in Charge Transport through Single-Molecule Junctions

*Yang Yang<sup>1#</sup>, Markus Gantenbein<sup>2#</sup>, Afaf Alqorashi<sup>3#</sup>, Junying Wei<sup>1</sup>, Sara Sangtarash<sup>3</sup>, Duan Hu<sup>1</sup>, Hatef Sadeghi<sup>3</sup>, Rui Zhang<sup>1</sup>, Jiuchan Pi<sup>1</sup>, Lichuan Chen<sup>1</sup>, Xiaoyan Huang<sup>1</sup>, Ruihao Li<sup>1</sup>, Junyang Liu<sup>1</sup>, Jia Shi<sup>1</sup>, Wenjing Hong<sup>\*1</sup>, Colin J. Lambert<sup>\*3</sup>, Martin R. Bryce<sup>\*2</sup>*

1. State Key Laboratory of Physical Chemistry of Solid Surfaces, Pen-Tung Sah Institute of Micro-Nano Science and Technology, College of Chemistry and Chemical Engineering, iChEM, Xiamen University, 361005, Xiamen, China

2. Department of Chemistry, Durham University, DH1 3LE, Durham, UK

3. Department of Physics, Lancaster University, LA1 4YB, Lancaster, UK

Corresponding Author

\* Wenjing Hong, Email: [whong@xmu.edu.cn](mailto:whong@xmu.edu.cn)

\* Martin R. Bryce, Email: [m.r.bryce@durham.ac.uk](mailto:m.r.bryce@durham.ac.uk)

\* Colin J. Lambert, Email: [c.lambert@lancaster.ac.uk](mailto:c.lambert@lancaster.ac.uk)

## Table of Contents

1	Synthesis and characterization of molecules.....	S3
1.1	General information.....	S3
1.2	Experimental procedures.....	S4
1.3	$^1\text{H}$ NMR and $^{13}\text{C}$ NMR spectra.....	S22
2	Single-molecule conductance measurements for solvent and compounds <b>1-8</b> .....	S44
3	Theory .....	S50
4	References.....	S52

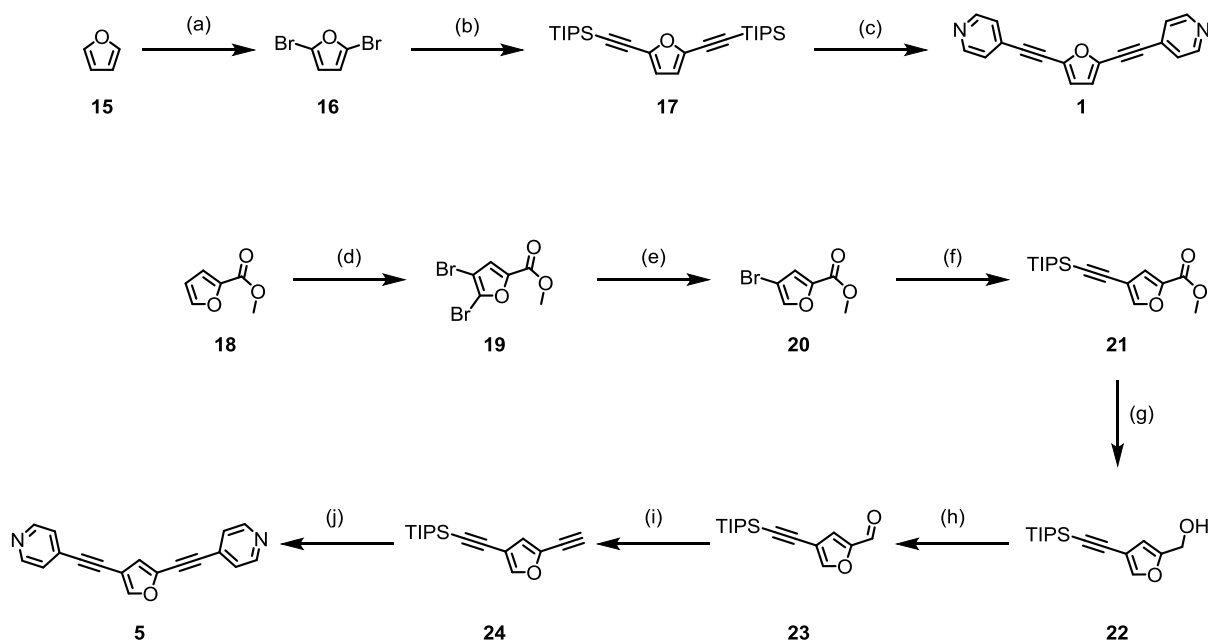
## 1. Synthesis and Characterization of Molecules

### 1.1 General Information

All reactions were carried out under an argon atmosphere unless otherwise stated. Starting materials were purchased commercially and were used as received. Solvents were dried using an Innovative Technology solvent purification system and were stored in ampoules under argon. Analytical thin layer chromatography (TLC) was performed on 20 mm pre-coated plates of silica gel (Merck, silica gel 60 F<sub>254</sub>) TLC plates and spots were visualised using a TLC lamp emitting at 365, 312 or 254 nm. Silica gel column chromatography was performed using silica gel 60 purchased from Sigma Aldrich. UV–Visible absorption spectra were recorded at room temperature on a Thermo Scientific Evolution 220 spectrometer. <sup>1</sup>H and <sup>13</sup>C NMR spectroscopy was carried out on Bruker AV400, Varian VNMRS 500 and 700, and Varian Inova 500 NMR spectrometers. Chemical shifts are reported in ppm relative to CHCl<sub>3</sub> (7.26 ppm), and residual protons in DMSO-d<sub>6</sub> (2.50 ppm) or Acetone-d<sub>6</sub> (2.05 ppm) and all NMR data was processed in MestReNova V10. Melting points were recorded on a Stuart SMP40 machine using open ended capillaries with a ramping rate of 1 °C min<sup>-1</sup>. Videos were replayed manually to determine the melting point. High resolution mass spectrometry was carried out on a Waters LCT Premier XE using ASAP ionization. Samples were analyzed directly as solids. Elemental analysis was performed on an Exeter Analytical E-440 machine.

## 1.2 Experimental Procedures

### 1.2.1 Synthesis of furan derivatives 1 and 5



Scheme S1-1: Reagents and Conditions: (a) EtOAc, NBS, ultra-sonication, rt, 1 h, 84%; (b) TIPS, PdCl<sub>2</sub>(PPh<sub>3</sub>)<sub>2</sub>, CuI, THF, DIPA, 80 °C, 12 h, 86%; (c) TBAF (1 M in THF) THF, rt, 30 min; then Pd<sub>2</sub>(dba)<sub>3</sub>, CuI, 4-iodopyridine, THF, DIPA, 40 °C, 12 h, 78% (over two steps); (d) Br<sub>2</sub>, CHCl<sub>3</sub>, reflux, 12 h, 92% (e) *i*-PrMgCl, THF, -40 °C, 2 h, 85%; (f) PdCl<sub>2</sub>(PhCN)<sub>2</sub>, CuI, (*t*-Bu)<sub>3</sub>P, TIPS, DIPA, 1,4-dioxane, 80 °C, 12 h, 90%; (g) LiAlH<sub>4</sub>, THF, 0 °C to rt, 2 h, 99%; (h) MnO<sub>2</sub>, CH<sub>2</sub>Cl<sub>2</sub>, rt, 16 h, 86%; (i) Zn, PPh<sub>3</sub>, CBr<sub>4</sub>, CH<sub>2</sub>Cl<sub>2</sub>, 0 °C to rt, 48 h, then *t*-BuLi, Et<sub>2</sub>O, -78 °C to 0 °C, 16 h, 78%; (j) TBAF (1 M in THF), THF, rt, 30 min, then 4-iodopyridine, PdCl<sub>2</sub>(PPh<sub>3</sub>)<sub>2</sub>, CuI, THF, DIPA, 40 °C, 12 h, 82% (over two steps).

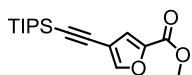
The compounds **16**, **17**, **19** and **20** were synthesized according to literature procedures. Their <sup>1</sup>H- and <sup>13</sup>C-NMR spectra matched previously reported data.<sup>1-4</sup>

### 2,5-bis(4-ethynylpyridyl)furan (**1**)



A solution of furan derivative **17** (1.00 g, 2.3 mmol) in dry THF (40 mL) was degassed for 30 min. TBAF (1 M in THF, 4.6 mL) was then added and resulting reaction mixture (A) was stirred in the dark for 30 min at room temperature under inert atmosphere. A separate flask was charged with 4-iodopyridine (0.90 g, 4.6 mmol), CuI (44 mg, 10% mmol), PPh<sub>3</sub> (184 mg, 30% mmol) and dry (*i*-Pr)<sub>2</sub>NH (20 mL). The resulting mixture (B) was degassed for 30 min, followed by the addition of Pd<sub>2</sub>(dba)<sub>3</sub> (214 mg, 10% mmol). After deprotection of **17** was completed, the solution (A) was degassed for 10 min and subsequently cannulated into the reaction mixture (B). The resulting reaction mixture was stirred at room temperature overnight under inert atmosphere. After completion, the reaction was filtered through a pad of Celite<sup>TM</sup>, and solvents were removed at reduced pressure. The residue was diluted in ethyl acetate, washed sequentially with saturated aqueous NH<sub>4</sub>Cl, water and brine. The organic layer was dried over MgSO<sub>4</sub> and evaporated *in vacuo*. The crude product was further purified by flash column chromatography (SiO<sub>2</sub>, acetone/toluene, 1:2 – 1:1 (v/v), 5% triethylamine) yielding **1** (542 mg, 2.0 mmol, 86% over two steps) as a pale yellow solid. mp: 151.5–152.5 °C. <sup>1</sup>H NMR (400 MHz, CDCl<sub>3</sub>, δ): 8.64–8.62 (m, 4H), 7.38–7.37 (m, 4H), 6.79 (s, 2H). <sup>13</sup>C NMR (101 MHz, CDCl<sub>3</sub>, δ): 150.07, 137.70, 130.05, 125.17, 118.16, 92.03, 83.25. HRMS–ASAP+ (m/z): calcd for C<sub>18</sub>H<sub>11</sub>N<sub>2</sub>O [M]<sup>+</sup>+H, 271.0871; found, 271.0867. Anal. calcd for C<sub>18</sub>H<sub>10</sub>N<sub>2</sub>O: C 79.99; H 3.73; N 10.36; found: C 79.93; H 3.72; N 10.25.

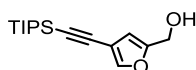
### Methyl 4-((triisopropylsilyl)ethynyl)furan-2-carboxylate (**21**)



Methyl 4-bromofuran-2-carboxylate (**20**, 2.00 g, 9.8 mmol) was dissolved in dry 1,4-dioxane (30 mL) and dry DIPA (15 mL). The resulting solution was degassed for 30 min, followed by the addition of PdCl<sub>2</sub>(PhCN)<sub>2</sub> (187 mg, 5% mmol) and CuI (93 mg, 5% mmol). After further degassing for 10 min, *t*-Bu<sub>3</sub>P (197 mg, 10% mmol) and TIPS-acetylene (2.70 mL, 12.2 mmol) were added sequentially. The reaction mixture was stirred at 80 °C overnight. After

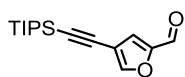
cooling to room temperature, the reaction mixture was filtered through a pad of Celite<sup>TM</sup>, and solvents were evaporated. The residue was diluted in ethyl acetate, washed sequentially with saturated aqueous NH<sub>4</sub>Cl, water and brine. The organic layer was dried over MgSO<sub>4</sub> and removed at reduced pressure. The crude product was further purified by flash column chromatography (SiO<sub>2</sub>, hexanes/Et<sub>2</sub>O, 20:1 – 10:1 (v/v)) yielding **21** (2.70 g, 8.8 mmol, 90%) as a yellow oil. <sup>1</sup>H NMR (400 MHz, Acetone-d<sub>6</sub>, δ): 8.12 (d, *J* = 0.9 Hz, 1H), 7.28 (d, *J* = 0.9 Hz, 1H), 3.86 (s, 3H), 1.13–1.12 (m, 21H). <sup>13</sup>C NMR (101 MHz, Acetone-d<sub>6</sub>, δ): 158.93, 151.02, 145.80, 120.68, 110.91, 97.40, 94.41, 52.48, 19.11, 12.13. HRMS–ASAP+ (m/z): calcd for C<sub>17</sub>H<sub>27</sub>O<sub>3</sub>Si [M]+H, 307.1729; found, 307.1716.

#### (4-((triisopropylsilyl)ethynyl)furan-2-yl)methanol (**22**)



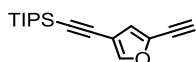
Methyl ester **21** (3.00 g, 9.8 mmol) dissolved in dry THF (70 mL) was added dropwise to a suspension of LiAlH<sub>4</sub> (312 mg, 8.22 mmol) in dry THF (35 mL) at 0 °C. After the addition was complete the reaction mixture was stirred for 2 h at room temperature. The reaction was quenched at 0 °C by carefully adding water followed by aq. HCl (1 M, 50 mL). The crude product was extracted with diethyl ether (3 x 20 mL). The combined organic layers were washed with brine, dried over MgSO<sub>4</sub>, filtered through a short plug of silica and evaporated at reduced pressure affording **22** (2.70 g, 9.7 mmol, 99%) as a pale yellow oil, which was used without further purification. <sup>1</sup>H NMR (400 MHz, DMSO-d<sub>6</sub>, δ): 7.98 (d, *J* = 0.9 Hz, 1H), 6.37 (d, *J* = 0.9 Hz, 1H), 5.27 (t, *J* = 5.8 Hz, 2H), 4.34 (dd, *J* = 5.8, 0.7 Hz, 2H), 1.07 (s, 21H). <sup>13</sup>C NMR (101 MHz, DMSO-d<sub>6</sub>, δ): 156.12, 146.43, 109.39, 107.24, 98.61, 91.50, 55.28, 18.46, 10.68. HRMS–ESI– (m/z): calcd for C<sub>16</sub>H<sub>25</sub>O<sub>2</sub>Si [M]–H, 277.1624; found, 277.1610.

#### 4-((triisopropylsilyl)ethynyl)furan-2-carbaldehyde (**23**)



To a solution of alcohol **22** (2.50 g, 8.9 mmol) in dry CH<sub>2</sub>Cl<sub>2</sub> (100 mL) was added MnO<sub>2</sub> (7.7 g, 88 mmol) in portions over 6 h and the resulting reaction mixture was stirred at room temperature for 12 h. The reaction was filtered through a pad of Celite<sup>TM</sup>. The organic layer was washed with brine, dried over MgSO<sub>4</sub> and evaporated at reduced pressure. The crude product was further purified by flash column chromatography (SiO<sub>2</sub>, hexanes/Et<sub>2</sub>O, 20:1 – 10:1 (v/v)) affording **23** (2.10 g, 7.6 mmol, 86%) as a colorless oil. <sup>1</sup>H NMR (400 MHz, Acetone-d<sub>6</sub>, δ): 9.66 (d, *J* = 0.7 Hz, 1H), 8.24 (t, *J* = 0.8 Hz, 1H), 7.52 (d, *J* = 0.8 Hz, 1H) 3.90 (s, 3H), 1.14–1.13 (m, 21H). <sup>13</sup>C NMR (101 MHz, Acetone-d<sub>6</sub>, δ): 178.69, 153.95, 152.34, 123.99, 111.44, 97.12, 94.86, 19.10, 12.12. HRMS–ASAP+ (m/z): calcd for C<sub>16</sub>H<sub>25</sub>O<sub>2</sub>Si [M]+H, 277.1624; found, 277.1610.

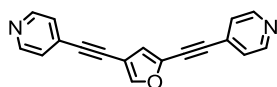
#### 2-ethenyl-4-((triisopropylsilyl)ethynyl)furan (**24**)



A flask was charged with PPh<sub>3</sub> (2.40 g, 9.0 mmol), CBr<sub>4</sub> (3.00 g, 9.0 mmol), Zn dust (0.60 g, 9.0 mmol) and dry methylene chloride (25 mL). The resulting suspension was stirred for 24 h under inert atmosphere at room temperature. The reaction mixture was cooled to 0 °C and a solution of **23** (1.00 g, 3.6 mmol) in dry methylene chloride (5 mL) was slowly added. After completed addition the cooling bath was removed and stirring was continued for 16 h at room temperature. The reaction mixture was diluted with methylene chloride (50 mL) and filtered through a pad of Celite<sup>TM</sup>. The organic layer was washed with 10% aqueous Na<sub>2</sub>S<sub>2</sub>O<sub>3</sub>, saturate aqueous NH<sub>4</sub>Cl, brine, dried over MgSO<sub>4</sub> and removed at reduced pressure. The crude product was further purified by flash column chromatography (SiO<sub>2</sub>, hexanes/methylene chloride, 95:5 (v/v)) affording the corresponding dibromo-olefin product (1.50 g, 3.5 mmol, 96%) which was not purified further. <sup>1</sup>H NMR (400 MHz, CDCl<sub>3</sub>, δ): 7.60 (d, *J* = 0.7 Hz, 1H), 7.34 (d, *J* = 0.6 Hz, 1H), 7.00 (t, *J* = 0.7 Hz, 1H), 1.11 (s, 21H). <sup>13</sup>C NMR (101 MHz, CDCl<sub>3</sub>, δ): 150.03, 145.89, 126.02, 113.99, 110.01, 96.95, 93.75, 88.98, 18.78, 11.41. To a flask charged with the dibromo-olefin product (1.50 g, 3.5 mmol) and Et<sub>2</sub>O (25

mL) was added *t*-BuLi (1.7 M in pentane, 7.8 mL, 13.2 mmol) at  $-78\text{ }^{\circ}\text{C}$ . The resulting reaction mixture was warmed to room temperature over the course of 16 h. The reaction was quenched by the addition of aqueous saturated  $\text{NH}_4\text{Cl}$  and extracted with  $\text{Et}_2\text{O}$  (3x 50 mL). The combined organic layers were washed with brine, over  $\text{MgSO}_4$  and removed at reduced pressure. The crude product was further purified by flash column chromatography ( $\text{SiO}_2$ , hexanes/methylene chloride, 95:5 (v/v)) yielding **24** (745 mg, 2.7 mmol, 79%) as a light yellow oil.  $^1\text{H}$  NMR (400 MHz,  $\text{CDCl}_3$ ,  $\delta$ ): 7.55 (d,  $J = 0.8$  Hz, 1H), 6.67 (d,  $J = 0.8$  Hz, 1H), 3.37 (s, 1H), 1.10 (s, 21H).  $^{13}\text{C}$  NMR (101 MHz,  $\text{CDCl}_3$ ,  $\delta$ ): 146.99, 136.41, 118.85, 109.27, 96.50, 93.64, 82.32, 73.14, 18.76, 11.39. HRMS–ASAP+ (m/z): calcd for  $\text{C}_{17}\text{H}_{25}\text{OSi}$  [M]<sup>+</sup>H, 273.1675; found, 273.1668.

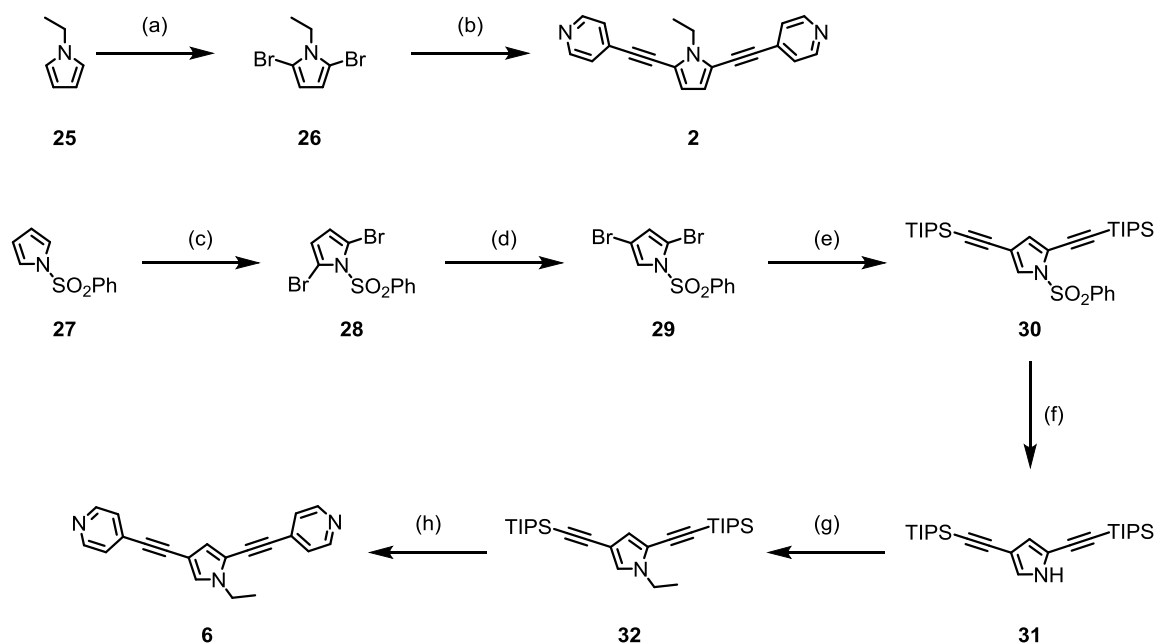
### 2,4-bis(4-ethynylpyridyl)furan (**5**)



A solution of furan derivative **24** (0.60 g, 2.2 mmol) in dry THF (30 mL) was degassed for 20 min. TBAF (1 M in THF, 2.2 mL) was then added and the resulting reaction mixture (A) was stirred in the dark for 30 min at room temperature under inert atmosphere. A separate flask was charged with 4-iodopyridine (1.0 g, 4.8 mmol), CuI (42 mg, 10% mmol) and dry triethylamine (15 mL). The resulting mixture (B) was degassed for 10 min, followed by the addition of  $\text{PdCl}_2(\text{PPh}_3)_2$  (154 mg, 10% mmol). After deprotection of **24** was completed, the solution (A) was degassed for 5 min and subsequently, cannulated into the reaction mixture (B). The resulting reaction mixture was stirred at room temperature for 12 h under inert atmosphere. After completion, the reaction was filtered through a pad of Celite<sup>TM</sup>, and solvents were removed at reduced pressure. The residue was diluted in ethyl acetate, washed sequentially with saturated aqueous  $\text{NH}_4\text{Cl}$ , water and brine. The organic layer was dried over  $\text{MgSO}_4$  and evaporated *in vacuo*. The crude product was further purified by flash column chromatography ( $\text{SiO}_2$ , acetone/toluene, 1:5 – 1:2 (v/v), 5% triethylamine) yielding **5** (486 mg, 1.8 mmol, 82% over two steps) as a white solid. mp: 122.5–123.3  $^{\circ}\text{C}$ .  $^1\text{H}$  NMR (400 MHz, Acetone- $\text{d}_6$ ,  $\delta$ ): 8.67–8.66 (m, 2H), 8.63–8.62 (m, 2H), 8.16 (d,  $J = 0.8$  Hz, 1H), 7.52–7.50 (m, 2H), 7.45–7.44 (m, 2H), 7.12 (d,  $J = 0.8$  Hz, 1H).  $^{13}\text{C}$  NMR (101 MHz, Acetone- $\text{d}_6$ ,  $\delta$ ): 151.22, 151.13, 149.99, 137.83, 131.38, 130.23, 126.16, 125.95, 119.74,

109.50, 92.33, 89.83, 84.44, 82.75. HRMS–ASAP+ (m/z): calcd for C<sub>18</sub>H<sub>11</sub>N<sub>2</sub>O [M]<sup>+</sup>H, 271.0871; found, 271.0882. Anal. calcd for C<sub>18</sub>H<sub>10</sub>N<sub>2</sub>O: C 79.99; H 3.73; N 10.36; found: C 79.56; H 3.73; N 10.31.

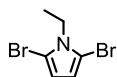
### 1.2.2 Synthesis of pyrrole derivatives 2 and 6



Scheme S1-2: Reagents and Conditions: (a) NBS, DMF, 0 °C, 1 h, 85%; (b) 4-ethynylpyridine, PdCl<sub>2</sub>(PhCN)<sub>2</sub>, CuI, (*t*-Bu)<sub>3</sub>P, DIPA, 1,4-dioxane, 80 °C, 12 h, 79%; (c) NBS, DMF, rt, 30 min; (d) CF<sub>3</sub>SO<sub>3</sub>H, MePh, 0 °C, 1 h; then TEA, rt, 24 h, 54% (over two steps); (e) TIPS-protected ethynylpyridine, PdCl<sub>2</sub>(PhCN)<sub>2</sub>, CuI, (*t*-Bu)<sub>3</sub>P, DIPA, 1,4-dioxane, 80 °C, 12 h, 83%; (f) KOH, THF, MeOH, rt, 1 h, 93%; (g) EtI, K<sub>2</sub>CO<sub>3</sub>, DMF, rt, 12 h, 85%; (h) TBAF (1 M in THF), THF, rt, 30 min; then Pd<sub>2</sub>(dba)<sub>3</sub>, CuI, PPh<sub>3</sub>, 4-iodopyridine, DIPA, 40 °C, 12 h, 67% (over two steps).

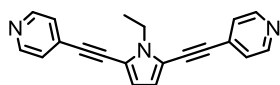
The compounds 28 and 29 were synthesized according to literature procedures. Their <sup>1</sup>H- and <sup>13</sup>C-NMR spectra matched previously reported data.<sup>5-6</sup>

### 2,5-dibromo-1-ethyl-1H-pyrrole (26)



An oven-dried argon-flushed flask was charged with dry DMF (20 mL) and 1-ethyl-1*H*-pyrrole (**25**) (1.0 g, 1.1 mL, 10.5 mmol). The resulting reaction mixture was cooled at 0 °C, while NBS (3.74 g, 21.02 mmol) was added as a solution in DMF (10 mL). The reaction was stirred at 0 °C before water was added and the product was extracted with hexanes (3 x 50 mL). The combined organic layers were washed sequentially with aq. sat. Na<sub>2</sub>S<sub>2</sub>O<sub>3</sub> (50 mL), water (50 mL), brine (50 mL), and dried over MgSO<sub>4</sub>. Before the organic layer was removed at reduced pressure a few drops of TEA were added to prevent decomposition of the product. Further purification by column chromatography (SiO<sub>2</sub>, hexanes, 5% triethylamine) afforded **26** (2.2 g, 8.9 mmol, 85%) as a clear very volatile oil. <sup>1</sup>H NMR (400 MHz, CDCl<sub>3</sub>, δ): 6.17 (s, 2H), 4.05 (q, *J* = 7.2 Hz, 2H), 1.28 (t, *J* = 7.2 Hz, 3H). <sup>13</sup>C NMR (101 MHz, CDCl<sub>3</sub>, δ): 111.76, 100.29, 42.46, 15.63. HRMS–ASAP+ (*m/z*): calcd for C<sub>18</sub>H<sub>11</sub>N<sub>2</sub>S [M]<sup>+</sup>, 250.8945; found, 250.8956.

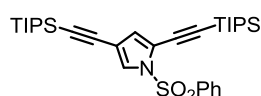
### 2,5-bis(4-pyridylethynyl)-1-ethyl-1*H*-pyrrole (**2**)



A solution of 4-((trimethylsilyl)ethynyl)pyridine (0.70 g, 3.9 mmol) in dry 1,4-dioxane (30 mL) was degassed for 30 min. Tetrabutylammonium fluoride (TBAF, 1 M in THF, 3.9 mL) was then added and the resulting reaction mixture (A) was stirred in the dark for 30 min at room temperature under inert atmosphere. A separate flask was charged with pyrrole derivative **26** (0.40 g, 1.78 mmol), PdCl<sub>2</sub>(PhCN)<sub>2</sub> (68.2mg, 10% mmol), CuI (33.9 mg, 10% mmol), and (*i*-Pr)<sub>2</sub>NH, (20 mL). The resulting mixture (B) was degassed for 30 min, followed by the addition of *t*-Bu<sub>3</sub>P (72.0 mg, 20% mmol). After deprotection of 4-((trimethylsilyl)ethynyl)pyridine was completed, the solution (A) was degassed for 15 min and subsequently, cannulated into the reaction mixture (B). The resulting reaction mixture was stirred at room temperature for 12 h under inert atmosphere. The reaction was then filtered through a pad of Celite<sup>TM</sup>, and solvents were removed at reduced pressure. The residue was diluted in ethyl acetate, washed sequentially with saturated aqueous NH<sub>4</sub>Cl, water and brine. The organic layer was dried over MgSO<sub>4</sub> and removed *in vacuo*. The crude

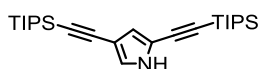
product was further purified by flash column chromatography (SiO<sub>2</sub>, acetone/toluene, 1:2 – 1:1 (v/v), 5% triethylamine) affording **2** (0.42 g, 1.40 mmol, 79%) as a yellow solid. mp: 152.8–153.7 °C. <sup>1</sup>H NMR (400 MHz, CDCl<sub>3</sub>, δ): 8.61–8.59 (m, 4H), 7.35–7.33 (m, 4H), 6.56 (s, 2H), 4.27 (q, *J* = 7.2 Hz, 2H), 1.48 (t, *J* = 7.2 Hz, 3H). <sup>13</sup>C NMR (101 MHz, CDCl<sub>3</sub>, δ): 149.97, 131.15, 124.95, 116.67, 116.33, 91.92, 85.52, 41.80, 16.36. HRMS–ASAP+ (*m/z*): calcd for C<sub>20</sub>H<sub>16</sub>N<sub>3</sub> [M]<sup>+</sup>H, 298.1344; found, 298.1340. Anal. calcd for C<sub>20</sub>H<sub>15</sub>N<sub>3</sub>: C 80.78; H 5.08; N 14.13; found: C 80.73; H 5.15; N 13.98.

### 1-(phenylsulfonyl)-2,4-bis((triisopropylsilyl)ethynyl)-1*H*-pyrrole (**30**)



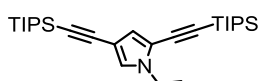
Pyrrole derivative **29** (1.40 g, 3.84 mmol) was dissolved in a mixture of dry 1,4-dioxane (40 mL) and dry DIPA (20 mL). The resulting solution was degassed for 30 min, followed by the addition of PdCl<sub>2</sub>(PhCN)<sub>2</sub> (147 mg, 10% mmol) and CuI (73 mg, 10% mmol). After further degassing for 10 min, *t*-Bu<sub>3</sub>P (194 mg, 25% mmol) and TIPS-acetylene (1.90 mL, 8.4 mmol) were added sequentially. The reaction mixture was stirred at 80 °C for 12 h. After cooling to room temperature, the reaction mixture was filtered through a pad of Celite<sup>TM</sup>, and solvents were evaporated. The residue was diluted in ethyl acetate, washed sequentially with saturated aqueous NH<sub>4</sub>Cl, water and brine. The organic layer was dried over MgSO<sub>4</sub> and removed at reduced pressure. The crude product was further purified by flash column chromatography (SiO<sub>2</sub>, hexanes/toluene, 10:1 – 5:1 (v/v)) yielding **30** (1.80 g, 3.2 mmol, 83%) as a pale yellow oil. <sup>1</sup>H NMR (400 MHz, CDCl<sub>3</sub>, δ): 8.03–8.00 (m, 2H), 7.65–7.61 (m, 1H), 7.52–7.48 (m, 2H), 7.45 (d, *J* = 1.8 Hz, 1H), 6.60 (d, *J* = 1.8 Hz, 1H) 1.13–1.08 (m, 42H). <sup>13</sup>C NMR (101 MHz, CDCl<sub>3</sub>, δ): 138.29, 134.39, 129.39, 127.83, 126.29, 125.01, 115.86, 108.74, 98.82, 98.52, 95.20, 92.03, 18.75, 18.73, 11.48, 11.39. HRMS–ASAP+ (*m/z*): calcd for C<sub>32</sub>H<sub>50</sub>NO<sub>2</sub>SSi<sub>2</sub> [M]<sup>+</sup>H, 568.3101; found, 568.3086.

### 2,4-bis((triisopropylsilyl)ethynyl)-1*H*-pyrrole (**31**)



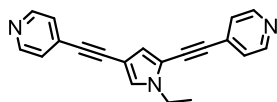
Finely ground KOH (5.2 g, 92.4 mmol) was dissolved in HPLC grade MeOH (75 mL) followed by the addition of pyrrole derivative **30** (1.50 g, 2.6 mmol) in HPLC grade THF (75 mL). The reaction mixture was stirred at room temperature for 1 h then quenched by pouring into iced water (100 mL) and extracted with Et<sub>2</sub>O (3 x 100 mL). The combined organic layers were washed with brine, dried over MgSO<sub>4</sub> and filtered. A few drops of triethylamine were added and solvents were evaporated at reduced pressure. Further purification by flash column chromatography (SiO<sub>2</sub>, hexanes/ethyl acetate, 10:1 – 5:1 (v/v), 5% triethylamine) afforded **31** (1.10 g, 2.5 mmol, 93%) as a beige solid. <sup>1</sup>H NMR (400 MHz, CDCl<sub>3</sub>, δ): 8.24 (broad s, 1H), 6.91 (dd, *J* = 2.9, 1.5 Hz, 1H), 6.56 (dd, *J* = 2.6, 1.5 Hz, 1H), 1.10 (s, 42H). <sup>13</sup>C NMR (101 MHz, CDCl<sub>3</sub>, δ): 123.34, 118.77, 113.65, 106.11, 101.36, 97.89, 92.69, 88.70, 18.84, 18.78, 11.53, 11.41. HRMS–ASAP+ (*m/z*): calcd for C<sub>26</sub>H<sub>46</sub>NSi<sub>2</sub> [M]<sup>+</sup>+H, 428.3169; found, 428.3159.

### 1-ethyl-2,4-bis((triisopropylsilyl)ethynyl)-1*H*-pyrrole (**32**)



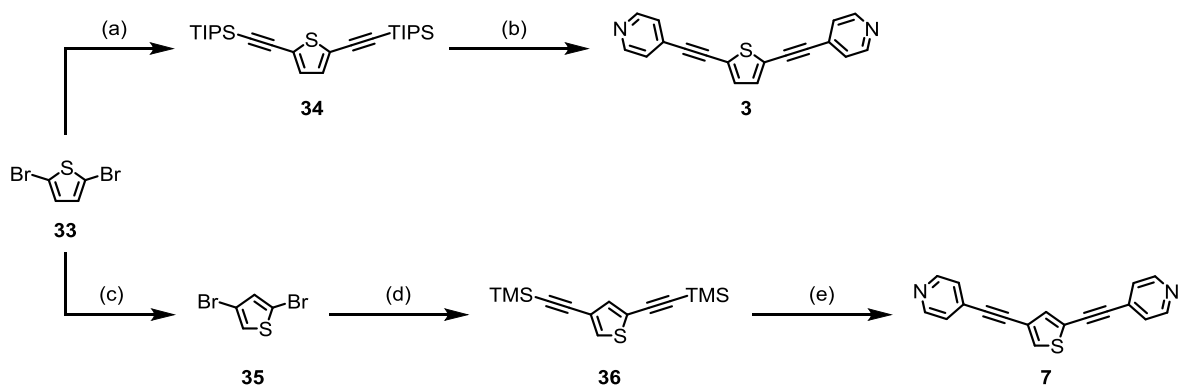
An oven-dried argon-flushed flask was charged with K<sub>2</sub>CO<sub>3</sub> (646 mg 4.7 mmol) and dry DMF (50 mL), ethyl iodide (729 mg, 0.4 mL, 4.7 mmol) and pyrrole derivative **31** (1.00 g, 2.3 mmol). The reaction mixture was stirred for 12 h under inert atmosphere at room temperature. The reaction was poured into iced water (100 mL) and extracted with Et<sub>2</sub>O (3 x 100 mL). The combined organic layers were washed with aqueous HCl (1 M), brine, dried over MgSO<sub>4</sub> and filtered. A few drops of triethylamine were added and solvents were removed at reduced pressure. Further purification by flash column chromatography (SiO<sub>2</sub>, hexanes/dichloromethane, 10:1 (v/v), 5% triethylamine) afforded **32** (0.90 g, 2.0 mmol, 85%) as a pale yellow oil. <sup>1</sup>H NMR (400 MHz, CDCl<sub>3</sub>, δ): 6.87 (d, *J* = 1.7 Hz, 1H), 6.53 (d, *J* = 1.7 Hz, 1H), 3.98 (q, *J* = 7.2 Hz, 2H), 1.38 (t, *J* = 7.2 Hz, 3H), 1.13–1.12 (m, 42H). <sup>13</sup>C NMR (101 MHz, CDCl<sub>3</sub>, δ): 125.90, 118.87, 115.35, 104.39, 101.84, 97.34, 95.18, 88.15, 43.17, 18.84, 18.79, 16.49, 11.55, 11.44. HRMS–ASAP+ (*m/z*): calcd for C<sub>28</sub>H<sub>50</sub>NSi<sub>2</sub> [M]<sup>+</sup>+H, 456.3482; found, 456.3474.

### 2,4-bis(4-pyridylethynyl)-1-ethyl-1H-pyrrole (**6**)



A solution of pyrrole derivative **32** (0.60 g, 1.3 mmol) in dry THF (25 mL) was degassed for 30 min. TBAF (1 M in THF, 2.63 mL) was then added and the resulting reaction mixture (A) was stirred in the dark for 30 min at room temperature under inert atmosphere. A separate flask was charged with 4-iodopyridine (0.60 g, 2.9 mmol), CuI (25 mg, 10% mmol), PPh<sub>3</sub> (103 mg, 30% mmol) and dry (*i*-Pr)<sub>2</sub>NH (12 mL). The resulting mixture (B) was degassed for 20 min, followed by the addition of Pd<sub>2</sub>(dba)<sub>3</sub> (120 mg, 10% mmol). After deprotection of **32** was completed, the solution (A) was degassed for 5 min and subsequently cannulated into the reaction mixture (B). The resulting reaction mixture was stirred at room temperature for 12 h under inert atmosphere. After completion, the reaction was filtered through a pad of Celite<sup>TM</sup>, and solvents were removed at reduced pressure. The residue was diluted in ethyl acetate, washed sequentially with saturated aqueous NH<sub>4</sub>Cl, water and brine. The organic layer was dried over MgSO<sub>4</sub> and removed *in vacuo*. The crude product was further purified by flash column chromatography (SiO<sub>2</sub>, acetone/toluene, 1:2 – 1:1 (v/v), 5% triethylamine) yielding **6** (262 mg, 0.9 mmol, 67% over two steps) as a yellow solid. mp: 111.7–112.7 °C. <sup>1</sup>H NMR (400 MHz, CDCl<sub>3</sub>, δ): 8.61–8.59 (m, 2H), 8.56–8.55 (m, 2H), 7.34–7.30 (m, 4H), 7.09 (d, *J* = 1.7 Hz, 1H), 6.71 (d, *J* = 1.7 Hz, 1H), 4.10 (q, *J* = 7.3 Hz, 2H), 1.49 (t, *J* = 7.2 Hz, 3H). <sup>13</sup>C NMR (101 MHz, CDCl<sub>3</sub>, δ): 149.97, 149.80, 132.20, 131.14, 127.43, 125.29, 124.94, 119.51, 114.61, 103.80, 91.58, 89.26, 86.11, 84.86, 43.49, 16.42. HRMS–ASAP+ (*m/z*): calcd for C<sub>20</sub>H<sub>15</sub>N<sub>3</sub> [M]<sup>+</sup>, 297.1266; found, 297.1293. Anal. calcd for C<sub>20</sub>H<sub>15</sub>N<sub>3</sub>: C 80.78; H 5.08; N 14.13; found: C 80.34; H 5.05; N 14.07.

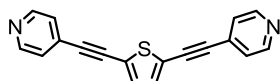
### 1.2.3 Synthesis of thiophene derivatives **3** and **7**



Scheme S1-3: Reagents and Conditions: (a) (Triisopropylsilyl)acetylene,  $\text{PdCl}_2(\text{PPh}_3)_2$ ,  $\text{CuI}$ , THF,  $(i\text{-Pr})_2\text{NH}$ ,  $80\text{ }^\circ\text{C}$ , 12 h, 93%; (b) TBAF (1 M in THF), THF, rt, 30 min; then  $\text{Pd}_2(\text{dba})_3$ ,  $\text{CuI}$ , 4-iodopyridine,  $(i\text{-Pr})_2\text{NH}$ ,  $25\text{ }^\circ\text{C}$ , 12 h, 73% (over two steps); (c) Lithium diisopropylamide, THF,  $-78\text{ }^\circ\text{C}$ , 2 h; then MeOH,  $-78\text{ }^\circ\text{C}$  to rt, 1 h, 89%; (d) (Trimethylsilyl)acetylene,  $\text{Pd}(\text{PPh}_3)_4$ ,  $\text{CuI}$ ,  $\text{Et}_3\text{N}$ , THF,  $60\text{ }^\circ\text{C}$ , 12 h, 71%; (e) TBAF (1 M in THF), THF, rt, 30 min; then  $\text{Pd}_2(\text{dba})_3$ ,  $\text{CuI}$ , 4-iodopyridine,  $(i\text{-Pr})_2\text{NH}$ ,  $25\text{ }^\circ\text{C}$ , 12 h, 64 (89% over two steps).

The compounds **33**, **34**, **35**, and **36** were synthesized according to literature procedures. Their  $^1\text{H}$ - and  $^{13}\text{C}$ -NMR spectra matched previously reported data.<sup>1, 7-9</sup>

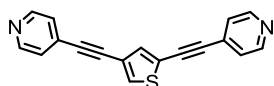
### 2,5-bis(pyridin-4-ylethynyl)thiophene (**3**)



A solution of 2,5-bis((triisopropylsilyl)ethynyl)thiophene (**34**) (1.20 g, 2.7 mmol) in dry THF (40 mL) was degassed for 30 min. Tetrabutylammonium fluoride (TBAF, 1 M in THF, 5.4 mL) was then added and the resulting reaction mixture (A) was stirred in the dark for 30 min at room temperature under inert atmosphere. A separate flask was charged with 4-iodopyridine (1.1 g, 5.4 mmol),  $\text{CuI}$  (51.4 mg, 10% mmol),  $\text{PPh}_3$  (212.0 mg, 30% mmol) and dry diisopropylamine (25 mL). The resulting mixture (B) was degassed for 30 min, followed by the addition of  $\text{Pd}_2(\text{dba})_3$  (247 mg, 10% mmol). After deprotection of **34** was completed, solution (A) was degassed for 15 min and subsequently cannulated into the reaction mixture

(B). The resulting reaction mixture was stirred at room temperature for 12 h under inert atmosphere. The reaction was then filtered through a pad of Celite<sup>TM</sup>, and solvents were removed at reduced pressure. The residue was diluted in ethyl acetate, washed sequentially with saturated aqueous NH<sub>4</sub>Cl, water and brine. The organic layer was dried over MgSO<sub>4</sub> and solvent was removed *in vacuo*. The crude product was further purified by flash column chromatography (SiO<sub>2</sub>, acetone/toluene, 1:2 – 1:1 (v/v), 5% triethylamine) yielding **3** (567.0 mg, 2.0 mmol, 73% over two steps) as a yellow solid. mp: 147.4–148.4 °C. <sup>1</sup>H NMR (400 MHz, DMSO-d<sub>6</sub>, δ): 8.66–8.64 (m, 4H), 7.57 (s, 2H), 7.56–7.55 (m, 4H). <sup>13</sup>C NMR (101 MHz, DMSO-d<sub>6</sub>, δ): 150.03, 134.63, 129.18, 125.09, 123.54, 91.91, 85.74. HRMS–ASAP+ (m/z): calcd for C<sub>18</sub>H<sub>11</sub>N<sub>2</sub>S [M]+H, 287.0643; found, 287.0652. Anal. calcd for C<sub>18</sub>H<sub>10</sub>N<sub>2</sub>S: C 75.50; H 3.52; N 9.78; found: C 75.15; H 3.42; N 10.04.

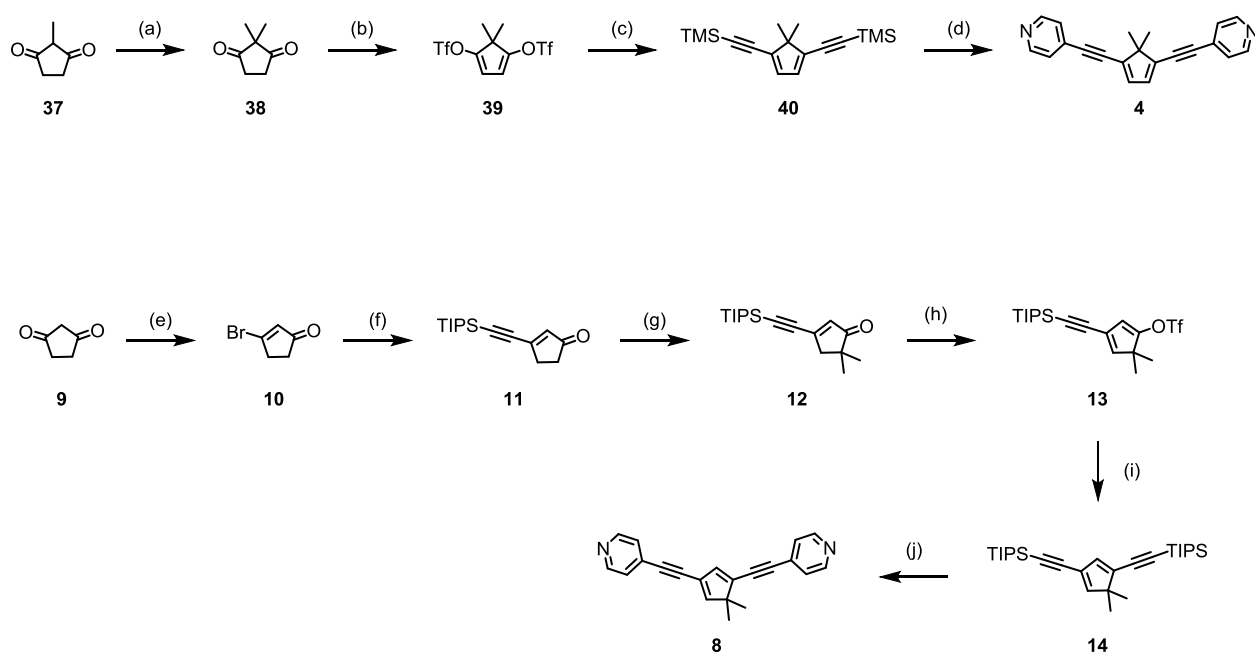
### 2,4-bis(pyridin-4-ylethynyl)thiophene (**7**)



A solution of 2,4-bis((trimethylsilyl)ethynyl)thiophene (**36**) (0.80 g, 2.9 mmol) in dry THF (40 mL) was degassed for 30 min. Tetrabutylammonium fluoride (TBAF, 1 M in THF, 5.8 mL) was then added and the resulting reaction mixture (A) was stirred in the dark for 30 min at room temperature under inert atmosphere. A separate flask was charged with 4-iodopyridine (1.20 g, 5.8 mmol), CuI (55.1 mg, 10% mmol), PPh<sub>3</sub> (227.6 mg, 30% mmol) and dry diisopropylamine (25 mL). The resulting mixture (B) was degassed for 30 min, followed by the addition of Pd<sub>2</sub>(dba)<sub>3</sub> (265 mg, 10% mmol). After deprotection of **36** was completed, the solution (A) was degassed for 15 min and subsequently cannulated into the reaction mixture (B). The resulting reaction mixture was stirred at room temperature overnight under inert atmosphere. After completion, reaction was filtered through a pad of Celite<sup>TM</sup>, and solvents were removed at reduced pressure. The residue was diluted in ethyl acetate, washed sequentially with saturated aqueous NH<sub>4</sub>Cl, water and brine. The organic layer was dried over MgSO<sub>4</sub> and removed *in vacuo*. The crude product was further purified by flash column chromatography (SiO<sub>2</sub>, acetone/toluene, 1:2 – 1:1 (v/v), 5% triethylamine) yielding **7** (743 mg, 2.6 mmol, 89% over two steps) as a white solid. mp: 138.4–139.4 °C. <sup>1</sup>H

NMR (400 MHz, CDCl<sub>3</sub>,  $\delta$ ): 8.63–8.60 (m, 4H), 7.59 (d,  $J$  = 1.3 Hz, 1H), 7.42 (d,  $J$  = 1.3 Hz, 1H), 7.42–7.36 (m, 4H), <sup>13</sup>C NMR (101 MHz, CDCl<sub>3</sub>,  $\delta$ ): 150.03, 150.00, 135.23, 132.53, 131.09, 130.70, 125.58, 125.34, 122.81, 121.75, 91.30, 88.04, 86.86, 86.07. HRMS–ASAP+ (m/z): calcd for C<sub>18</sub>H<sub>11</sub>N<sub>2</sub>S [M]<sup>+</sup>H, 287.0643; found, 287.0640. Anal. calcd for C<sub>18</sub>H<sub>10</sub>N<sub>2</sub>S: C 75.50; H 3.52; N 9.78; found: C 75.47; H 3.55; N 9.68.

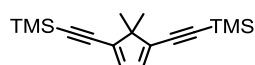
### 1.2.4 Synthesis of cyclopentadiene derivatives 4 and 8



Scheme S1-4: Reagents and Conditions: (a) KOH, MeI, dioxane, H<sub>2</sub>O, reflux, 24 h, 69%; (b) KHMDS, Comins' reagent, THF, –78 °C to rt, 5 h, 76%; (c) TMSA, PdCl<sub>2</sub>(PPh<sub>3</sub>)<sub>2</sub>, CuI, THF, TEA, rt, 12 h, 96%; (d) TBAF (1 M in THF), THF, rt, 30 min, then Pd<sub>2</sub>(dba)<sub>3</sub>, CuI, PPh<sub>3</sub>, 4-iodopyridine, THF, DIPA, 40 °C, 12 h, 80% (over two steps). (e) PPh<sub>3</sub>, Br<sub>2</sub>, TEA, CH<sub>2</sub>Cl<sub>2</sub>, 0 °C to rt, 2 h, 71%; (f) PdCl<sub>2</sub>(PPh<sub>3</sub>)<sub>2</sub>, CuI, TIPSA, DIPA, 10 min, 94%; (g) LiHMDS, MeI, THF, –78 °C to rt, 12 h, 64%; (h) KHMDS, Comins' reagent, THF, –78 °C to rt, 12 h, 87%; (i) TIPSA, PdCl<sub>2</sub>(PPh<sub>3</sub>)<sub>2</sub>, CuI, TEA, THF, rt, 4 h, 91%; (j) TBAF (1 M in THF), THF, rt, 30 min, then 4-iodopyridine, PdCl<sub>2</sub>(PPh<sub>3</sub>)<sub>2</sub>, CuI, THF, DIPA, 40 °C, 12 h, 61% (over two steps).

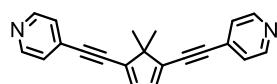
The compounds **10**, **38**, and **39** were synthesized according to literature procedures. Their <sup>1</sup>H- and <sup>13</sup>C-NMR spectra matched previously reported data.<sup>10-11</sup>

### 1,4-bis(ethynyltrimethylsilane)-5,5-dimethylcyclopenta-1,3-diene (**40**)



Triflate derivative **39** (2.00 g, 5.1 mmol) was dissolved in dry THF (40 mL) and dry triethylamine (15 mL). The resulting solution was degassed for 30 min, followed by the addition of CuI (98 mg, 10% mmol) and PdCl<sub>2</sub>(PPh<sub>3</sub>)<sub>2</sub> (360 mg, 10% mmol). After further degassing for 10 min TMS-acetylene (1.50 g, 2.1 mL, 14.9 mmol) was added and the reaction mixture was stirred at room temperature for 12 h. The reaction mixture was filtered through a pad of Celite<sup>TM</sup>, and solvents were evaporated. The residue was diluted in ethyl acetate, washed sequentially with saturated aqueous NH<sub>4</sub>Cl, water and brine. The organic layer was dried over MgSO<sub>4</sub> and removed at reduced pressure. The crude product was further purified by flash column chromatography (SiO<sub>2</sub>, hexanes/methylene chloride, 95:5 (v/v)) yielding **40** (1.40 g, 4.9 mmol, 96%) as a beige solid. <sup>1</sup>H NMR (400 MHz, CDCl<sub>3</sub>, δ): 6.51 (s, 2H), 1.17 (s, 6H), 0.23 (s, 18H). <sup>13</sup>C NMR (101 MHz, CDCl<sub>3</sub>, δ): 140.42, 133.99, 102.42, 100.61, 57.42, 22.28, 0.25. HRMS–ASAP+ (m/z): calcd for C<sub>17</sub>H<sub>27</sub>Si<sub>2</sub> [M]<sup>+</sup>H, 287.1651; found, 287.1655.

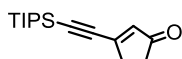
### 1,4-bis(4-ethynylpyridine)-5,5-dimethylcyclopenta-1,3-diene (**4**)



A solution of cyclopentadiene derivative **40** (1.00 g, 3.5 mmol) in dry THF (40 mL) was degassed for 30 min. TBAF (1 M in THF, 7.0 mL) was then added and the resulting reaction mixture (A) was stirred in the dark for 30 min at room temperature under inert atmosphere. A separate flask was charged with 4-iodopyridine (1.00 g, 4.8 mmol), CuI (46 mg, 10% mmol), PPh<sub>3</sub> (188 mg, 30% mmol) and dry DIPA (20 mL). The resulting mixture (B) was degassed for 10 min, followed by the addition of Pd<sub>2</sub>(dba)<sub>3</sub> (219 mg, 10% mmol). After deprotection of **40** was completed, the solution (A) was degassed for 5 min and subsequently, cannulated into the reaction mixture (B). The resulting reaction mixture was stirred at room temperature for 12 h under inert atmosphere. After completion, the reaction was filtered through a pad of

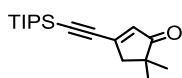
Celite<sup>TM</sup>, and solvents were removed at reduced pressure. The residue was diluted in ethyl acetate, washed sequentially with saturated aqueous NH<sub>4</sub>Cl, water and brine. The organic layer was dried over MgSO<sub>4</sub> and evaporated *in vacuo*. The crude product was further purified by flash column chromatography (SiO<sub>2</sub>, acetone/toluene, 1:5 – 1:2 (v/v), 5% triethylamine) yielding **4** (567 mg, 1.9 mmol, 80% over two steps) as a white solid. mp: 91.8–92.5 °C. <sup>1</sup>H NMR (400 MHz, CDCl<sub>3</sub>, δ): 8.60–8.59 (m, 4H), 7.34–7.33 (m, 4H), 6.74 (s, 2H), 1.33 (s, 6H). <sup>13</sup>C NMR (101 MHz, CDCl<sub>3</sub>, δ): 149.95, 140.23, 135.61, 131.43, 125.44, 94.95, 89.45, 57.66, 22.37. HRMS–ASAP+ (m/z): calcd for C<sub>21</sub>H<sub>17</sub>N<sub>2</sub> [M]+H, 297.1392; found, 297.1405. Anal. calcd for C<sub>18</sub>H<sub>10</sub>N<sub>2</sub>O: C 85.11; H 5.44; N 9.45; found: C 85.11; H 5.38; N 9.44.

### 3-((triisopropylsilyl)ethynyl)cyclopent-2-en-1-one (**11**)



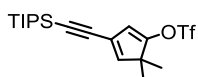
Cyclohexenone derivative **10** (3.20 g, 19.9 mmol) was dissolved in dry THF (35 mL) and dry DIPA (20 mL). The resulting solution was degassed for 30 min, followed by the addition of CuI (114 mg, 3% mmol) and PdCl<sub>2</sub>(PPh<sub>3</sub>)<sub>2</sub> (419 mg, 3% mmol). After further degassing for 10 min TIPS-acetylene (4.40 g, 5.4 mL, 23.9 mmol) was added and the reaction mixture was stirred for 10 min at room temperature. The reaction mixture was filtered through a pad of Celite<sup>TM</sup>, and solvents were evaporated. The residue was diluted in Et<sub>2</sub>O, washed sequentially with saturated aqueous NH<sub>4</sub>Cl, water and brine. The organic layer was dried over MgSO<sub>4</sub> and removed at reduced pressure. The crude product was further purified by bulb to bulb distillation (140 °C, 1.0 · 10<sup>-1</sup> mbar) yielding **11** (4.90 g, 18.7 mmol, 94%) as a clear oil. <sup>1</sup>H NMR (400 MHz, CDCl<sub>3</sub>, δ): 6.28 (t, *J* = 1.9 Hz, 1H), 2.77–2.74 (m, 2H), 2.45–2.42 (m, 2H), 1.12–1.10 (m, 21H). <sup>13</sup>C NMR (101 MHz, CDCl<sub>3</sub>, δ): 209.80, 157.10, 136.67, 109.13, 101.98, 34.91, 32.89, 18.70, 11.26. HRMS–ASAP+ (m/z): calcd for C<sub>16</sub>H<sub>27</sub>OSi<sub>2</sub> [M]+H, 263.1831; found, 263.1840.

### 5,5-dimethyl-3-((triisopropylsilyl)ethynyl)cyclopent-2-en-1-one (**12**)



A solution of LiHMDS (1 M in THF, 69.5 mL) was added dropwise to a solution of cyclopentenone derivative **11** (4.60 g, 17.4 mmol) in dry THF (80 mL) at  $-78\text{ }^{\circ}\text{C}$  under an inert atmosphere. The reaction mixture was stirred at  $0\text{ }^{\circ}\text{C}$  for 1 h and was then cooled to  $-78\text{ }^{\circ}\text{C}$  followed by the slow addition of MeI (12.3 g, 5.4 mL, 86.9 mmol). After completed addition, the reaction mixture was allowed to warm to room temperature overnight. The reaction was quenched by the addition of saturated aqueous  $\text{NH}_4\text{Cl}$  and the aqueous layer was extracted with  $\text{Et}_2\text{O}$  (3 x 50 mL). The combined organic layers were dried over  $\text{MgSO}_4$  and removed *in vacuo*. The crude product was further purified by flash column chromatography ( $\text{SiO}_2$ , hexanes/  $\text{Et}_2\text{O}$ , 95:5 (v/v)) affording **12** (3.70 g, 12.9 mmol, 74%) as a clear oil.  $^1\text{H}$  NMR (400 MHz,  $\text{CDCl}_3$ ,  $\delta$ ): 6.20 (t,  $J = 1.9\text{ Hz}$ , 1H), 2.61 (d,  $J = 1.9\text{ Hz}$ , 1H), 1.13 (s, 6H), 1.12–1.10 (m, 21H).  $^{13}\text{C}$  NMR (101 MHz,  $\text{CDCl}_3$ ,  $\delta$ ): 214.42, 154.08, 134.14, 108.71, 102.24, 49.26, 43.99, 25.11, 18.71, 11.27. HRMS–ASAP+ ( $m/z$ ): calcd for  $\text{C}_{18}\text{H}_{31}\text{OSi}_2$  [ $\text{M}$ ]+H, 291.2144; found, 291.2144.

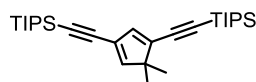
**5,5-dimethyl-3-((triisopropylsilyl)ethynyl)cyclopenta-1,3-dien-1-yl-trifluoromethanesulfonate (13)**



A solution of KHMDS (0.5 M in MePh, 30.3 mL) was added dropwise to a solution of cyclohexenone derivative **12** (2.02 g, 7.6 mmol) and 2-[*N,N*-bis(trifluoromethylsulfonyl)-amino]-5-chloropyridine (Comins' reagent, 5.70 g, 14.4 mmol) in dry THF (50 mL) at  $-78\text{ }^{\circ}\text{C}$  under an inert atmosphere. After stirring the reaction mixture for 2 h at  $-78\text{ }^{\circ}\text{C}$ , the solution was allowed to warm to  $0\text{ }^{\circ}\text{C}$  and stirred for an additional 1 h. The reaction mixture was diluted with hexanes (100 mL) and the organic layer was sequentially washed with water (50 mL), 10% aqueous NaOH, and brine. The organic layer was dried over  $\text{MgSO}_4$  and removed at reduced pressure. The crude product was further purified by flash column chromatography ( $\text{SiO}_2$ , hexanes/  $\text{Et}_2\text{O}$ , 95:5 (v/v)) yielding **13** (2.80 g, 6.6 mmol, 88%) as a yellow oil.  $^1\text{H}$  NMR (400 MHz,  $\text{CDCl}_3$ ,  $\delta$ ): 6.26 (d,  $J = 1.8\text{ Hz}$ , 1H), 5.99 (d,  $J = 1.8\text{ Hz}$ , 1H),

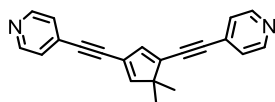
1.23 (s, 6H), 1.10 (s, 21H).  $^{13}\text{C}$  NMR (101 MHz,  $\text{CDCl}_3$ ,  $\delta$ ): 159.57, 144.79, 120.95, 118.71 (q,  $J = 320.8$  Hz), 114.27, 101.70, 100.14, 93.64, 50.68, 20.37, 18.77, 11.39.  $^{19}\text{F}$  NMR (377 MHz,  $\text{CDCl}_3$ ,  $\delta$ ): -73.29. HRMS-ASAP+ ( $m/z$ ): calcd for  $\text{C}_{19}\text{H}_{30}\text{F}_3\text{O}_3\text{SSi}_2$  [ $\text{M}$ ]+H, 423.1637; found, 423.1627.

### 1,3-bis(ethynyltriisopropylsilane)-5,5-dimethylcyclopenta-1,3-diene (14)



Triflate derivative **13** (2.80 g, 6.6 mmol) was dissolved in dry THF (50 mL) and dry triethylamine (50 mL). The resulting solution was degassed for 30 min, followed by the addition of CuI (63 mg, 5% mmol) and  $\text{PdCl}_2(\text{PPh}_3)_2$  (233 mg, 5% mmol). After further degassing for 10 min TIPS-acetylene (1.80 g, 2.2 mL, 9.9 mmol) was added and the reaction mixture was stirred for 12 h at room temperature. The reaction mixture was filtered through a pad of Celite<sup>TM</sup>, and solvents were evaporated. The residue was diluted in  $\text{Et}_2\text{O}$ , washed sequentially with saturated aqueous  $\text{NH}_4\text{Cl}$ , water and brine. The organic layer was dried over  $\text{MgSO}_4$  and removed at reduced pressure. The crude product was further purified by flash column chromatography ( $\text{SiO}_2$ , hexanes) affording **14** (2.90 g, 6.4 mmol, 96%) as a clear oil.  $^1\text{H}$  NMR (400 MHz,  $\text{CDCl}_3$ ,  $\delta$ ): 6.49 (d,  $J = 1.5$  Hz, 1H), 6.41 (d,  $J = 1.5$  Hz, 1H), 1.19 (s, 6H), 1.10–1.09 (m, 42H).  $^{13}\text{C}$  NMR (101 MHz,  $\text{CDCl}_3$ ,  $\delta$ ): 151.34, 139.81, 135.28, 123.39, 102.47, 101.60, 98.39, 92.20, 55.42, 22.13, 18.81, 18.78, 11.43, 11.42. HRMS-ASAP+ ( $m/z$ ): calcd for  $\text{C}_{29}\text{H}_{51}\text{Si}_2$  [ $\text{M}$ ]+H, 455.3529; found, 455.3546.

### 1,3-bis(ethynylpyridine)-5,5-dimethylcyclopenta-1,3-diene (8)



A solution of cyclopentadiene derivative **14** (1.10 g, 2.3 mmol) in dry THF (40 mL) was degassed for 30 min. TBAF (1 M in THF, 4.6 mL) was then added and the resulting reaction mixture (A) was stirred in the dark for 30 min at room temperature under inert atmosphere. A separate flask was charged with 4-iodopyridine (1.00 g, 4.9 mmol), CuI (44 mg, 10% mmol),

PPh<sub>3</sub> (183 mg, 30% mmol) and dry DIPA (20 mL). The resulting mixture (B) was degassed for 20 min, followed by the addition of PdCl<sub>2</sub>(PPh<sub>3</sub>)<sub>2</sub> (164 mg, 10% mmol). After deprotection of **14** was completed, the solution (A) was degassed for 5 min and subsequently cannulated into the reaction mixture (B). The resulting reaction mixture was stirred at room temperature for 12 h under inert atmosphere. After completion, the reaction was filtered through a pad of Celite<sup>TM</sup>, and solvents were removed at reduced pressure. The residue was diluted in ethyl acetate, washed sequentially with saturated aqueous NH<sub>4</sub>Cl, water and brine. The organic layer was dried over MgSO<sub>4</sub> and evaporated *in vacuo*. The crude product was further purified by flash column chromatography (SiO<sub>2</sub>, acetone/toluene, 1:5 – 1:2 (v/v), 5% triethylamine) yielding **8** (486 mg, 1.6 mmol, 70% over two steps) as a beige solid. mp: 81.9–82.8 °C. <sup>1</sup>H NMR (400 MHz, CDCl<sub>3</sub>, δ): 8.60–8.59 (m, 4H), 7.34–7.33 (m, 4H), 6.75 (d, *J* = 1.5 Hz, 1H), 6.62 (d, *J* = 1.5 Hz, 1H), 1.30 (s, 6H). <sup>13</sup>C NMR (101 MHz, CDCl<sub>3</sub>, δ): 154.05, 149.96, 149.94, 139.04, 136.03, 131.47, 131.21, 125.62, 125.51, 122.59, 94.41, 89.05, 88.47, 88.24, 55.96, 22.01. HRMS–ASAP+ (m/z): calcd for C<sub>21</sub>H<sub>17</sub>N<sub>2</sub> [M]<sup>+</sup>H, 297.1392; found, 297.1387. Anal. calcd for C<sub>18</sub>H<sub>10</sub>N<sub>2</sub>O: C 85.11; H 5.44; N 9.45; found: C 85.12; H 5.44; N 9.44.

## 1.3 $^1\text{H}$ NMR and $^{13}\text{C}$ NMR Spectra

### 1.3.1 $^1\text{H}$ NMR and $^{13}\text{C}$ NMR Spectra of **1**

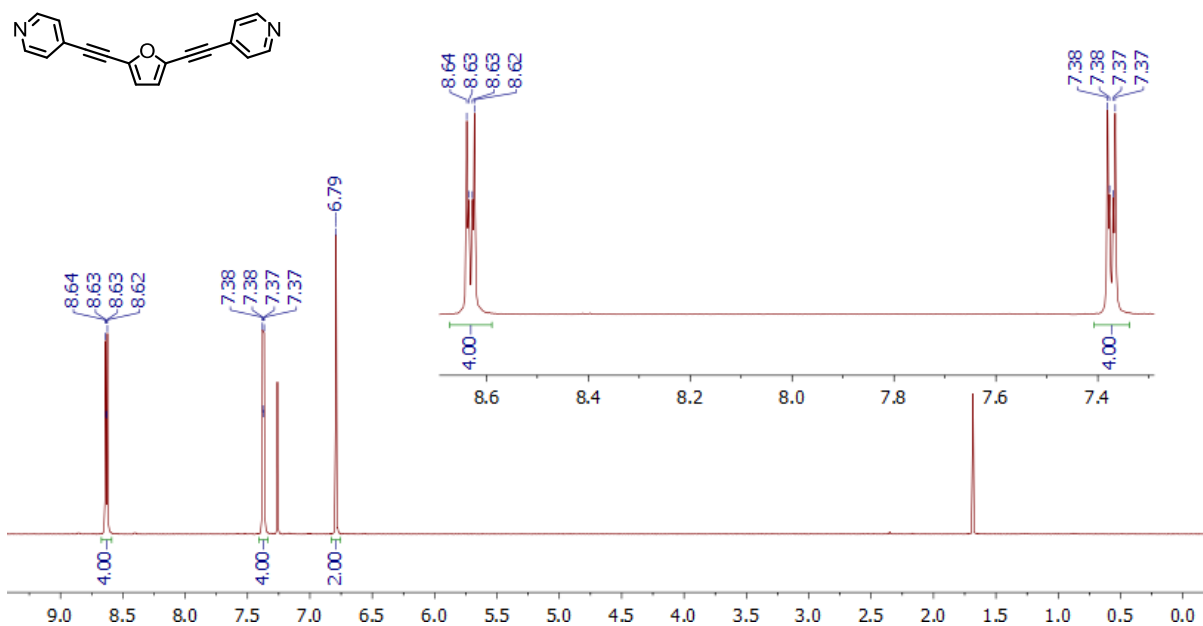


Figure S1-1:  $^1\text{H}$  NMR Spectrum of **1** in  $\text{CDCl}_3$  ( $\delta$   $\text{CHCl}_3$  7.26)

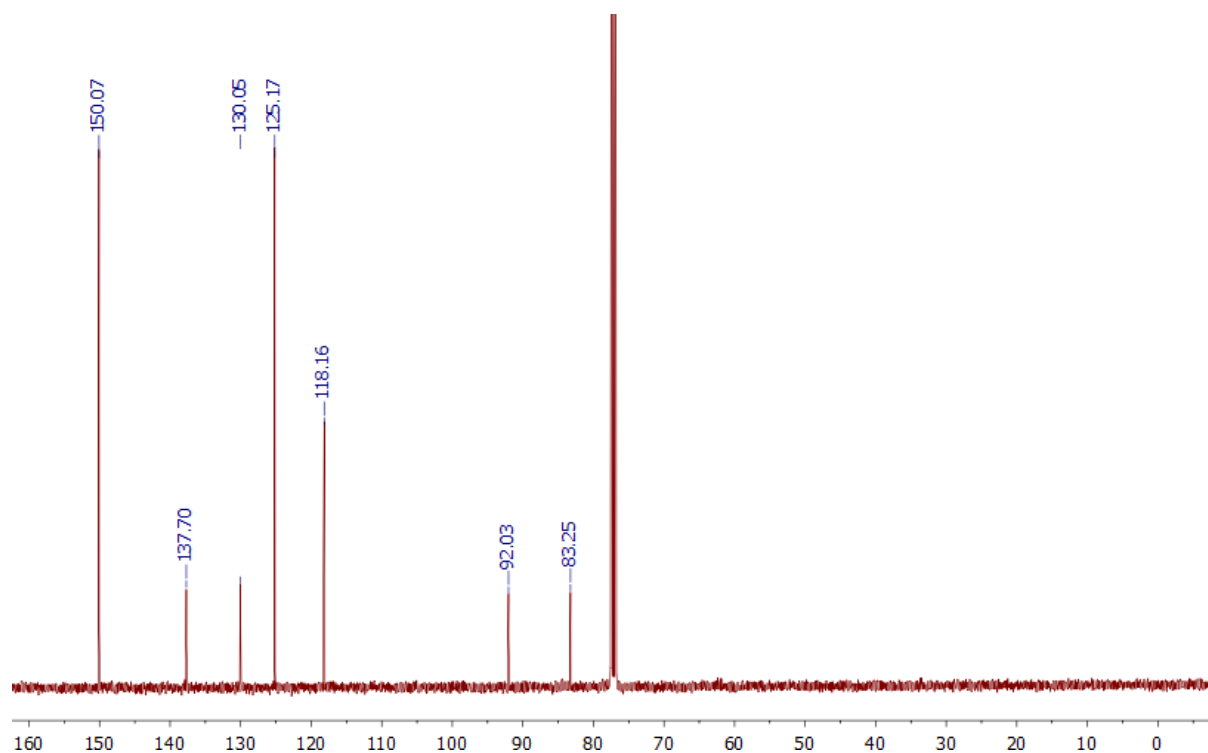


Figure S1-2:  $^{13}\text{C}$  NMR Spectrum of **1** in  $\text{CDCl}_3$  ( $\delta$  77.16)

### 1.3.2 $^1\text{H}$ NMR and $^{13}\text{C}$ NMR Spectra of **21**

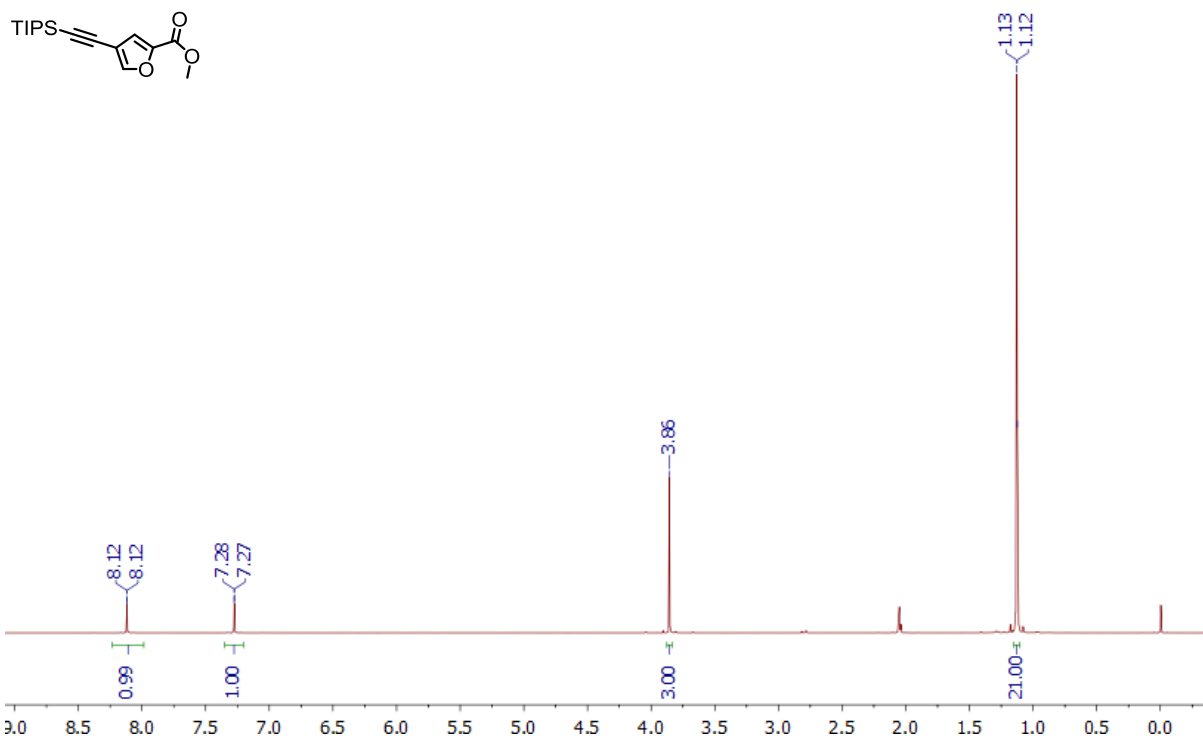


Figure S1-3:  $^1\text{H}$  NMR Spectrum of **21** in  $\text{Acetone-d}_6$  ( $\delta$  Acetone- $\text{d}_5$  2.05)

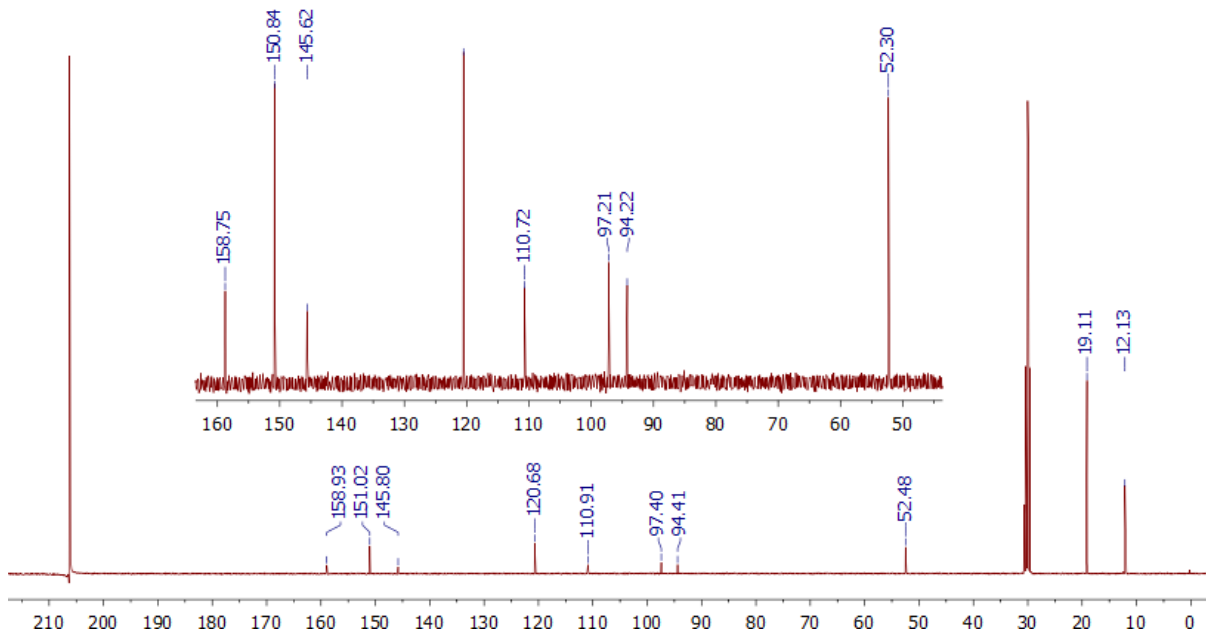


Figure S1-4:  $^{13}\text{C}$  NMR Spectrum of **21** in  $\text{Acetone-d}_6$  ( $\delta$  Acetone- $\text{d}_6$  206.26)

### 1.3.3 $^1\text{H}$ NMR and $^{13}\text{C}$ NMR Spectra of **22**

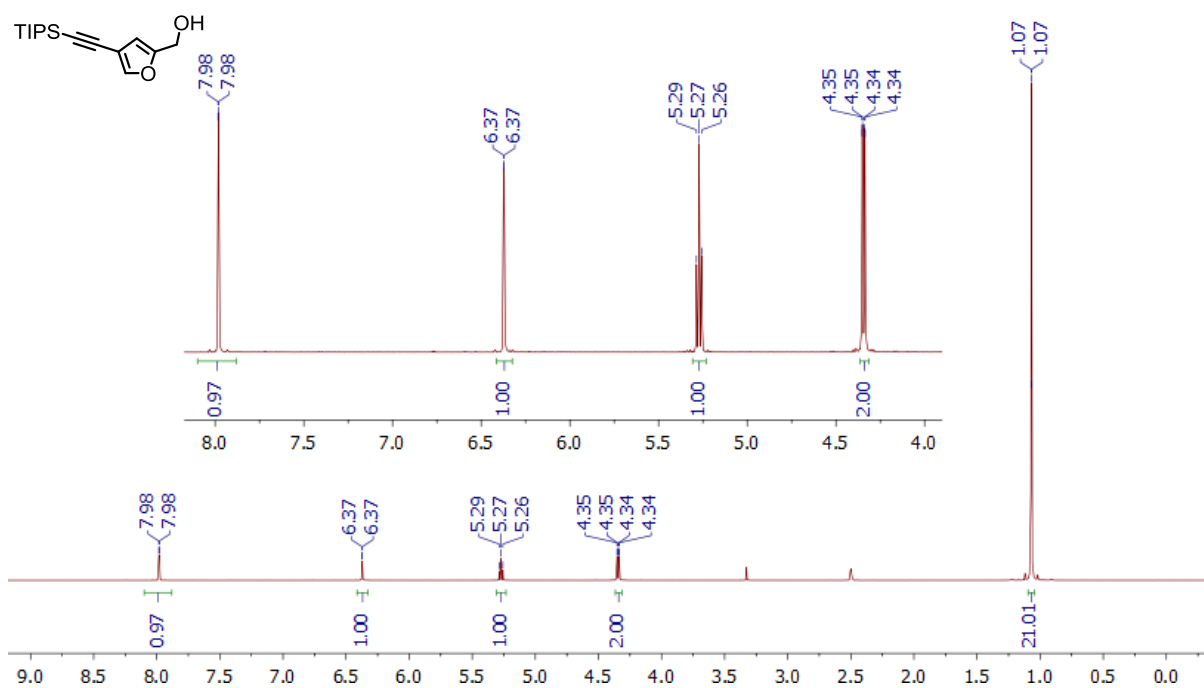


Figure S1-5:  $^1\text{H}$  NMR Spectrum of **22** in  $\text{DMSO-d}_6$  ( $\delta$  DMSO- $\text{d}_5$  2.50)

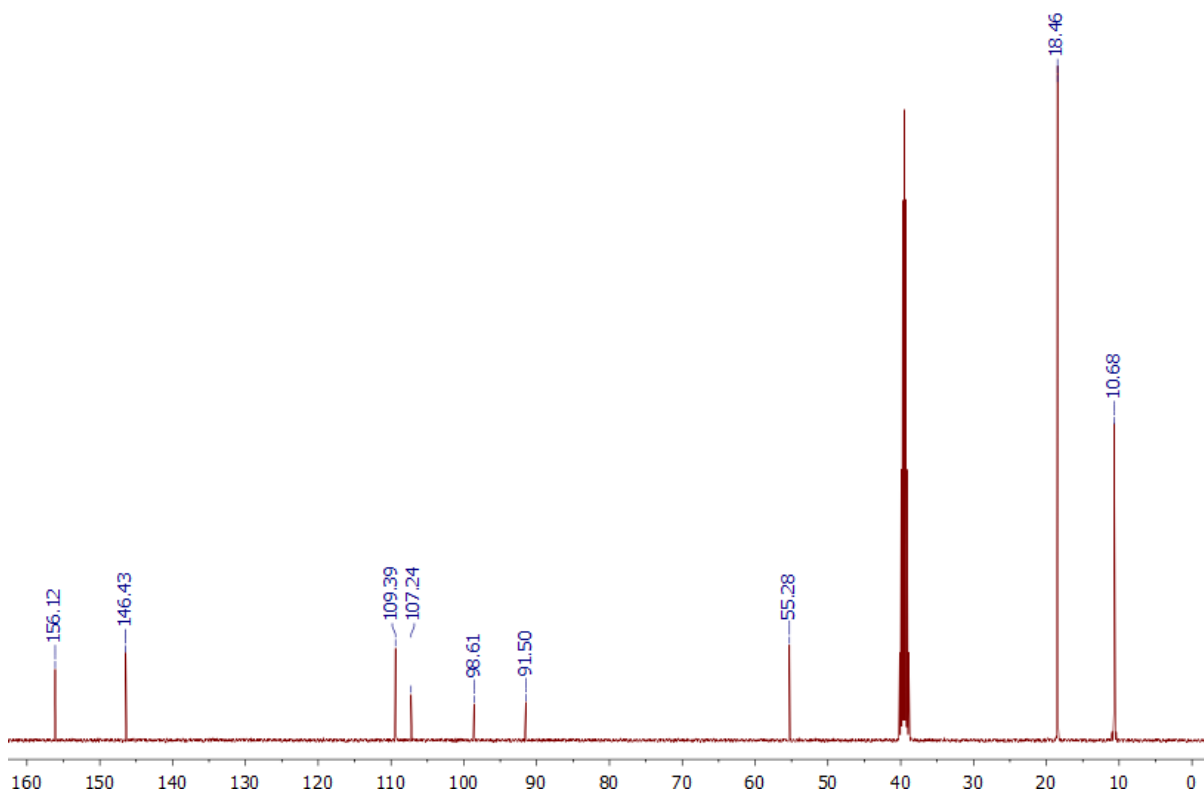


Figure S1-6:  $^{13}\text{C}$  NMR Spectrum of **22** in  $\text{DMSO-d}_6$  ( $\delta$  39.52)

### 1.3.4 $^1\text{H}$ NMR and $^{13}\text{C}$ NMR Spectra of **23**

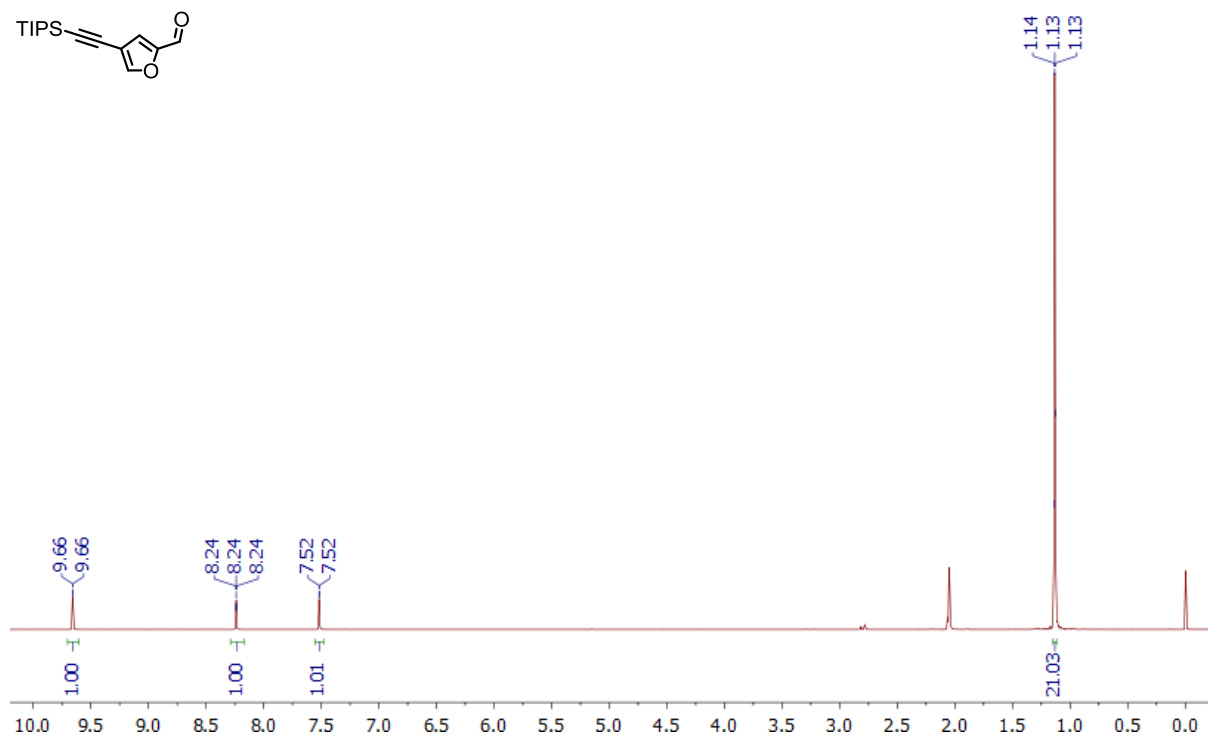
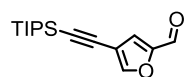


Figure S1-7:  $^1\text{H}$  NMR Spectrum of **23** in Acetone- $\text{d}_6$  ( $\delta$  Acetone- $\text{d}_5$  2.05)

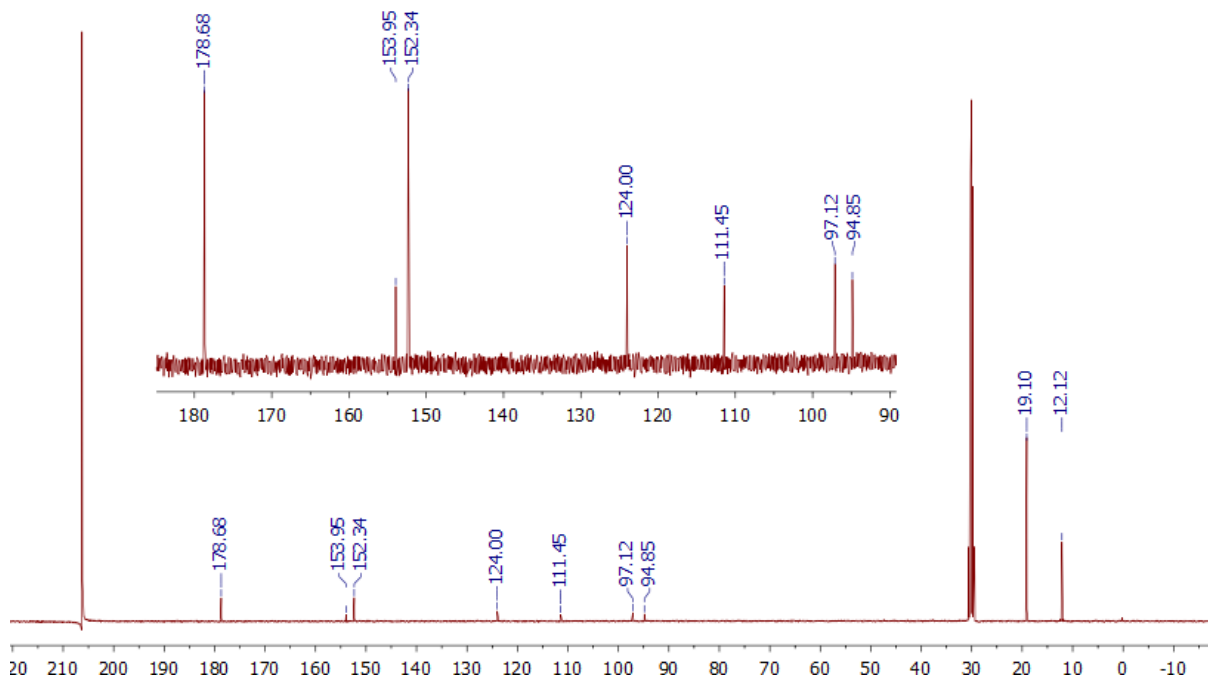


Figure S1-8:  $^{13}\text{C}$  NMR Spectrum of **23** in Acetone- $\text{d}_6$  ( $\delta$  Acetone- $\text{d}_6$  206.26)

### 1.3.5 $^1\text{H}$ NMR and $^{13}\text{C}$ NMR Spectra of **24**

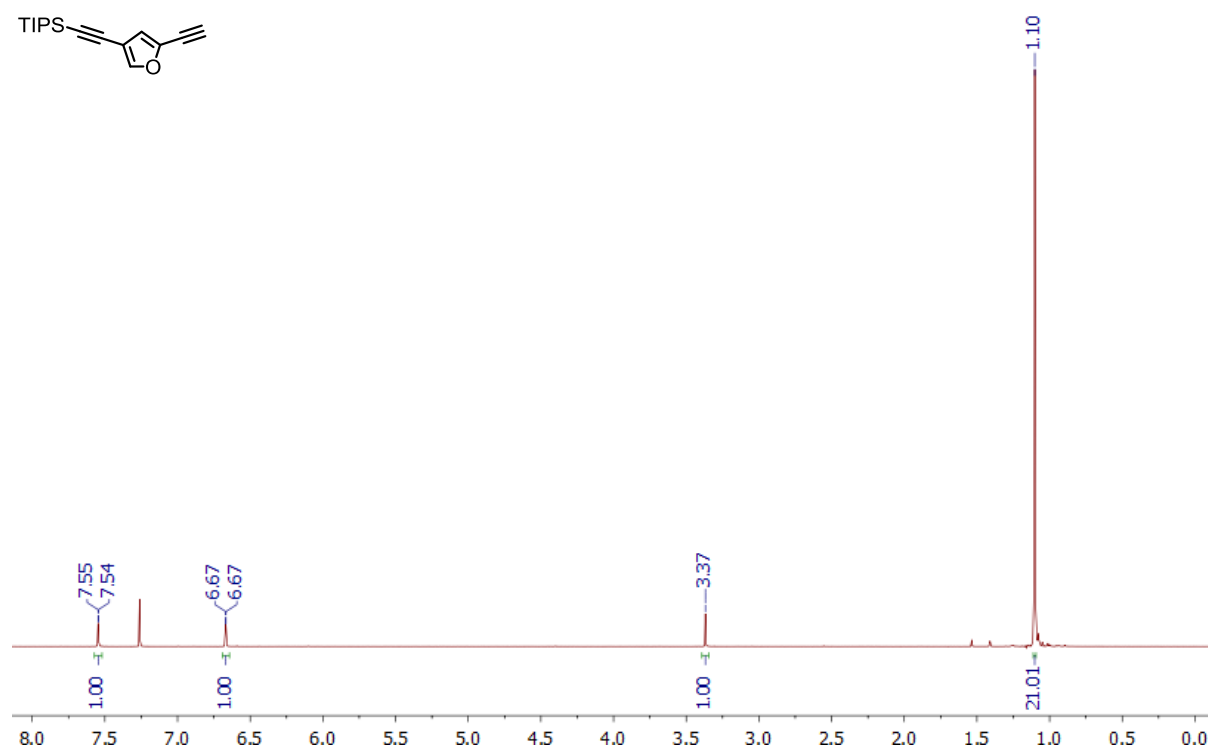
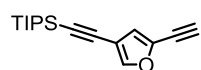


Figure S1-9:  $^1\text{H}$  NMR Spectrum of **24** in  $\text{CDCl}_3$  ( $\delta$   $\text{CHCl}_3$  7.26)

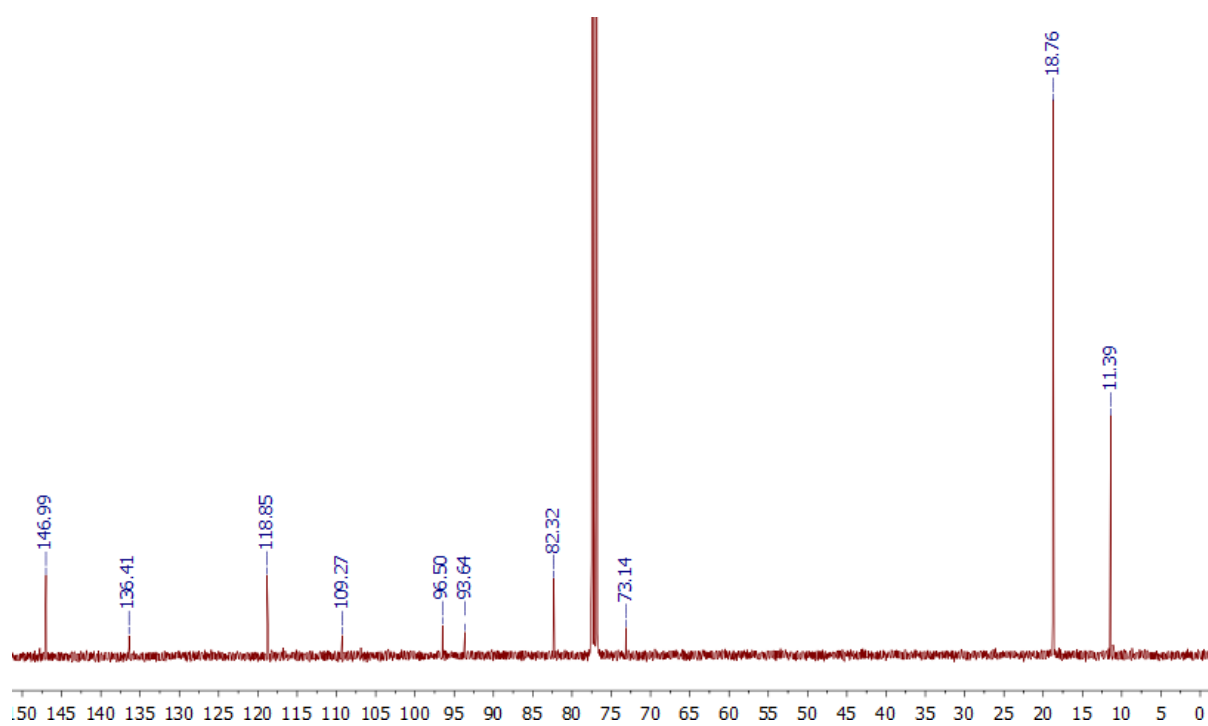


Figure S1-10:  $^{13}\text{C}$  NMR Spectrum of **24** in  $\text{CDCl}_3$  ( $\delta$  77.16)

### 1.3.6 $^1\text{H}$ NMR and $^{13}\text{C}$ NMR Spectra of **5**

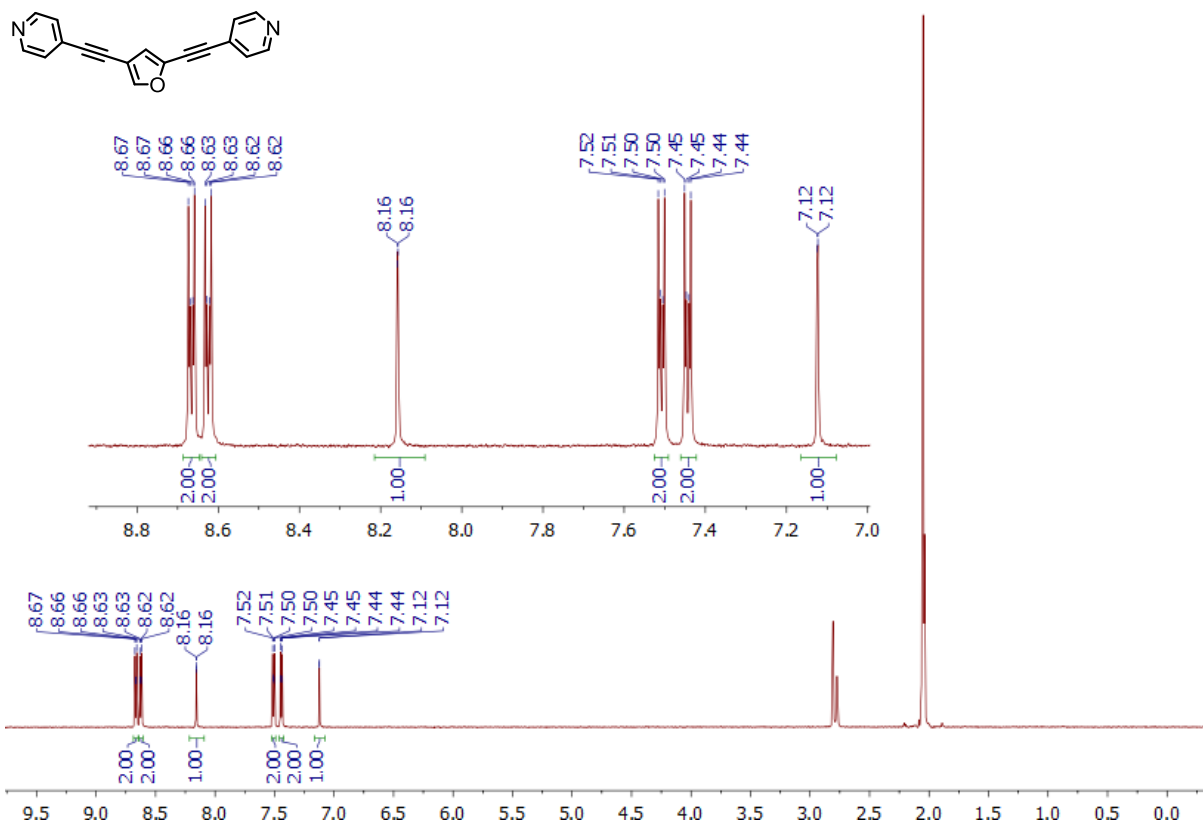


Figure S1-11:  $^1\text{H}$  NMR Spectrum of **5** in Acetone- $d_6$  ( $\delta$  Acetone- $d_5$  2.05)

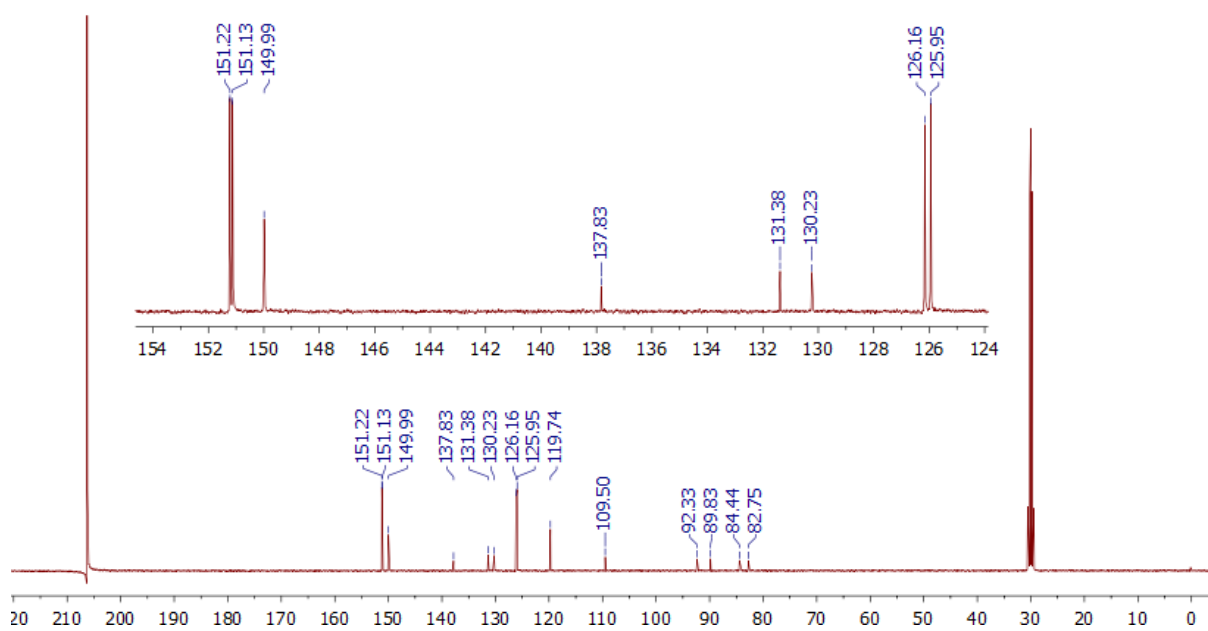


Figure S1-12:  $^{13}\text{C}$  NMR Spectrum of **5** in Acetone- $d_6$  ( $\delta$  Acetone- $d_6$  206.26)

### 1.3.7 $^1\text{H}$ NMR and $^{13}\text{C}$ NMR Spectra of **26**

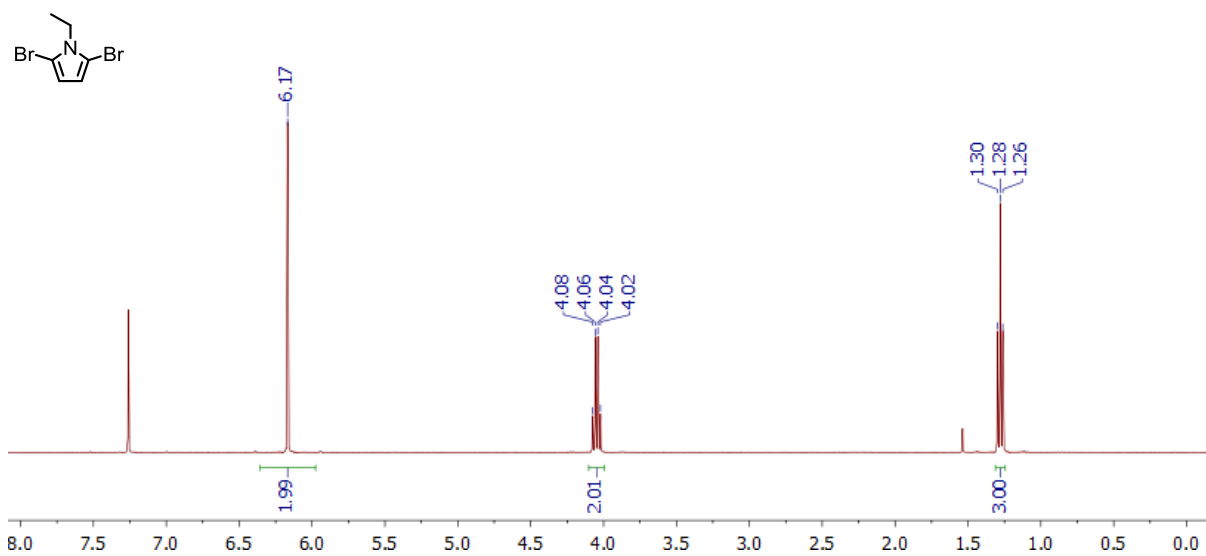


Figure S1-13:  $^1\text{H}$  NMR Spectrum of **26** in  $\text{CDCl}_3$  ( $\delta$   $\text{CHCl}_3$  7.26)

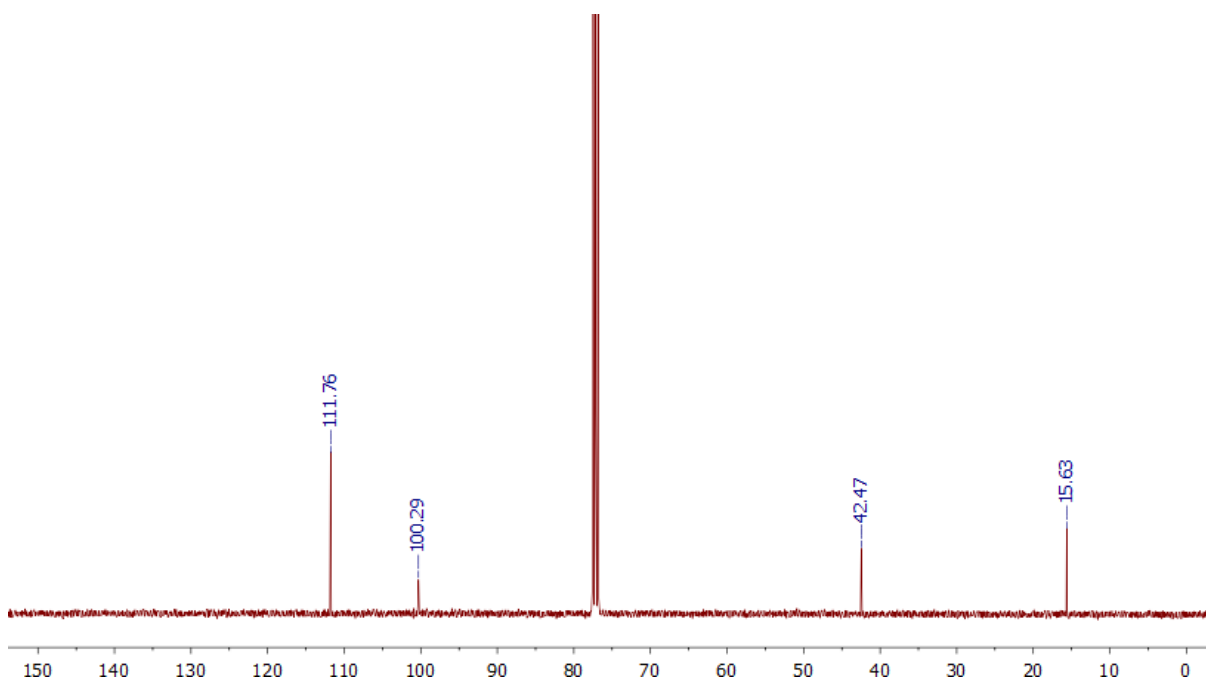


Figure S1-14:  $^{13}\text{C}$  NMR Spectrum of **26** in  $\text{CDCl}_3$  ( $\delta$  77.16)

### 1.3.8 $^1\text{H}$ NMR and $^{13}\text{C}$ NMR Spectra of **2**

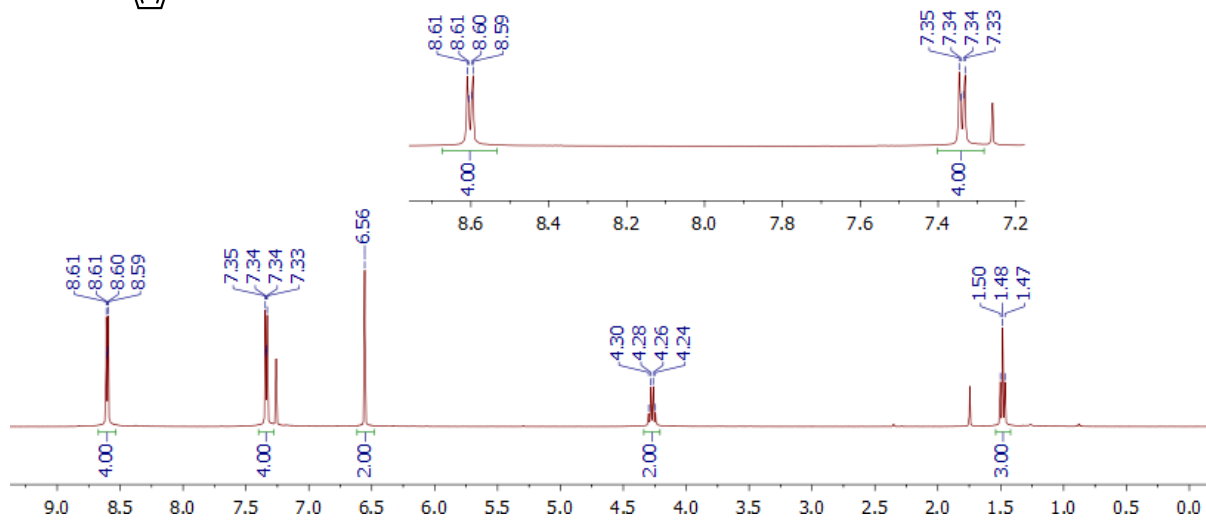
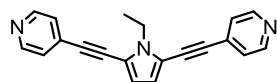


Figure S1-15:  $^1\text{H}$  NMR Spectrum of **2** in  $\text{CDCl}_3$  ( $\delta$   $\text{CHCl}_3$  7.26)

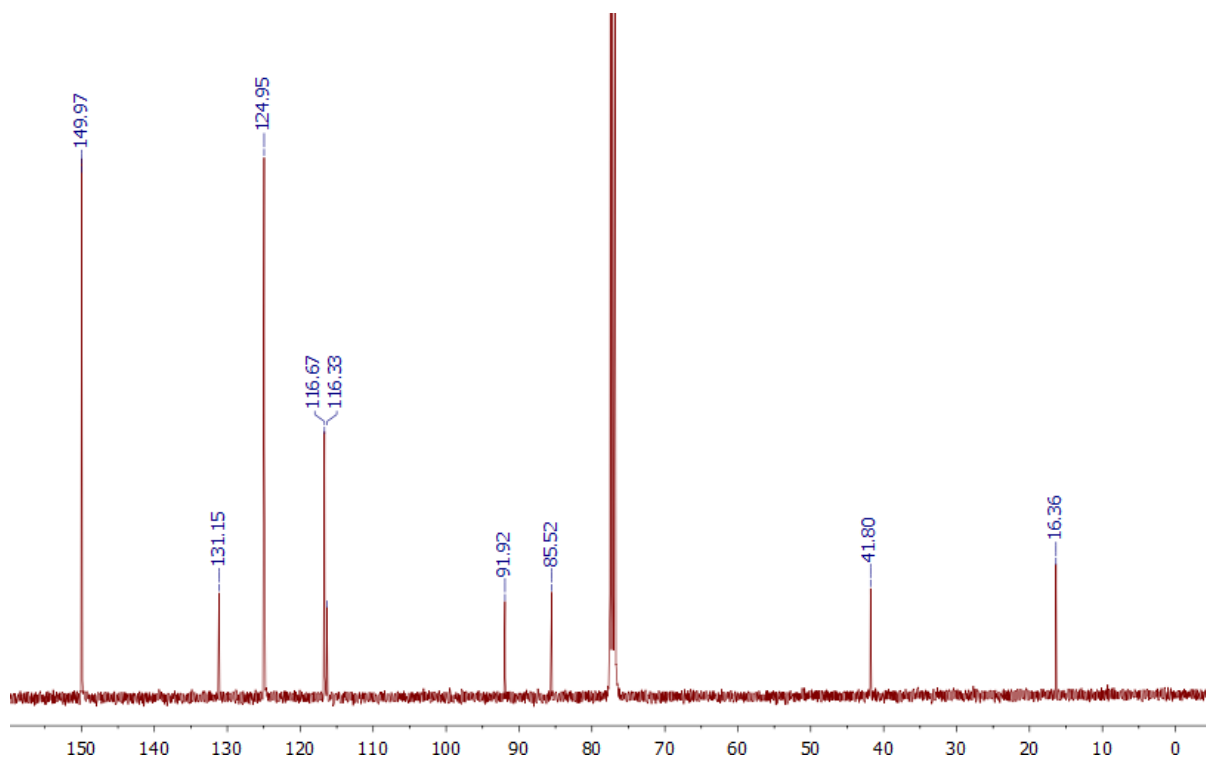


Figure S1-16:  $^{13}\text{C}$  NMR Spectrum of **2** in  $\text{CDCl}_3$  ( $\delta$  77.16)

### 1.3.9 $^1\text{H}$ NMR and $^{13}\text{C}$ NMR Spectra of **30**

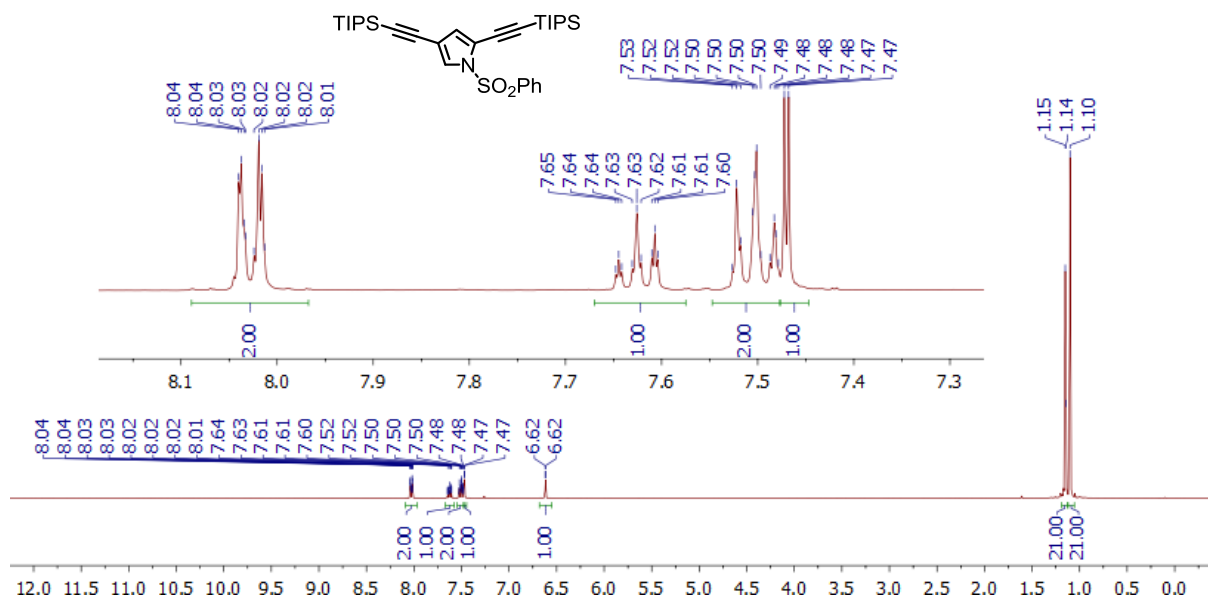


Figure S1-17:  $^1\text{H}$  NMR Spectrum of **30** in CDCl<sub>3</sub> ( $\delta$  CHCl<sub>3</sub> 7.26)

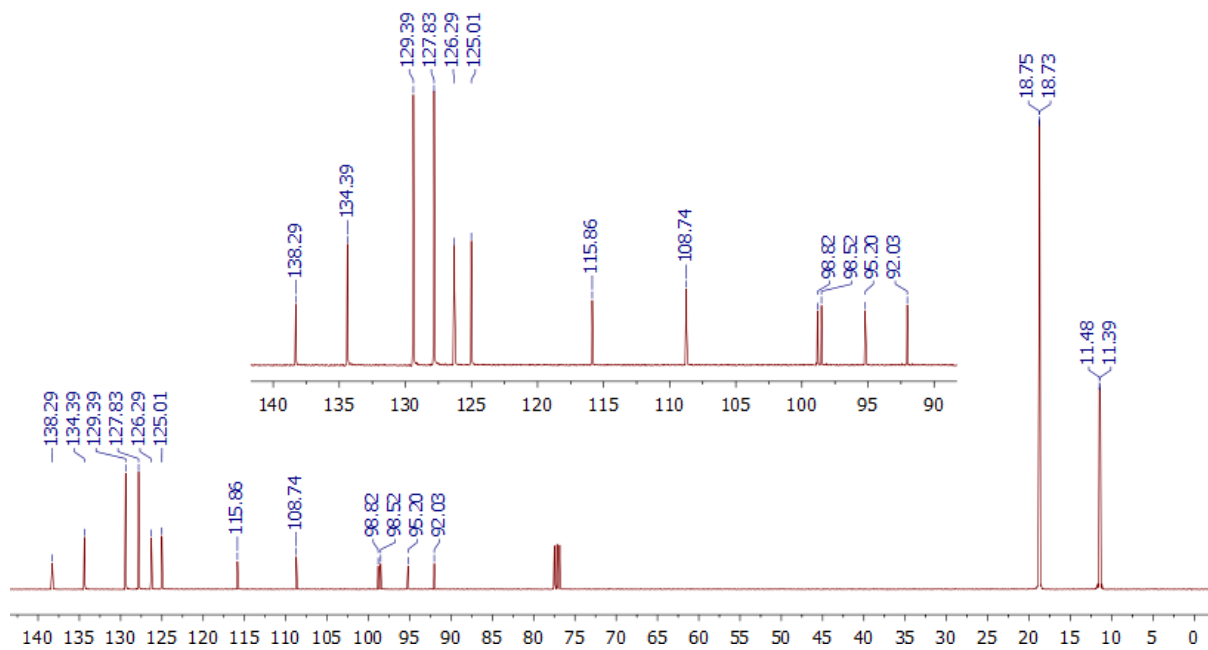


Figure S1-18:  $^{13}\text{C}$  NMR Spectrum of **30** in CDCl<sub>3</sub> ( $\delta$  77.16)

### 1.3.10 $^1\text{H}$ NMR and $^{13}\text{C}$ NMR Spectra of **31**

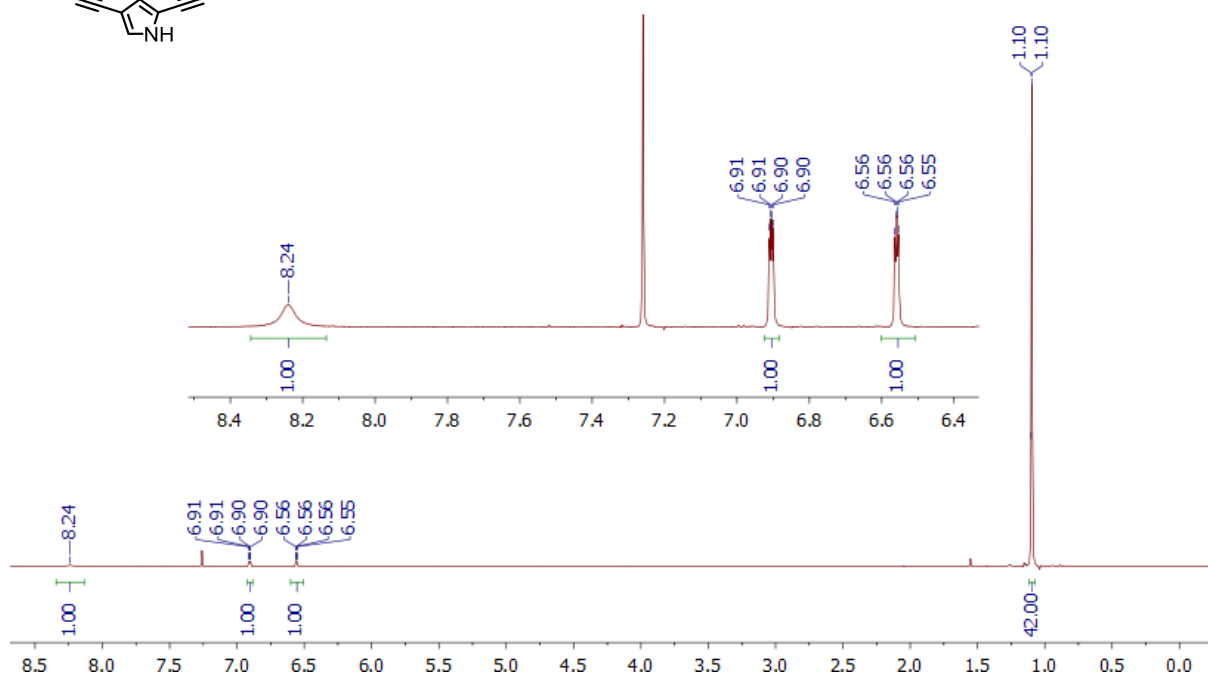
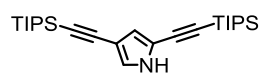


Figure S1-19:  $^1\text{H}$  NMR Spectrum of **31** in  $\text{CDCl}_3$  ( $\delta$   $\text{CHCl}_3$  7.26)

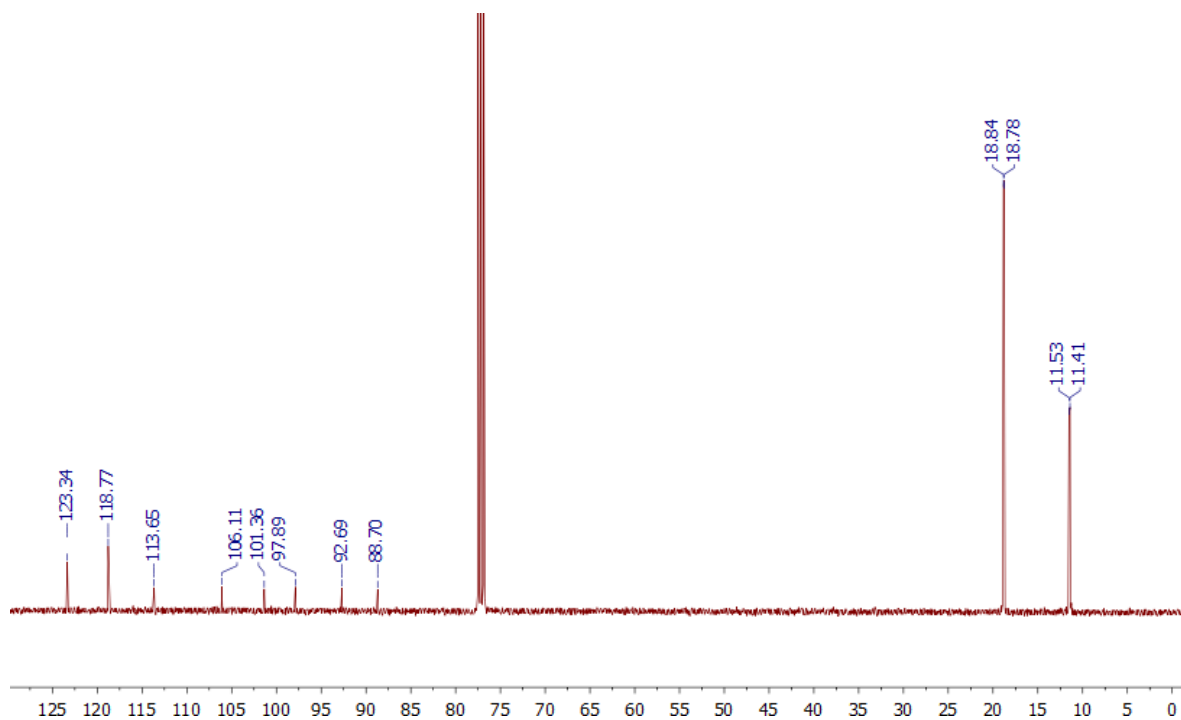


Figure S1-20:  $^{13}\text{C}$  NMR Spectrum of **31** in  $\text{CDCl}_3$  ( $\delta$  77.16)

### 1.3.11 $^1\text{H}$ NMR and $^{13}\text{C}$ NMR Spectra of **32**

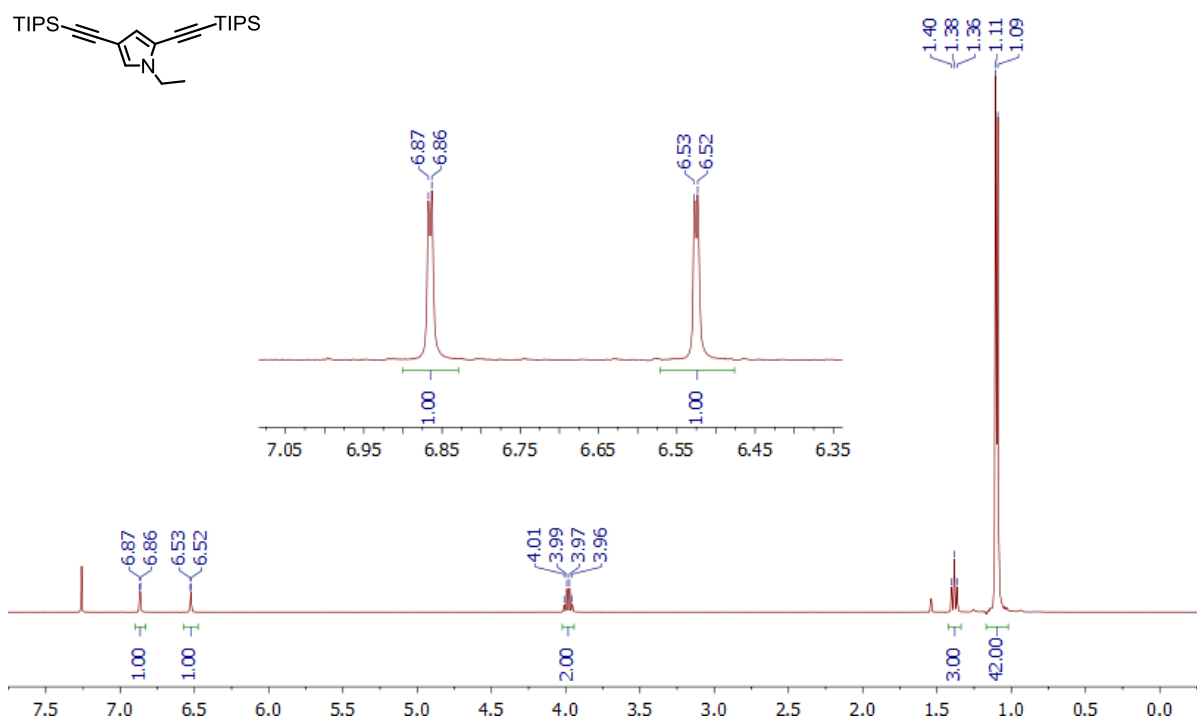


Figure S1-21:  $^1\text{H}$  NMR Spectrum of **32** in  $\text{CDCl}_3$  ( $\delta$   $\text{CHCl}_3$  7.26)

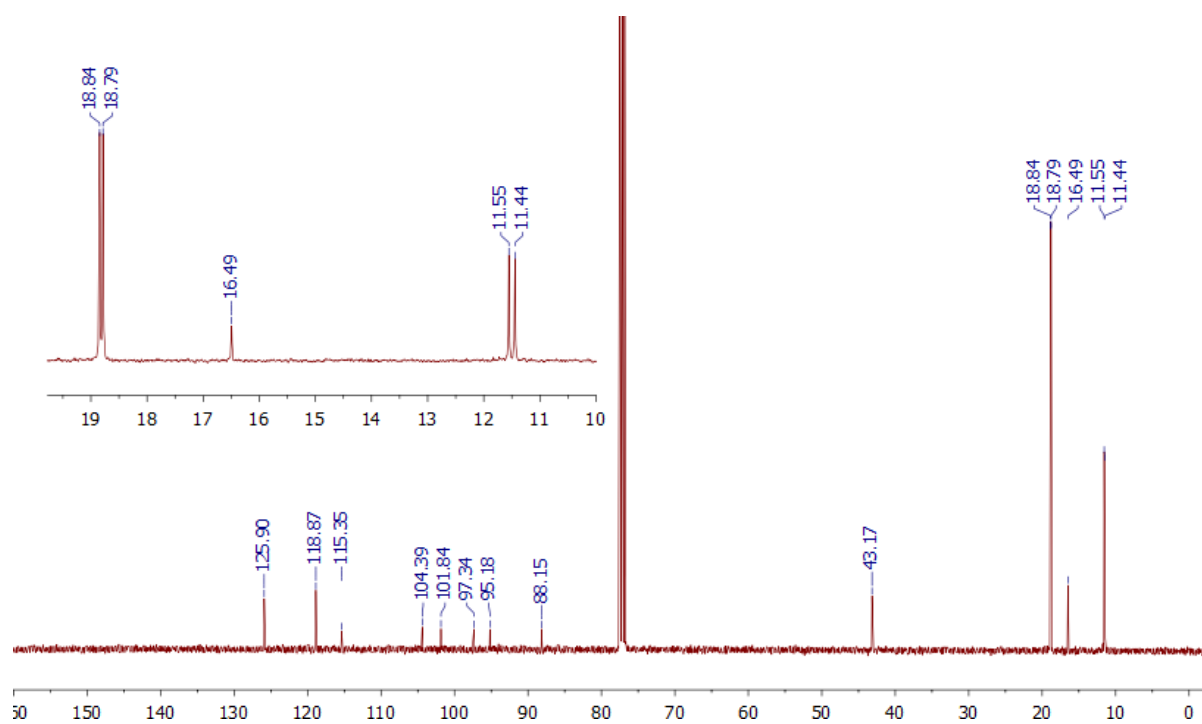


Figure S1-22:  $^{13}\text{C}$  NMR Spectrum of **32** in  $\text{CDCl}_3$  ( $\delta$  77.16)

### 1.3.12 $^1\text{H}$ NMR and $^{13}\text{C}$ NMR Spectra of **6**

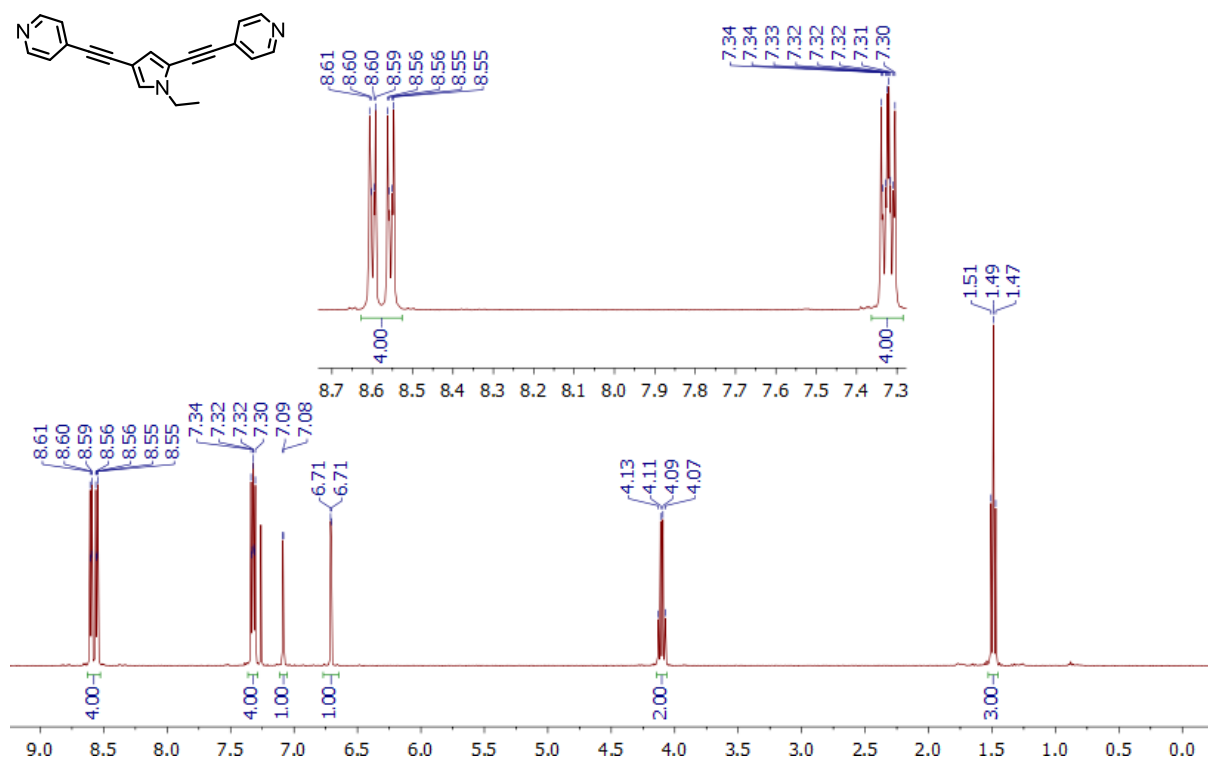


Figure S1-23:  $^1\text{H}$  NMR Spectrum of **6** in CDCl<sub>3</sub> ( $\delta$  CHCl<sub>3</sub> 7.26)

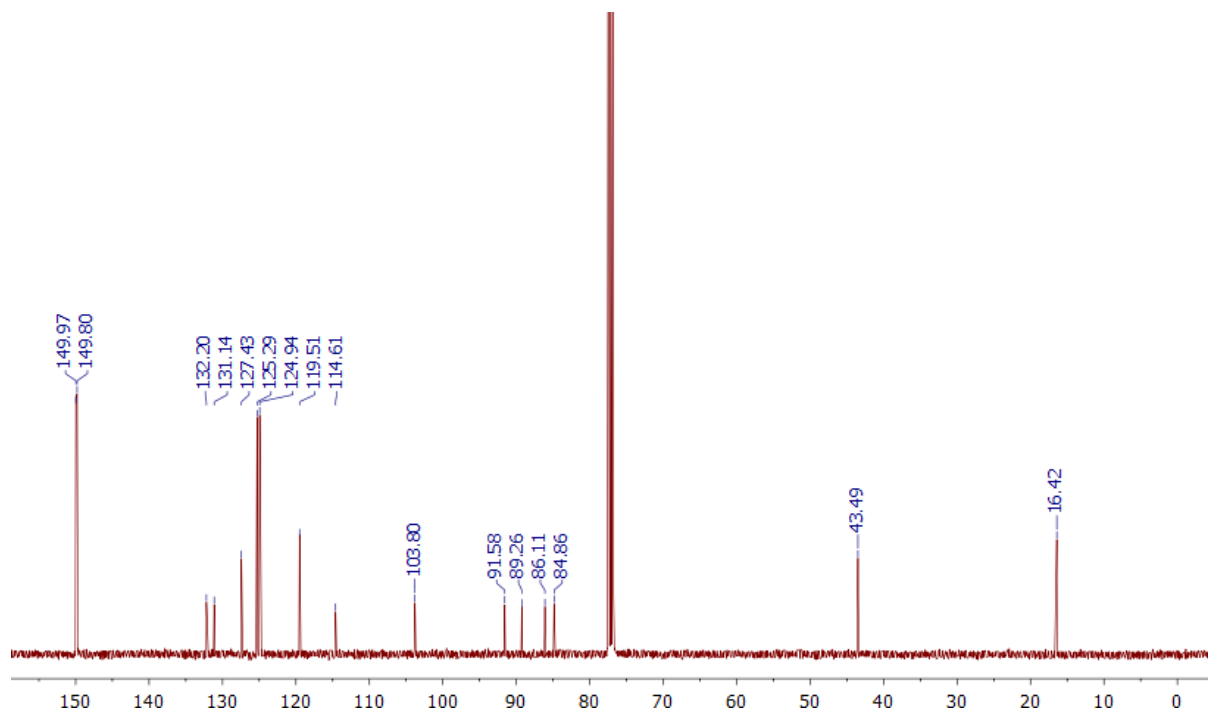


Figure S1-24:  $^{13}\text{C}$  NMR Spectrum of **6** in CDCl<sub>3</sub> ( $\delta$  77.16)

### 1.3.13 $^1\text{H}$ NMR and $^{13}\text{C}$ NMR Spectra of **3**

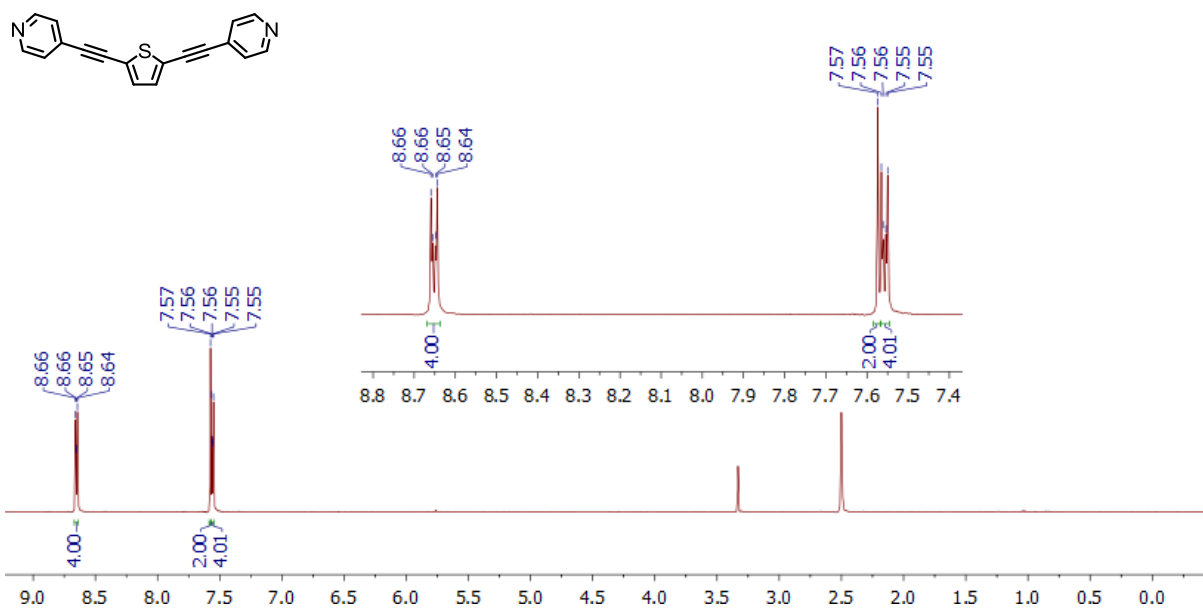


Figure S1-25:  $^1\text{H}$  NMR Spectrum of **3** in  $\text{DMSO-d}_6$  ( $\delta$   $\text{DMSO-d}_5$  2.50)

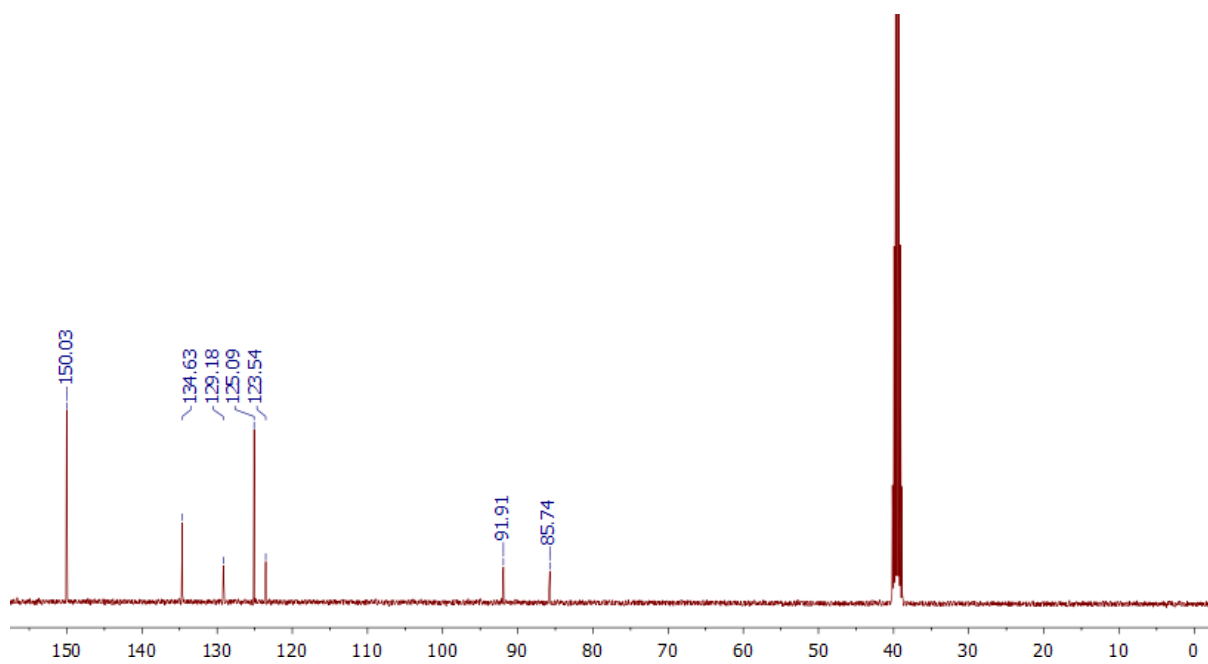


Figure S1-26:  $^{13}\text{C}$  NMR Spectrum of **3** in  $\text{DMSO-d}_6$  ( $\delta$  39.52)

### 1.3.14 $^1\text{H}$ NMR and $^{13}\text{C}$ NMR Spectra of 7

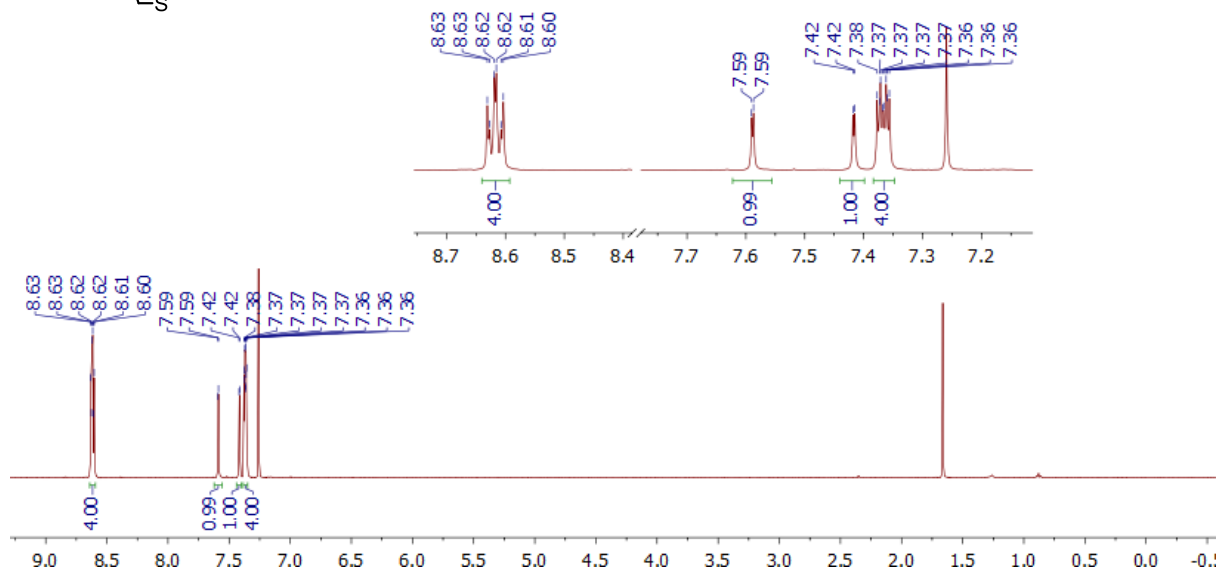
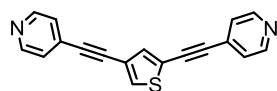


Figure S1-27:  $^1\text{H}$  NMR Spectrum of 7 in  $\text{CDCl}_3$  ( $\delta$   $\text{CHCl}_3$  7.26)

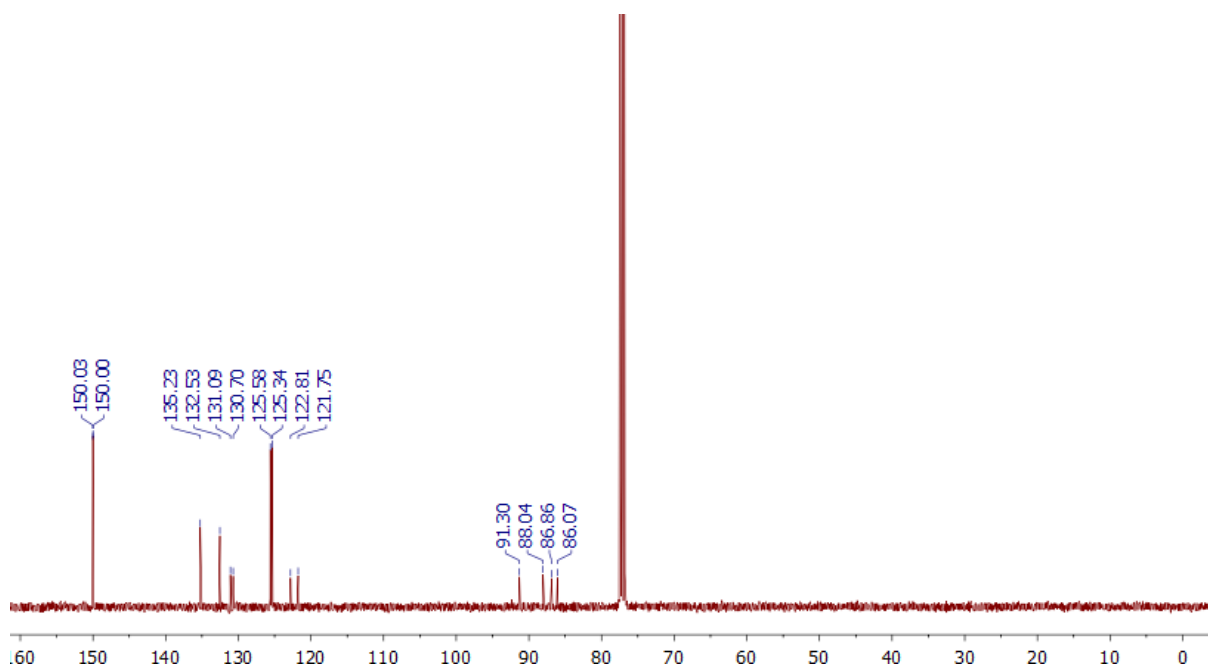


Figure S1-28:  $^{13}\text{C}$  NMR Spectrum of 7 in  $\text{CDCl}_3$  ( $\delta$  77.16)

### 1.3.15 $^1\text{H}$ NMR and $^{13}\text{C}$ NMR Spectra of **40**

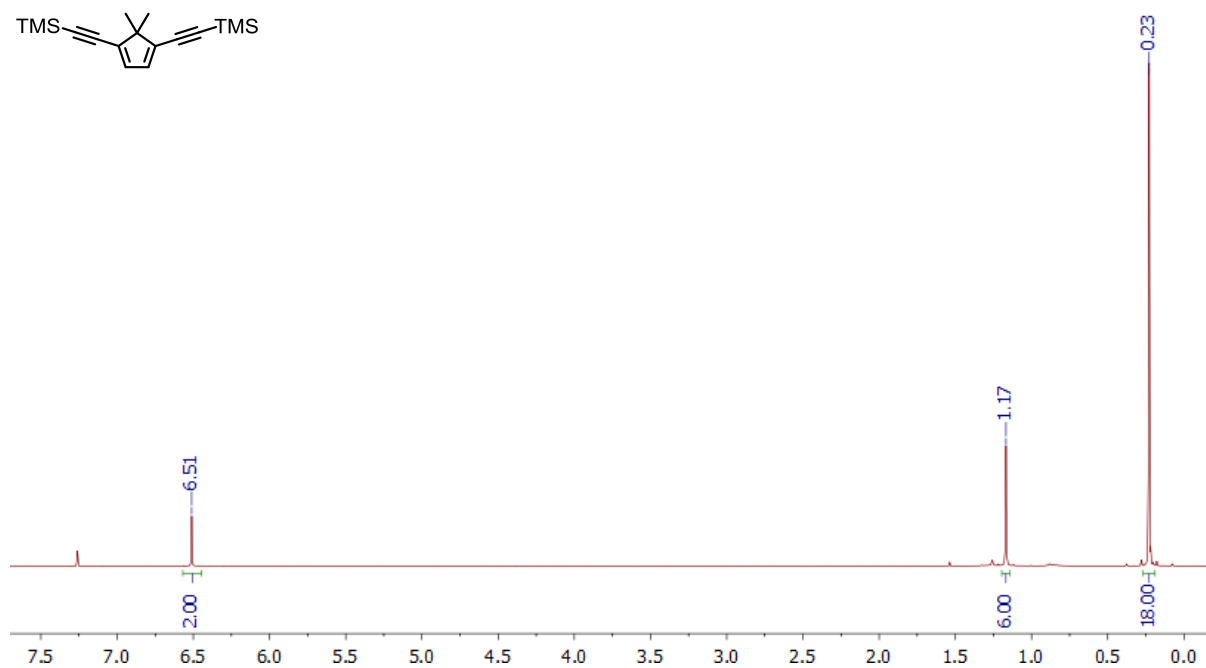
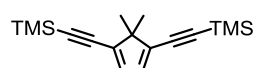


Figure S1-29:  $^1\text{H}$  NMR Spectrum of **40** in  $\text{CDCl}_3$  ( $\delta$   $\text{CHCl}_3$  7.26)

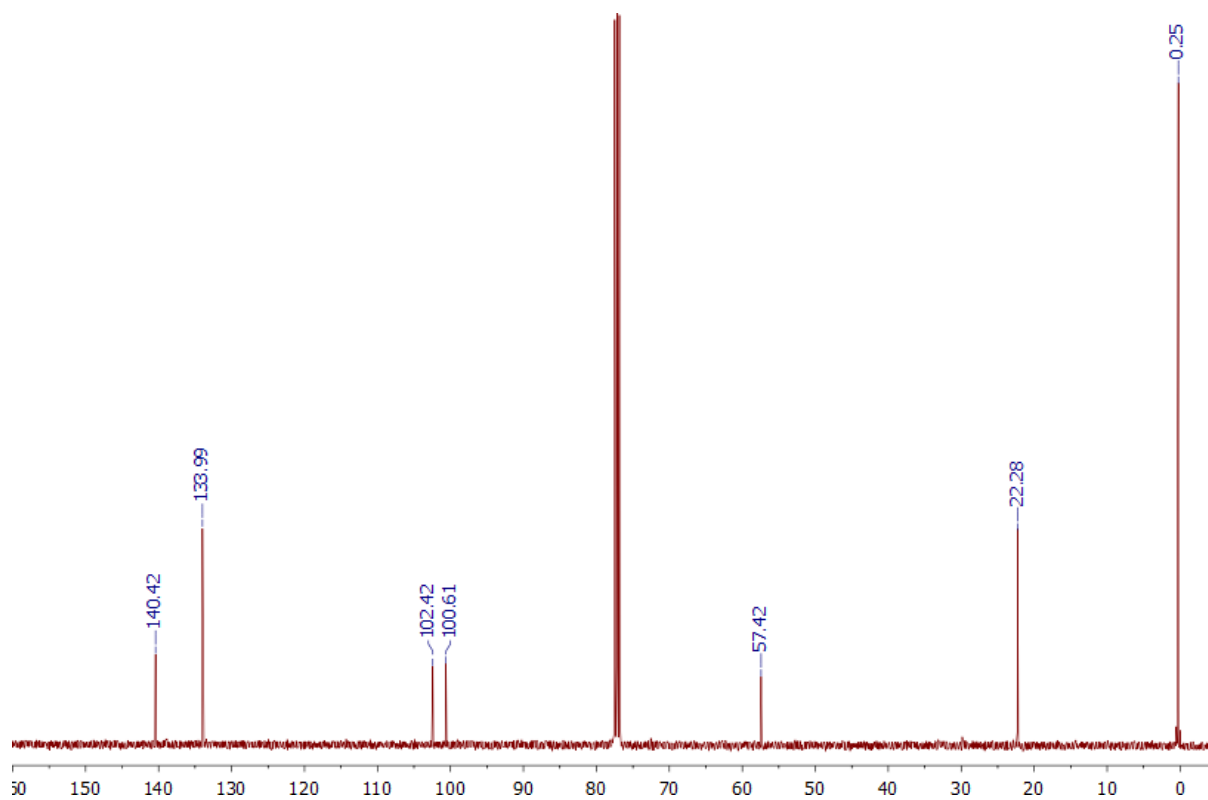


Figure S1-30:  $^{13}\text{C}$  NMR Spectrum of **40** in  $\text{CDCl}_3$  ( $\delta$  77.16)

### 1.3.16 $^1\text{H}$ NMR and $^{13}\text{C}$ NMR Spectra of **4**

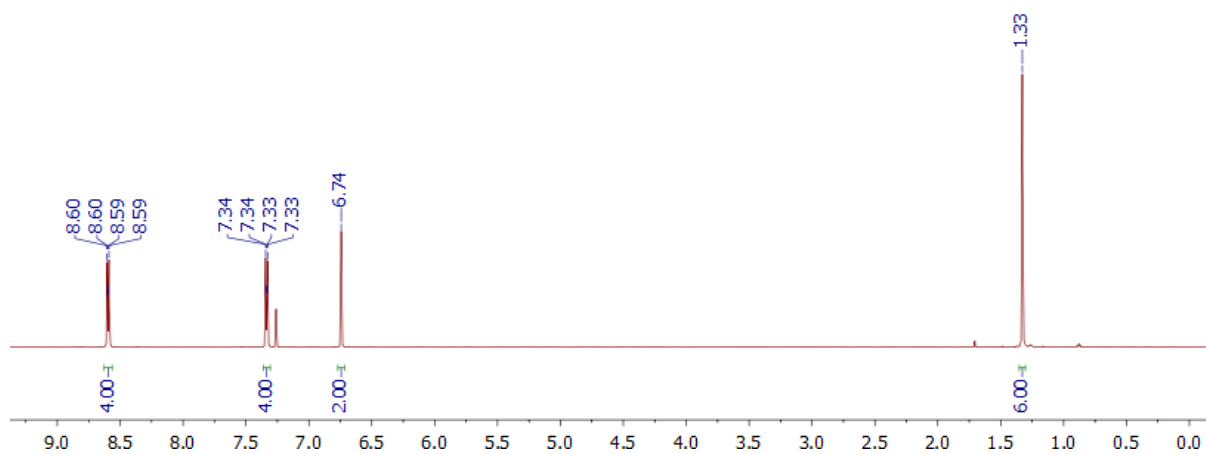
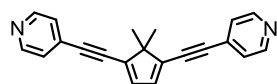


Figure S1-31:  $^1\text{H}$  NMR Spectrum of **4** in  $\text{CDCl}_3$  ( $\delta$   $\text{CHCl}_3$  7.26)

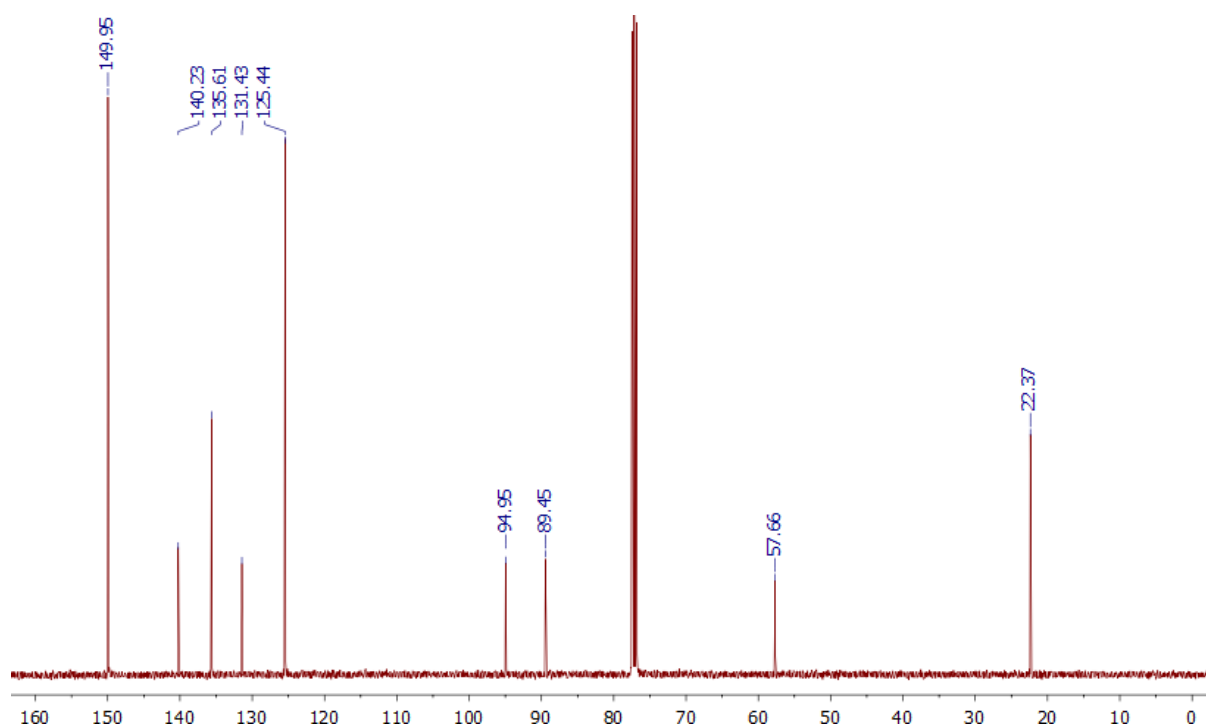


Figure S1-32:  $^{13}\text{C}$  NMR Spectrum of **4** in  $\text{CDCl}_3$  ( $\delta$  77.16)

### 1.3.17 $^1\text{H}$ NMR and $^{13}\text{C}$ NMR Spectra of **11**

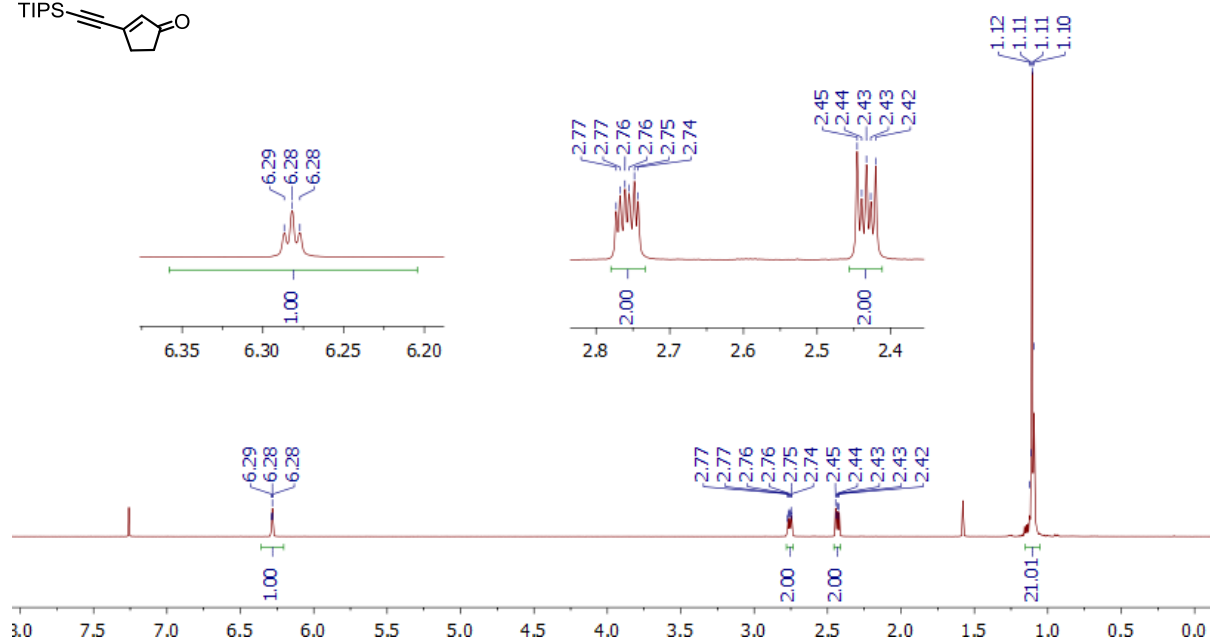
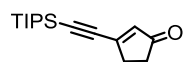


Figure S1-33:  $^1\text{H}$  NMR Spectrum of **11** in  $\text{CDCl}_3$  ( $\delta$   $\text{CHCl}_3$  7.26)

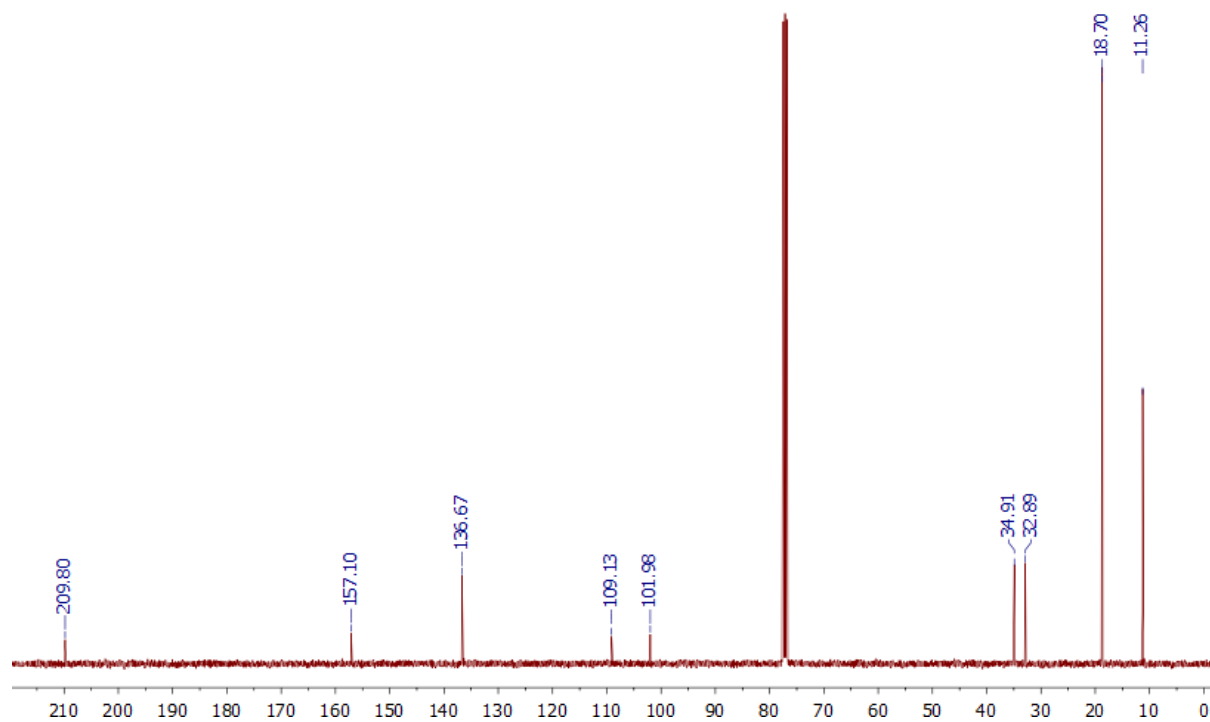


Figure S1-34:  $^{13}\text{C}$  NMR Spectrum of **11** in  $\text{CDCl}_3$  ( $\delta$  77.16)

### 1.3.18 $^1\text{H}$ NMR and $^{13}\text{C}$ NMR Spectra of **12**

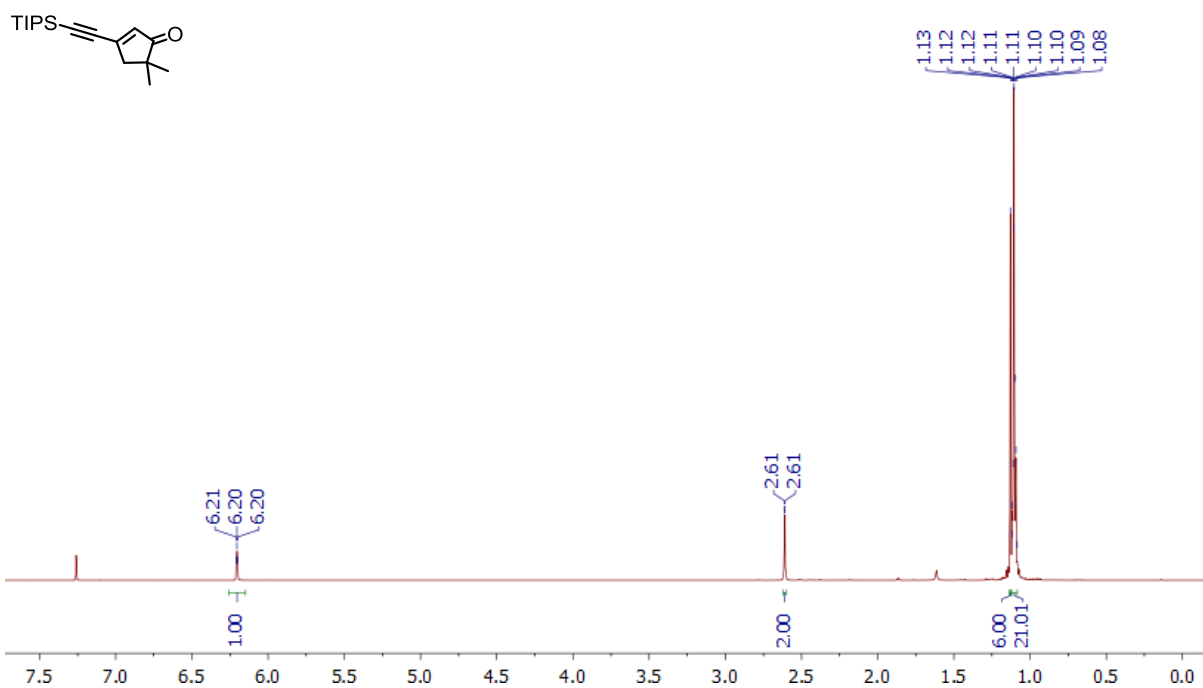


Figure S1-35:  $^1\text{H}$  NMR Spectrum of **12** in  $\text{CDCl}_3$  ( $\delta$   $\text{CHCl}_3$  7.26)

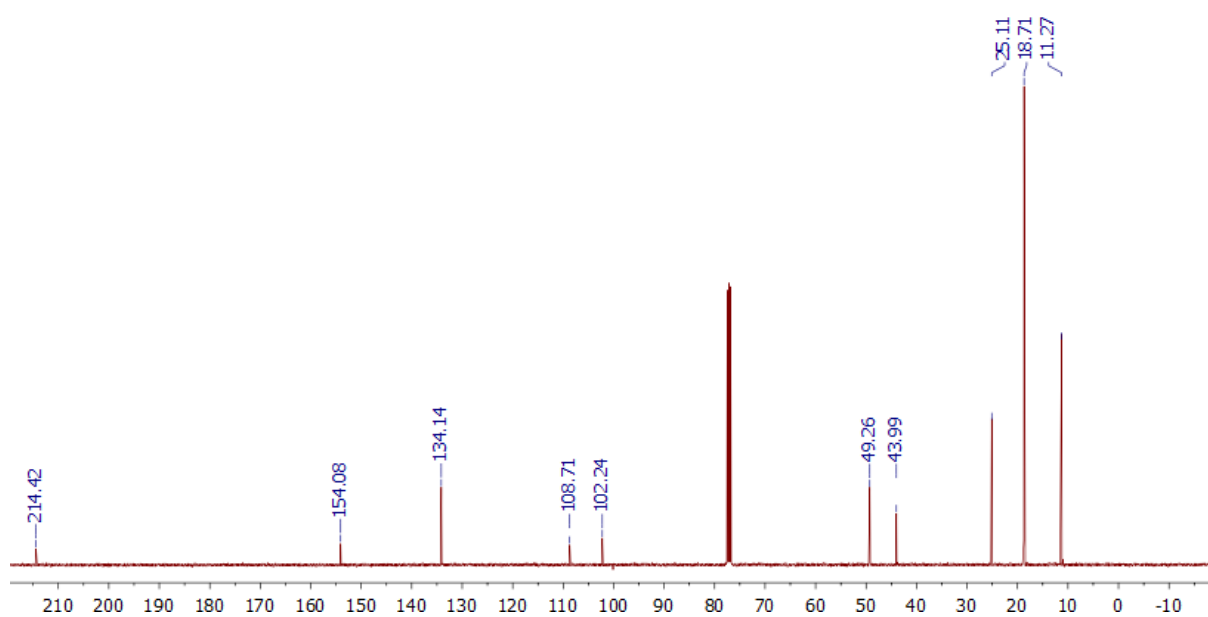


Figure S1-36:  $^{13}\text{C}$  NMR Spectrum of **12** in  $\text{CDCl}_3$  ( $\delta$  77.16)

### 1.3.19 $^1\text{H}$ NMR $^{13}\text{C}$ NMR and $^{19}\text{F}$ NMR Spectra of **13**

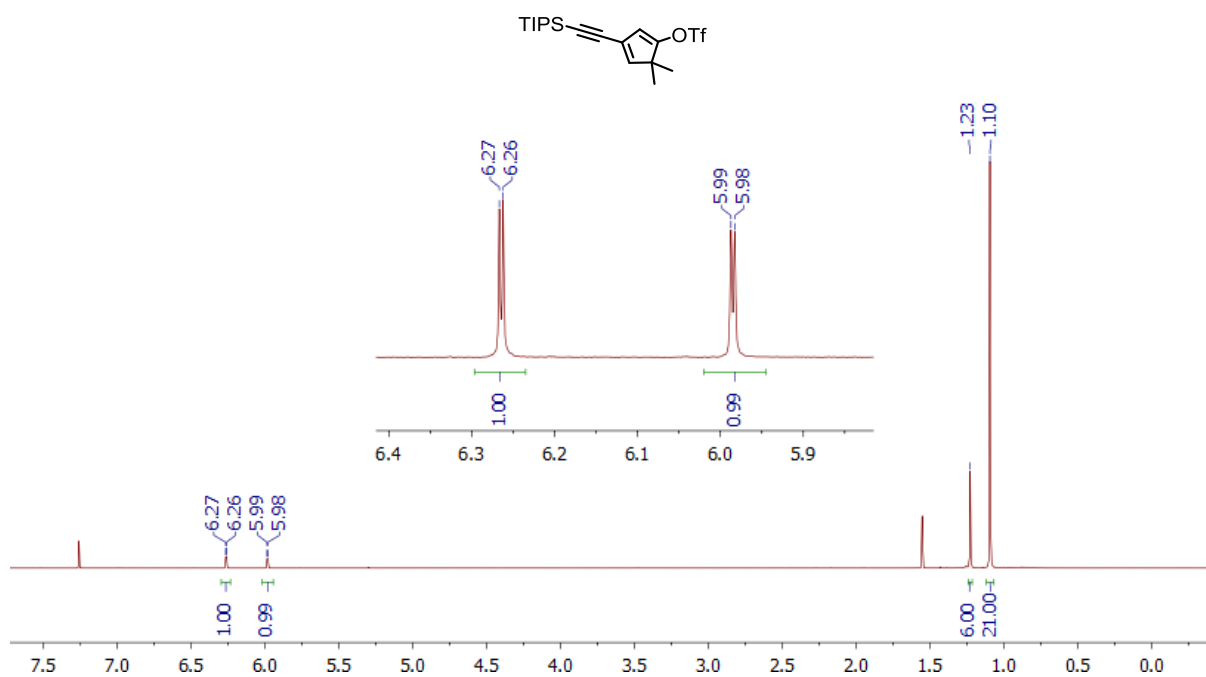


Figure S1-37:  $^1\text{H}$  NMR Spectrum of **13** in  $\text{CDCl}_3$  ( $\delta$   $\text{CHCl}_3$  7.26)

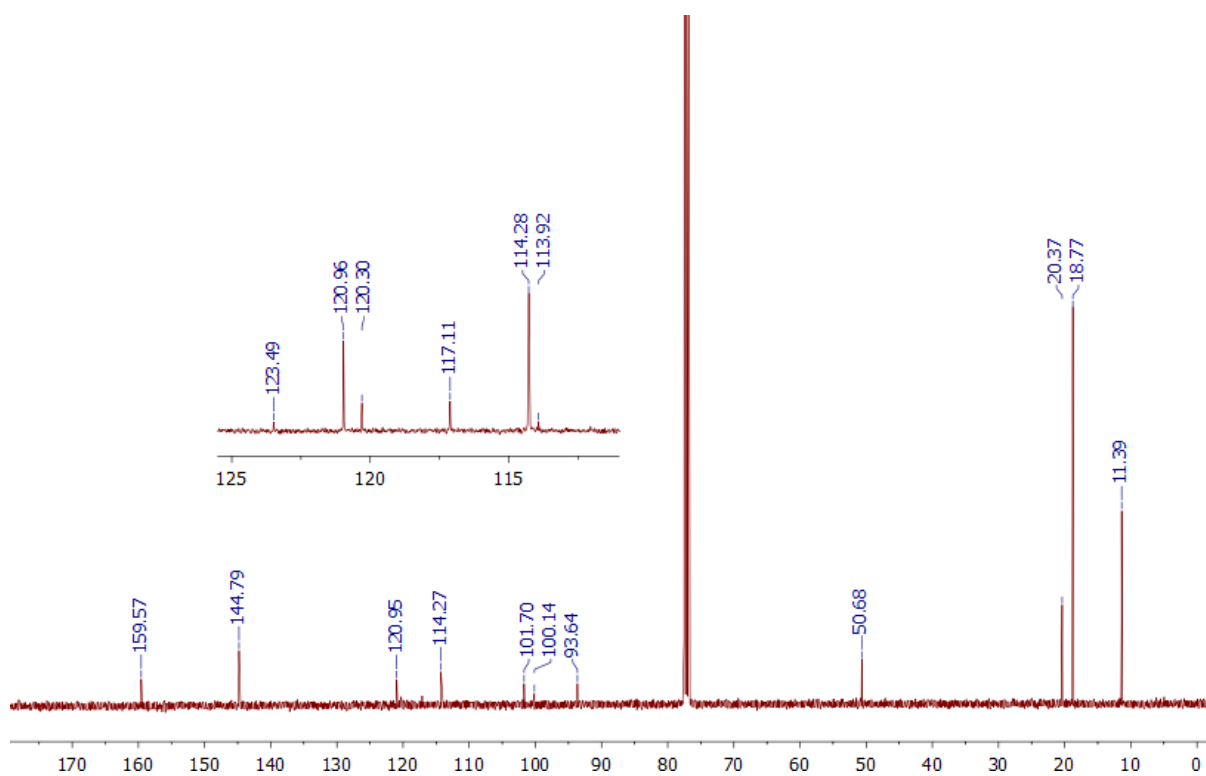


Figure S1-38:  $^{13}\text{C}$  NMR Spectrum of **13** in  $\text{CDCl}_3$  ( $\delta$  77.16)

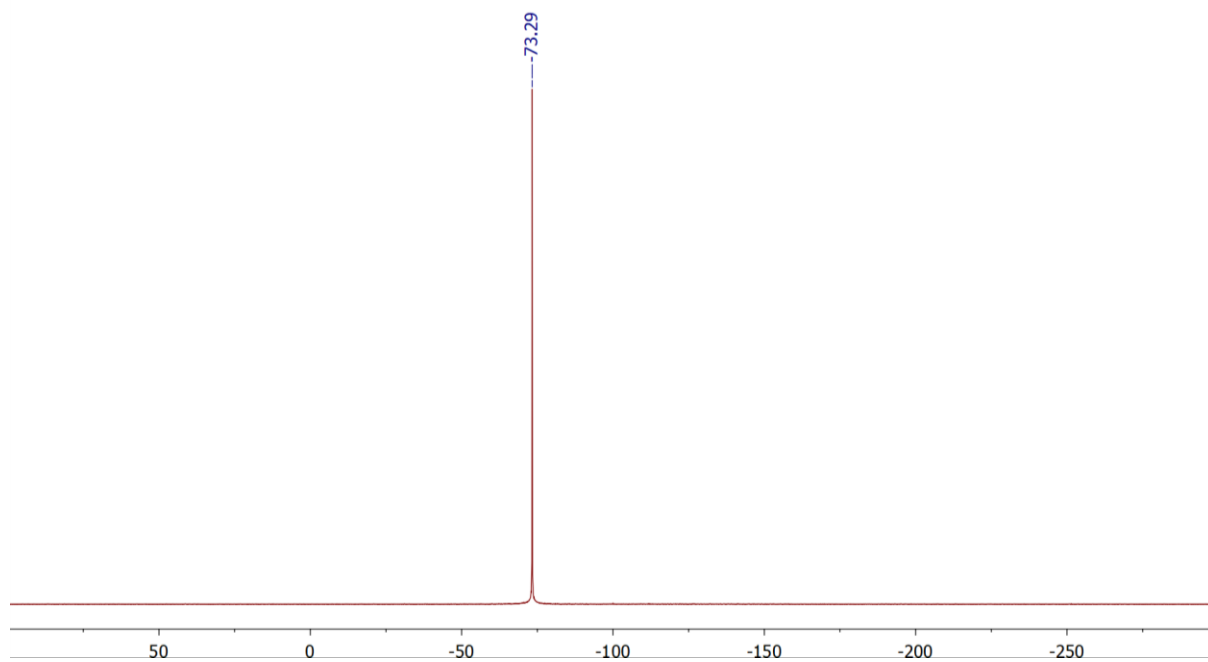


Figure S1-39:  $^{19}\text{F}$  NMR Spectrum of **13** in  $\text{CDCl}_3$

### 1.3.20 $^1\text{H}$ NMR and $^{13}\text{C}$ NMR Spectra of **14**

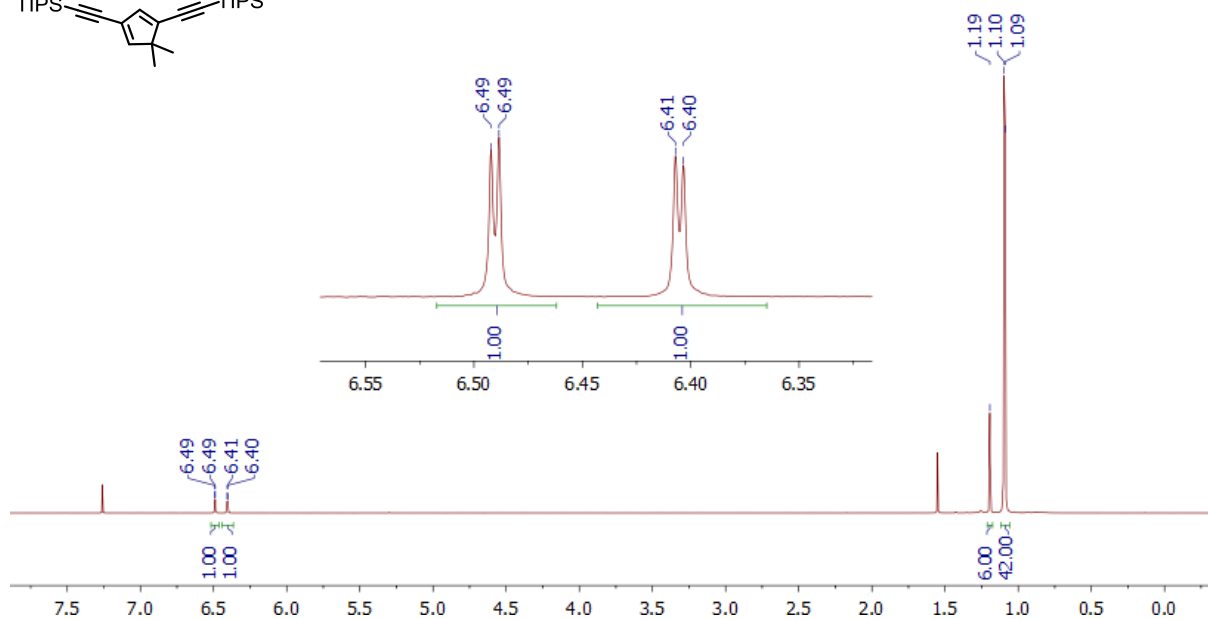
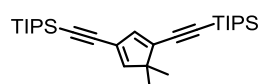


Figure S1-40:  $^1\text{H}$  NMR Spectrum of **14** in  $\text{CDCl}_3$  ( $\delta$   $\text{CHCl}_3$  7.26)

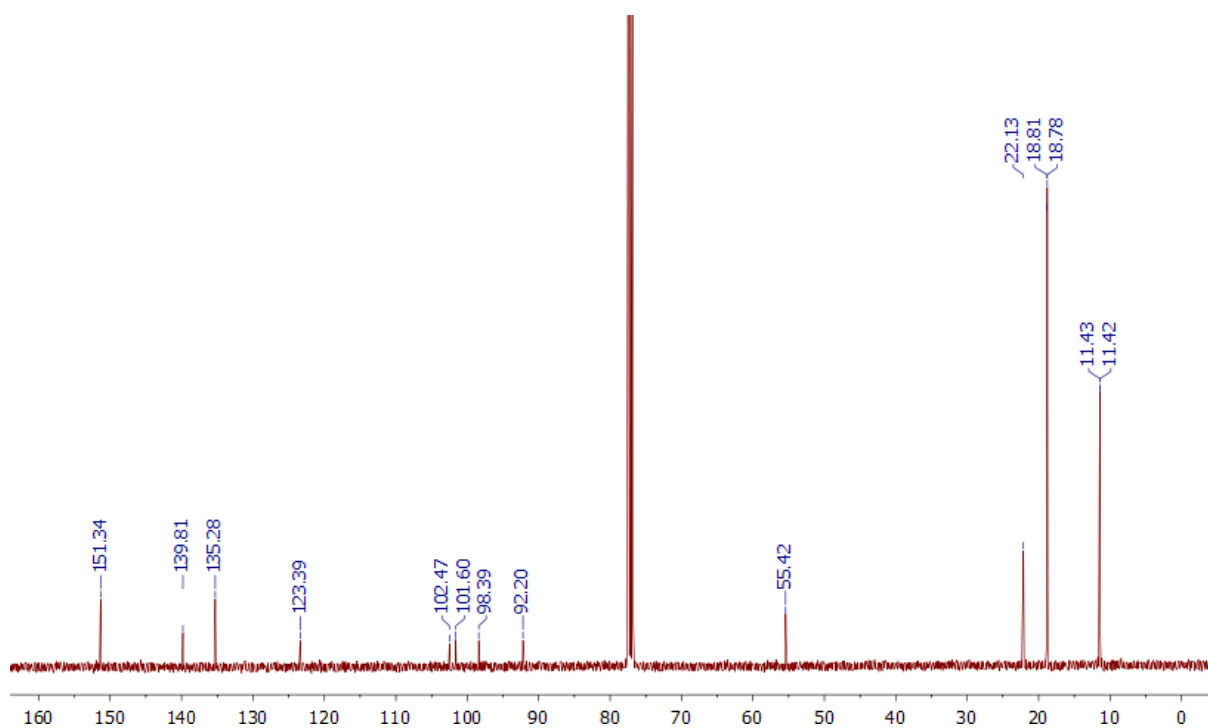


Figure S1-41:  $^{13}\text{C}$  NMR Spectrum of **14** in  $\text{CDCl}_3$  ( $\delta$  77.16)

### 1.3.21 $^1\text{H}$ NMR and $^{13}\text{C}$ NMR Spectra of **8**

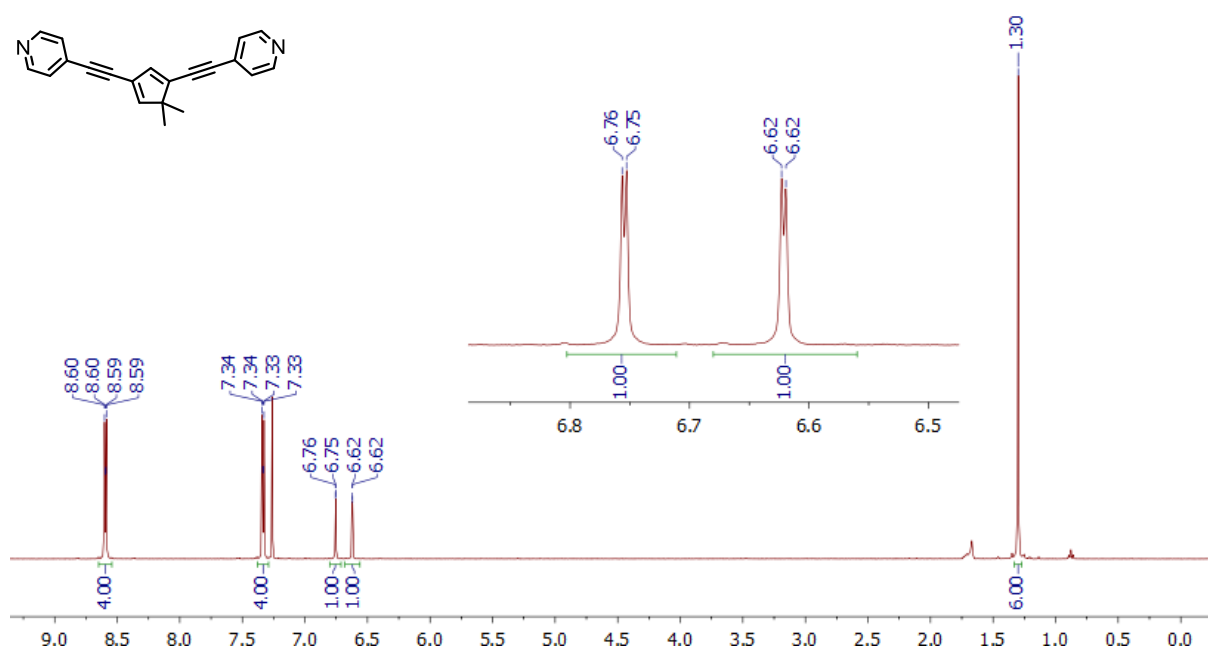


Figure S1-42:  $^1\text{H}$  NMR Spectrum of **8** in  $\text{CDCl}_3$  ( $\delta$   $\text{CHCl}_3$  7.26)

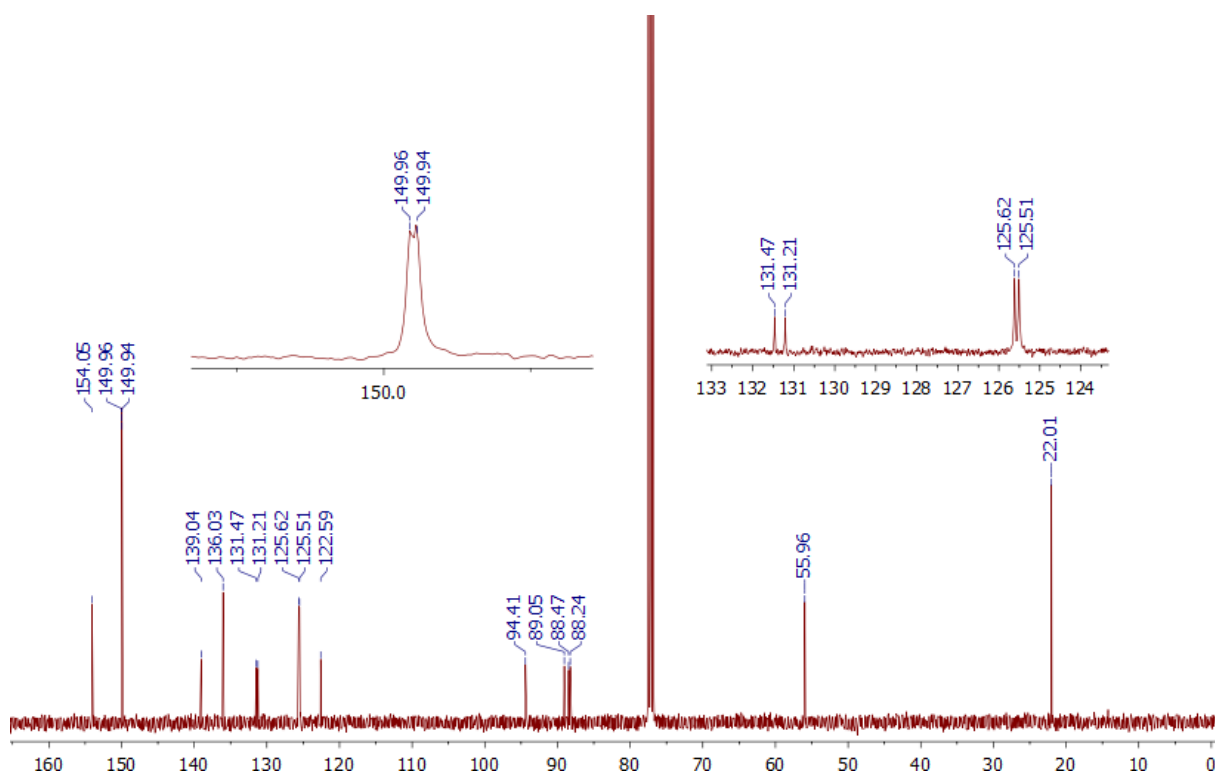


Figure S1-43:  $^{13}\text{C}$  NMR Spectrum of **8** in  $\text{CDCl}_3$  ( $\delta$  77.16)

## 2. Single-molecule conductance measurements for compounds 1-8

For the single-molecule conductance measurements, we employed an in-house constructed mechanically controllable break junction (MCBJ) setup. A notched gold wire with a diameter of 0.1 mm (99.99%, purity) was fixed on an elastic steel sheet (10 mm × 30 mm × 0.20 mm) using epoxy glue (Stycast 2850 FT with catalyst 9). Then a liquid cell made of polytef was placed onto the steel sheet. To open and close the nanogap repeatedly, a stepping motor (Zaber NA14B16 linear actuator), combined with a piezo stack (Thorlab AE0505D18F), was employed to bend and release the steel sheet. During the electrical measurements, a bias of 100 mV was applied at the two ends of the gold wire, and a logarithm  $IV$  converter with a sampling rate of 10 kHz was employed to collect the data. For each compound, at least 1,000 individual curves were collected without any data selection for further analysis. For each of the 8 compounds, the conductance measurements were performed at least three times to confirm their reproducibility.

## 2.1 Single-molecule conductance measurements for compound 1

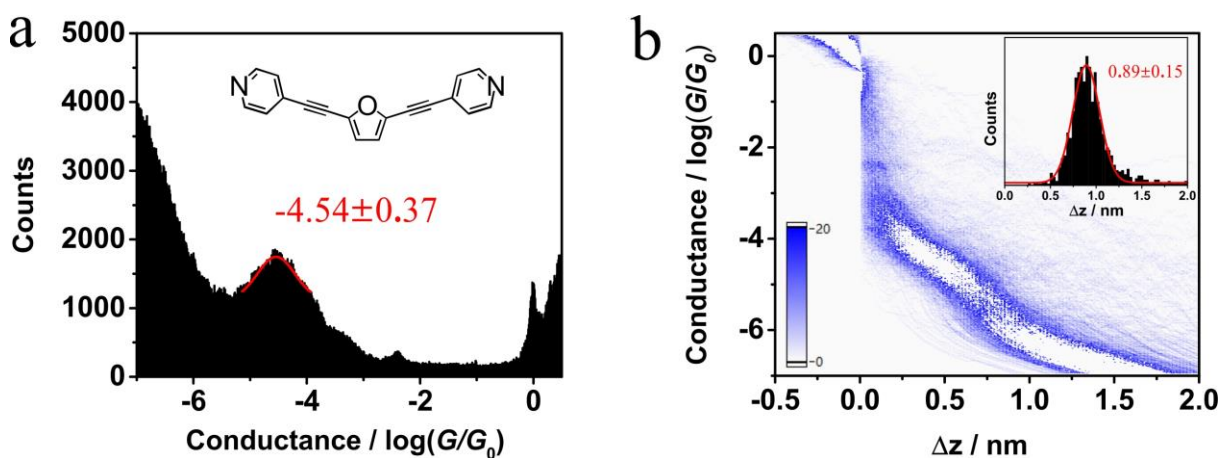


Figure S2-1: (a) One-dimensional conductance histogram for compound 1. Insert: the chemical structure of compound 1. (b) Two-dimensional conductance-distance cloud of compound 1. Insert: the distribution of the plateau length for compound 1.

## 2.2 Single-molecule conductance measurements for compound 2

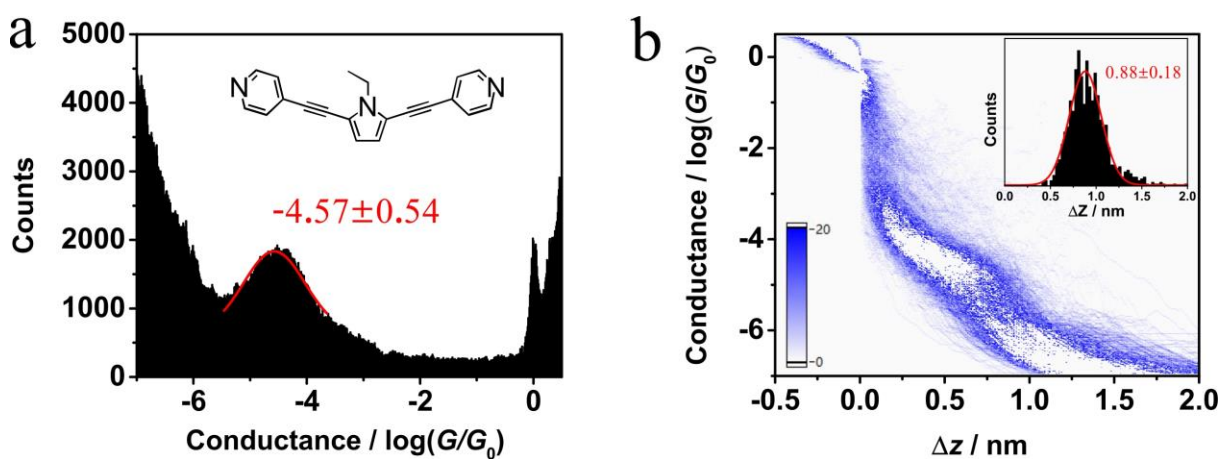


Figure S2-2: (a) One-dimensional conductance histogram for compound 2. Insert: the chemical structure of compound 2. (b) Two-dimensional conductance-distance cloud of compound 2. Insert: the distribution of the plateau length for compound 2.

### 2.3 Single-molecule conductance measurements for compound 3

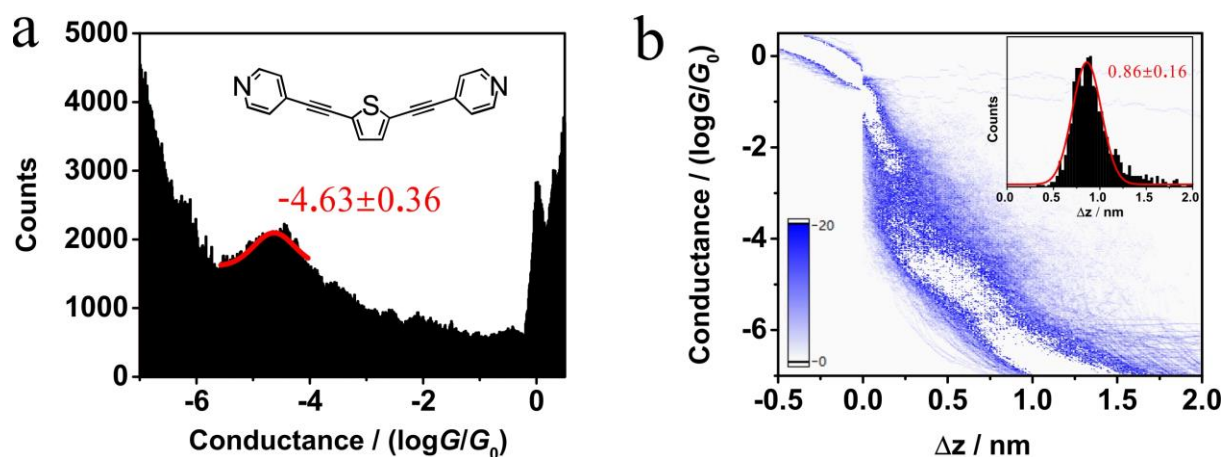


Figure S2-3: (a) One-dimensional conductance histogram for compound 3. Insert: the chemical structure of compound 3. (b) Two-dimensional conductance-distance cloud of compound 3. Insert: the distribution of the plateau length for compound 3.

### 2.4 Single-molecule conductance measurements for compound 4

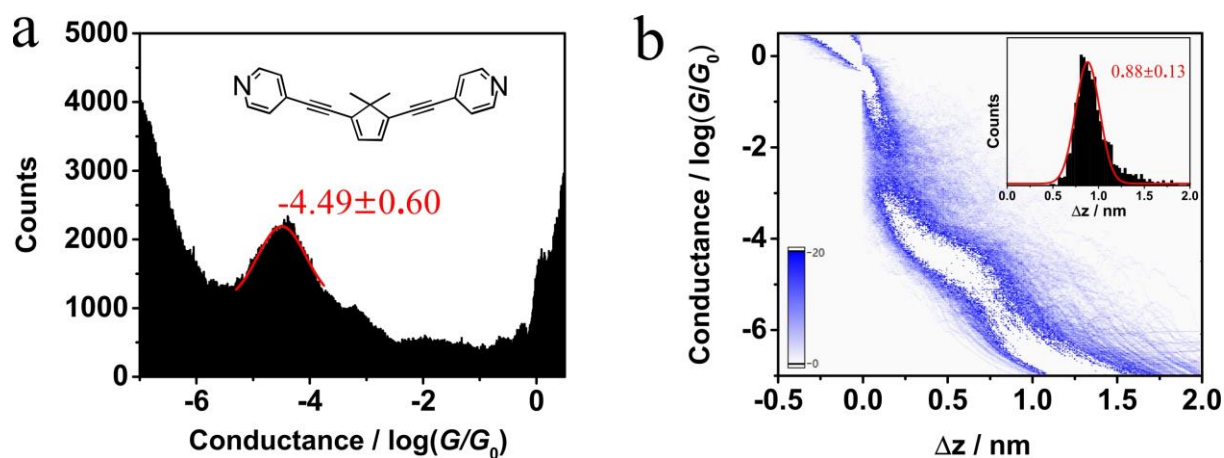


Figure S2-4: (a) One-dimensional conductance histogram for compound 4. Insert: the chemical structure of compound 4. (b) Two-dimensional conductance-distance cloud of compound 4. Insert: the distribution of the plateau length for compound 4.

### 2.5 Single-molecule conductance measurements for compound 5

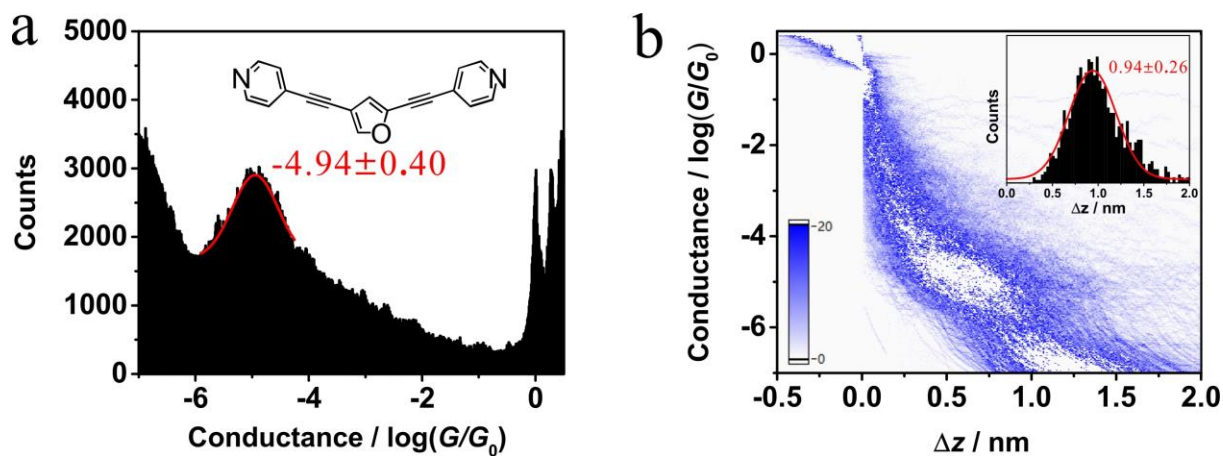


Figure S2-5: (a) One-dimensional conductance histogram for compound **5**. Insert: the chemical structure of compound **5**. (b) Two-dimensional conductance-distance cloud of compound **5**. Insert: the distribution of the plateau length for compound **5**.

## 2.6 Single-molecule conductance measurements for compound **6**

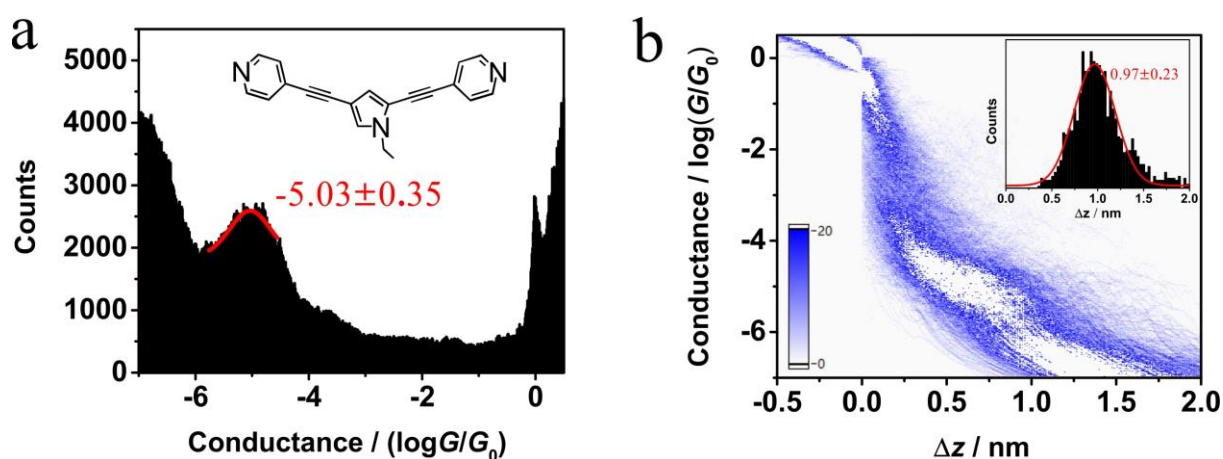


Figure S2-6: (a) One-dimensional conductance histogram for compound **6**. Insert: the chemical structure of compound **6**. (b) Two-dimensional conductance-distance cloud of compound **6**. Insert: the distribution of the plateau length for compound **6**.

## 2.7 Single-molecule conductance measurements for compound **7**

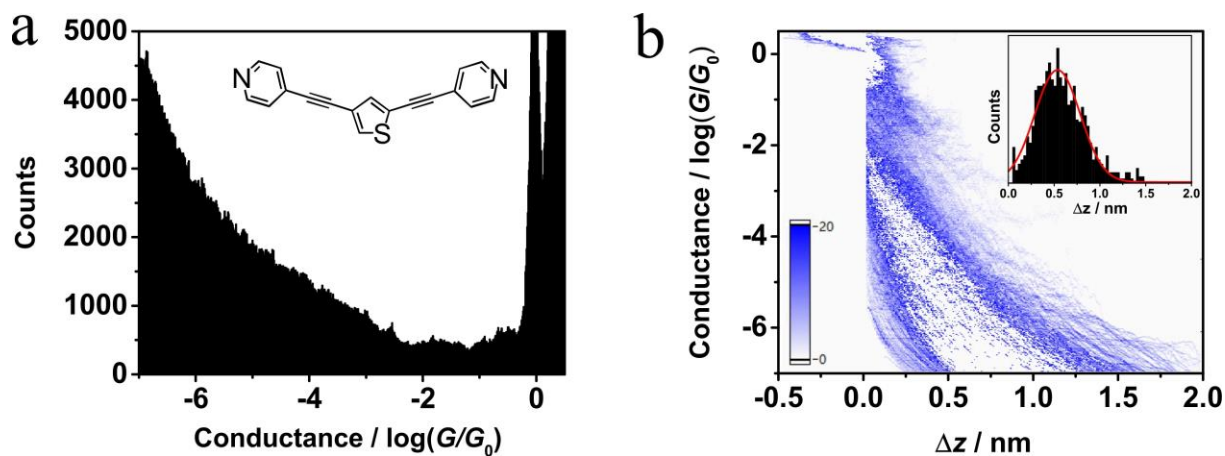


Figure S2-7: (a) One-dimensional conductance histogram for compound **7**. Insert: the chemical structure of compound **7**. (b) Two-dimensional conductance-distance cloud of compound **7**. Insert: the distribution of the plateau length for compound **7**.

## 2.8 Single-molecule conductance measurements for compound **8**

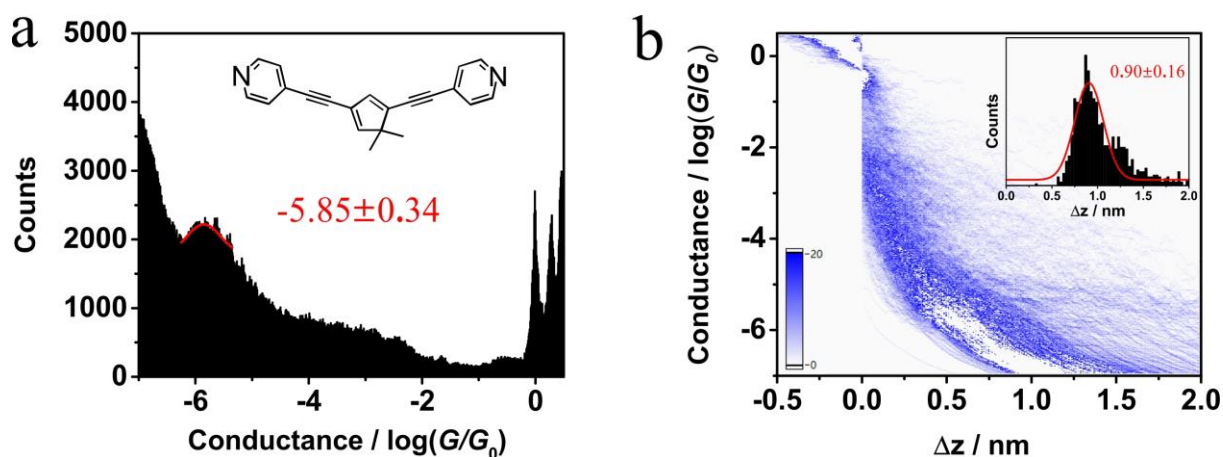


Figure S2-8: (a) One-dimensional conductance histogram for compound **8**. Insert: the chemical structure of compound **8**. (b) Two-dimensional conductance-distance cloud of compound **8**. Insert: the distribution of the plateau length for compound **8**.

## 2.9 Single-molecule conductance measurements for pure solvent

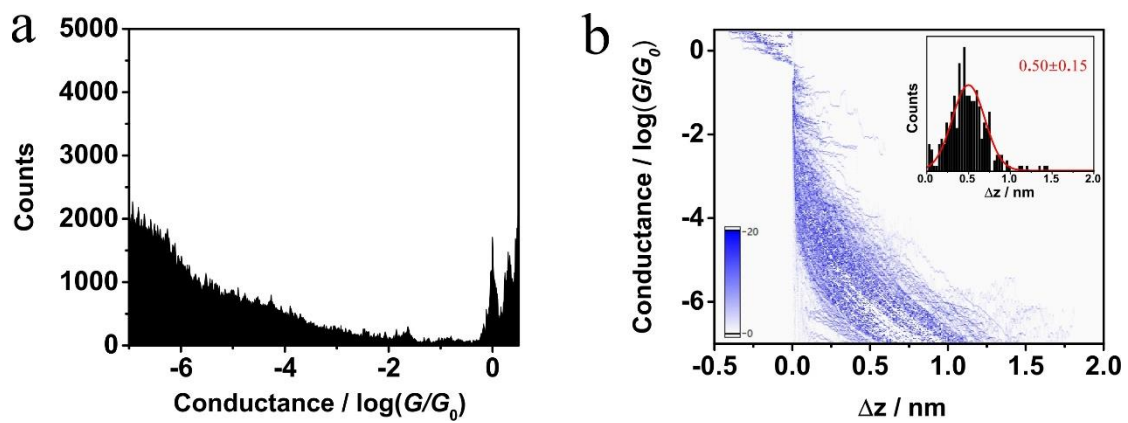


Figure S2-9: (a) One-dimensional conductance histogram for pure solvent. 2. (b) Two-dimensional conductance-distance cloud of pure solvent. Insert: the distribution of the plateau length.

### 3. Theory

#### DFT-based computational methods:

The optimized geometry and ground state Hamiltonian and overlap matrix elements of each structure were self-consistently obtained using the SIESTA<sup>12</sup> implementation of density functional theory (DFT). SIESTA employs norm-conserving pseudo-potentials to account for the core electrons and linear combinations of atomic orbitals to construct the valence states. The generalized gradient approximation (GGA) of the exchange and correlation functional is used with the Perdew-Burke-Ernzerhof parameterization (PBE),<sup>13</sup> a double- $\zeta$  polarized (DZP) basis set, a real-space grid defined with an equivalent energy cut-off of 250 Ry. The geometry optimization for each structure is performed to the forces smaller than 10 meV/Å. The mean-field Hamiltonian obtained from the converged DFT calculation was combined with our Gollum quantum transport code<sup>14</sup> to calculate the phase-coherent, elastic scattering properties of the each system consist of left (source) and right (drain) leads and the scattering region. The transmission coefficient  $T(E)$  for electrons of energy  $E$  (passing from the source to the drain) is calculated via the relation  $T(E) = \text{Trace}(\Gamma_R(E)G^R(E)\Gamma_L(E)G^{R\dagger}(E))$ . In this expression,  $\Gamma_{L,R}(E) = i(\Sigma_{L,R}(E) - \Sigma_{L,R}^\dagger(E))$  describe the level broadening due to the coupling between left (L) and right (R) electrodes and the central scattering region,  $\Sigma_{L,R}(E)$  are the retarded self-energies associated with this coupling and  $G^R = (ES - H - \Sigma_L - \Sigma_R)^{-1}$  is the retarded Green's function, where H is the Hamiltonian and S is overlap matrix. Using obtained transmission coefficient ( $T(E)$ ), the conductance could be calculated by Landauer formula ( $G = G_0 \int dE T(E)(-\partial f / \partial E)$ ) where  $G_0 = 2e^2/h$  is the conductance quantum,  $f(E) = (1 + \exp((E - E_F)/k_B T))^{-1}$  is the Fermi-Dirac distribution function, T is the temperature and  $k_B = 8.6 \times 10^{-5}$  eV/K is Boltzmann's const.

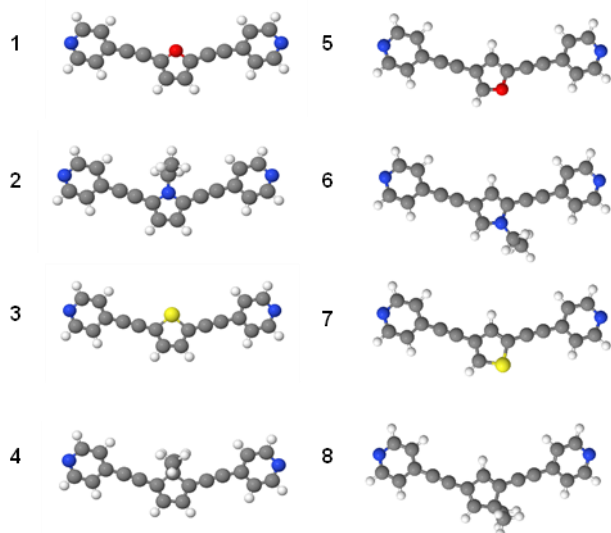


Figure S3-1: Relaxed structures of the molecules shown in Figure 1a.

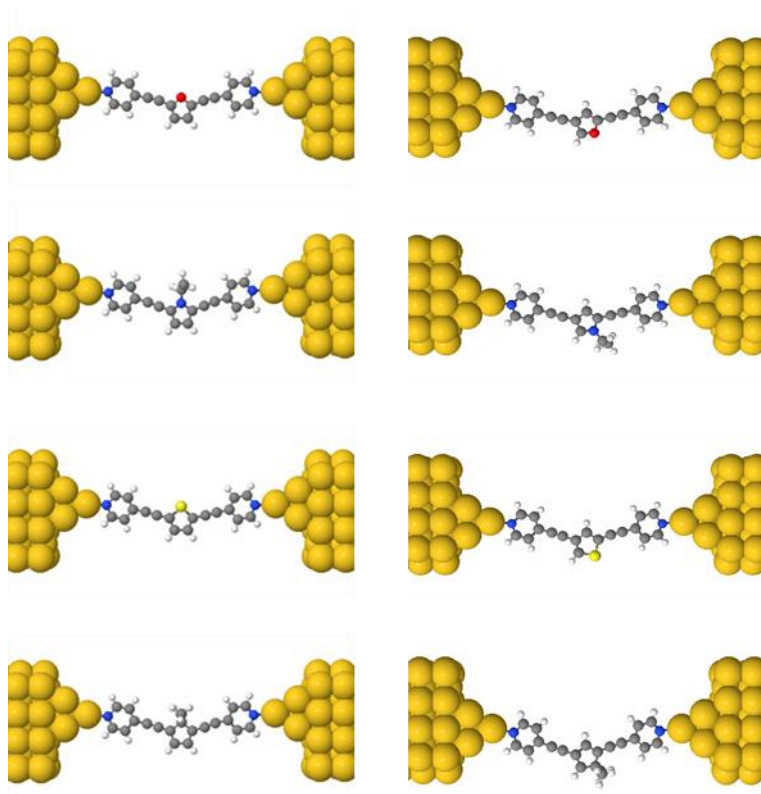


Figure S3-2: Relaxed structures of the molecules **1-8** between electrodes, when the electrodes are connected to the nitrogen atoms of the pyridyl anchor groups.

#### 4. References

- (1) Hein, S. J.; Arslan, H.; Keresztes, I.; Dichtel, W. R. Rapid Synthesis of Crowded Aromatic Architectures from Silyl Acetylenes. *Org. Lett.* **2014**, *16*, 4416-4419.
- (2) Zhan, W. H.; Xu, L.; Dong, X. W.; Dong, J.; Yi, X.; Ma, X. D.; Qiu, N.; Li, J.; Yang, B.; Zhou, Y. B.; Hu, Y. Z. Design, Synthesis and Biological Evaluation of Pyrazol-Furan Carboxamide Analogues as Novel Akt Kinase Inhibitors. *Eur. J. Med. Chem.* **2016**, *117*, 47-58.
- (3) Brucoli, F.; Natoli, A.; Marimuthu, P.; Borrello, M. T.; Stapleton, P.; Gibbons, S.; Schatzlein, A. Efficient Synthesis and Biological Evaluation of Proximicins a, B and C. *Bioorg. Med. Chem.* **2012**, *20*, 2019-2024.
- (4) Agosta, W. C.; Smith, A. B. Preparation and Reactions of 2,2-Dimethyl-4-Cyclopentene-1,3-Dione. *J. Org. Chem.* **1970**, *35*, 3856-3860.
- (5) Fukuda, T.; Ohta, T.; Sudo, E.; Iwao, M. Directed Lithiation of N-Benzenesulfonyl-3-Bromopyrrole. Electrophile-Controlled Regioselective Functionalization Via Dynamic Equilibrium between C-2 and C-5 Lithio Species. *Org. Lett.* **2010**, *12*, 2734-2737.
- (6) Arsenyan, P.; Paegle, E.; Belyakov, S. A Novel Method for the Bromination of Thiophenes. *Tetrahedron Lett.* **2010**, *51*, 205-208.
- (7) Keegstra, M. A.; Brandsma, L. Convenient High-Yield Procedures for 2-Bromothiophene and 2,5-Dibromothiophene. *Synthesis* **1988**, 890-891.
- (8) Ball, L. T.; Lloyd-Jones, G. C.; Russell, C. A. Gold-Catalyzed Oxidative Coupling of Arylsilanes and Arenes: Origin of Selectivity and Improved Precatalyst. *J. Am. Chem. Soc.* **2014**, *136*, 254-264.

- (9) Seidler, A.; Svoboda, J.; Dekoj, V.; Chocholousova, J. V.; Vacek, J.; Stara, I. G.; Stary, I. The Synthesis of Pi-Electron Molecular Rods with a Thiophene or Thieno[3,2-b]thiophene Core Unit and Sulfur Alligator Clips. *Tetrahedron Lett.* **2013**, *54*, 2795-2798.
- (10) Chen, L.; Mahmoud, S. M.; Yin, X.; Lalancette, R. A.; Pietrangelo, A. Decreasing Aromaticity in  $\Pi$ -Conjugated Materials: Efficient Synthesis and Electronic Structure Identification of Cyclopentadiene-Containing Systems. *Org. Lett.* **2013**, *15*, 5970-5973.
- (11) Marson, C. M.; Farrand, L. D.; Brettle, R.; Dunmur, D. A. Highly Efficient Syntheses of 3-Aryl-2-Cycloalken-1-Ones and an Evaluation of Their Liquid Crystalline Properties. *Tetrahedron* **2003**, *59*, 4377-4381.
- (12) José, M. S.; Emilio, A.; Julian, D. G.; Alberto, G.; Javier, J.; Pablo, O.; Daniel, S.-P. The Siesta Method for Ab Initio Order- N Materials Simulation. *J. Phys-Condens. Mat.* **2002**, *14*, 2745.
- (13) Perdew, J. P.; Burke, K.; Ernzerhof, M. Generalized Gradient Approximation Made Simple. *Phys. Rev. Lett.* **1996**, *77*, 3865-3868.
- (14) Ferrer, J.; Lambert, C. J.; García-Suárez, V. M.; Manrique, D. Z.; Visontai, D.; Oroszlany, L.; Rodríguez-Ferradás, R.; Grace, I.; Bailey, S. W. D.; Gillemot, K.; Sadeghi, H.; Algharagholy, L. A. Gollum: A Next-Generation Simulation Tool for Electron, Thermal and Spin Transport. *New J. Phys.* **2014**, *16*, 093029.